



# QUANTUM INNOVATION 2021

The International Symposium on Quantum Science,  
Technology and Innovation

T  
O  
K  
Y  
O



## Proceedings

Date 7-9 December 2021  
Virtual Conference

## Table of contents

### Program

---

02	Welcome to Quantum Innovation 2021
03	Organizing Committee
04-06	Symposium Outline

### Program

---

07-09	Program at a Glance
10	Plenary Sessions
11-12	Quantum Computing Track
13	Quantum Cryptography & Communication Track
14	Quantum Sensing Track
15-18	Quantum Sensing Track Short Presentations by Young Researchers

### Abstract

---

19-27	Plenary Sessions
28-58	Quantum Computing Track
59-78	Quantum Cryptography & Communication Track
79-100	Quantum Sensing Track
101-150	Quantum Sensing Track Short Presentations by Young Researchers SE-03A
151-166	Quantum Sensing Track Short Presentations by Young Researchers SE-03B



# QUANTUM INNOVATION 2021

## The International Symposium on Quantum Science, Technology and Innovation

### Welcome to Quantum Innovation 2021

It is our pleasure to invite all of you, scientists, engineers, academicians, young researchers, business delegates and students, from all over the world to attend Quantum Innovation 2021, the International Symposium on Quantum Science, Technology and Innovation, to be held on 7-9 December 2021 as Virtual Conference organized and served commemorating the birth of the Quantum Technology Innovation Hubs.

The aim of Quantum Innovation 2021 is to bring together, a multi-disciplinary group of scientists and engineers to present and exchange breaking-through ideas related to quantum technologies. The topics of the meeting cover broad aspects of quantum technology including quantum computing, quantum sensing, quantum cryptography and quantum communication with a focus on the latest outstanding achievements in the field of quantum technology and its future trends and needs.

We welcome you to Quantum Innovation 2021 and look forward to your participation in the meeting with distinguished speakers from different countries around the world sharing new and exciting results and promoting collaborations in Quantum Technology.

## Organizing Committee

### Chairs

---



General Chair  
**Yasunobu Nakamura**  
RIKEN



Track Chair  
Quantum Computing  
**Masahiro Kitagawa**  
Osaka University



Track Chair  
Quantum Sensing  
**Akinari Yokoya**  
National Institutes for  
Quantum Science and Technology  
(QST)



Track Chair  
Quantum Cryptography & Communication  
**Masahide Sasaki**  
National Institute of Information  
and Communications Technology (NICT)

### Committee members

---

**Keisuke Fujii**  
Osaka University

**Takayuki Iwasaki**  
Tokyo Institute of Technology

**Kae Nemoto**  
National Institute  
of Informatics (NII)

**Seichiro Tani**  
Nippon Telegraph  
and Telephone Corporation (NTT)

**Mikio Fujiwara**  
NICT

**Takashi Kuroda**  
National Institute  
for Materials Science (NIMS)

**Tadashi Sakai**  
Tokyo Institute of Technology

**Yoshimichi Tanizawa**  
Toshiba

**Takuya Hirano**  
Gakushuin University

**Takahiro Mori**  
National Institute  
of Advanced Industrial Science  
and Technology (AIST)

**Masahiro Takeoka**  
Keio University

**Akihisa Tomita**  
Hokkaido University

**Hiroshi Imai**  
The University of Tokyo

**Atsushi Mukaiyama**  
Osaka University

**Shu Tanaka**  
Keio University

**Rodney Van Meter**  
Keio University

## Symposium Outline

### Aims

---

Addressing the state-of-the-art  
quantum technology

Exploring cooperation on research,  
application, education and social awareness  
on quantum technology

We will bring together researchers working on quantum technology and offer a platform for discussions among them. Inviting prominent speakers from abroad and Japan, Quantum Innovation 2021 covers latest development of quantum computing, quantum sensing, quantum cryptography and quantum communication.

We also aim to give young researchers, future quantum working force candidates and aware citizens an overview of fast evolving quantum technology by listening to inspiring talks.

### Scope of the Symposium

---

Highlights of the development of quantum  
technology

Quantum Computing

Quantum Sensing

Quantum Cryptography & Communication

Development of Infrastructure for the progress  
of quantum technology

Promotion of practical applications of quantum technology

Development of human resources for quantum technology

Promotion of international collaborations

**Date**

---

**7-9 December 2021**

**Venue**

---

**Symposium is held on-line.**

**Schedule**

---

**7 December 2021      Plenary Sessions held in Tokyo**

---

**8-9 December 2021      Quantum Computing Track  
Quantum Sensing Track  
Quantum Cryptography & Communication Track**

**Speakers**

---

**All the speakers are to be invited.**

**Language**

---

**English**

**Participants**

---

Researchers, engineers, business delegates, policy makers, administrators, students and media. All participants are required to register in advance. Registration page is open!

## Symposium Sponsors

---

Cabinet Office  
Ministry of Education, Culture, Sports, Science and Technology (MEXT)  
RIKEN  
Japan Science and Technology Agency (JST)  
National Institutes for Quantum Science and Technology (QST)  
National Institute of Advanced Industrial Science and Technology (AIST)  
National Institute of Information and Communications Technology (NICT)  
Osaka University  
Tokyo Institute of Technology

## Symposium Supporters

---

Ministry of Internal Affairs and Communications  
Ministry of Economy, Trade and Industry  
National Institute for Materials Science (NIMS)  
The University of Tokyo

## About QIH

Quantum technology is bringing a great impact on a wide range of industry. In order to accelerate the progress and make best use of quantum technology, industry, academia and government are expected to collaborate on promoting basic research, technology demonstration, industrialization, intellectual property management and human resource development. For promoting these activities, Japan established Quantum Technology Innovation Hubs in February 2021.



- Quantum computer development hub in RIKEN
- Quantum device development hub in National Institute of Advanced Industrial Science and Technology (AIST)
- Quantum computer application hub represented by the University of Tokyo
- Quantum software innovation hub in Osaka University
- Quantum security network hub in National Institute of Information and Communications Technology (NICT)
- Quantum life science hub in National Institutes for Quantum Science and Technology (QST)
- Quantum materials research project in National Institute for Materials Science (NIMS)
- Quantum sensors hub represented by Tokyo Institute of Technology

RIKEN serves as Headquarters of the Hubs to incorporate efforts to advance quantum technology research in Japan.

## Program at a Glance

Tracks

# PL

### Plenary Sessions

Contents / Topics

Welcome from Organizing Committee and Hosting Ministries, Plenary Talks, Keynote Speeches

Tracks

# CP

### Quantum Computing Track

Contents / Topics

Quantum Computing with Atoms and Ions, Superconducting Quantum Computers(QC), Photonic QC, Young Researcher Session, Quantum Simulations, Semiconductor QC, Quantum Annealing Toward FTQC(Tutorial), Beyond NISQ/Toward FTQC Panel Discussion, Quantum Architecture, Quantum Algorithms, NISQ Algorithms, Quantum Algorithms for Chemistry

Tracks

# CC

### Quantum Cryptography & Communication Track

Contents / Topics

Quantum Internet, Quantum Cryptography(Up-to-date Technologies of Field and Satellite QKDs), Challenges for Quantum Technology Platform (QKD Networks, Satellite QKD and their integration), Industry Panel, Young Researcher Session  
\*\*CC-04 on 8th and CC-05, CC-06 on 9th Dec are supported by SIP (cross-ministerial Strategic Innovation promotion Program).

Tracks

# SE

### Quantum Sensing Track

Contents / Topics

Solid-State Quantum Sensors, Quantum Sensors for Life Sciences, Quantum Sensors and Quantum Life Sciences, Atom Interferometer, Cold Atom, Atomic/Ion Clocks, Short Presentations by Young Researchers  
\*8th Dec Sessions are a joint-program with The 4th IFQMS (The 4th International Forum on Quantum Metrology and Sensing).

All the times in the program are **Japan Standard Time(GMT+9)**

<b>7</b> Dec (Tue.)	9		
	10	10:00-10:30	Opening
	11	10:40-11:50	Plenary Talks <span style="float:right">PL-01</span>
	12		
	13		
	14	14:00-15:20	Keynote Speeches <span style="float:right">PL-02</span>
	15		
	16	15:50-17:50	Keynote Speeches (cont.) <span style="float:right">PL-03</span>
	17		
18			

\* 4th IFQMS(International Forum on Quantum Metrology and Sensing)  
 \*\* SIP(cross-ministerial Strategic Innovation promotion Program)

<b>8</b> Dec (Wed.)	8	8:00-9:45	Quantum Computing with Atoms and Ions <span style="float:right">CP-01</span>	8:00-10:10	Solid-State Quantum Sensors 1 <span style="float:right">SE-01*</span>			
	9				9:00-11:00	Quantum Internet 1 <span style="float:right">CC-01</span>		
	10	10:00-11:45	Superconducting Quantum Computers <span style="float:right">CP-02</span>					
	11			10:30-12:10	Quantum Sensors for Life Sciences <span style="float:right">SE-02*</span>			
	12							
	13	12:45-13:55	Photonic Quantum Computers <span style="float:right">CP-03</span>		13:10-16:10	Short Presentations by Young Researchers on SE-01,04,06,07 Topics	13:10-16:10	Short Presentations by Young Researchers on SE-02,05 Topics
	14	14:05-15:15	Young Researcher Session <span style="float:right">CP-04</span>					
	15	15:25-16:35	Quantum Simulations <span style="float:right">CP-05</span>		SE-03A*	SE-03B*	15:00-16:00	Young Researcher Session <span style="float:right">CC-02</span>
	16							
	17	16:45-18:30	Semiconductor Quantum Computers <span style="float:right">CP-06</span>		17:00-18:40	Solid-State Quantum Sensors 2 <span style="float:right">SE-04*</span>	17:00-19:30	Quantum Internet 2 <span style="float:right">CC-03</span>
	18							
	19				19:00-21:10	Quantum Sensors and Quantum Life Sciences <span style="float:right">SE-05*</span>		
	20							
	21						21:00-24:30	Quantum Cryptography (Up-to-date Technologies of Field and Satellite QKDs) <span style="float:right">CC-04**</span>
22								
23								
24								

\*\* SIP(cross-ministerial Strategic Innovation promotion Program)



## Plenary Sessions

All the times in the program are **Japan Standard Time**(GMT+9)

7 Dec (Tue.)	Session / Presentation	Chairperson / Presenter	Affiliation	Abstract PDF
10:00-10:30	Opening			
	Chairperson	Shigeo Koyasu	Executive Director, RIKEN	
	Welcome	Yasunobu Nakamura	General Chair, QI2021 Organizing Committee	
	Welcome	Takayuki Kobayashi	Minister of State for Science and Technology Policy	
	Welcome	Hideyuki Tanaka	State Minister of Education, Culture, Sports, Science and Technology	
	Congratulatory Speech	Keitaro Ohno	Parliamentary Association for Quantum Technology Promotion	
10:30	Break			
10:40-11:50	PL-01. Plenary Talks			
	Chairperson	Yasuhiko Arakawa	The University of Tokyo	
10:40	National Quantum Initiative	Charles Tahan	Assistant Director for QIS and Director of the NQCO, OSTP, White House, US	<a href="#">PL-01-01</a>
10:50	Quantum technology innovation for Society 5.0	Makoto Gonokami	The University of Tokyo /Chair, Quantum Technology Committee, Government of Japan	<a href="#">PL-01-03</a>
11:10	Introduction of quantum business creation consortium Q-STAR	Taro Shimada	Corporate Senior Vice President and Chief Digital Officer, Toshiba Corporation	<a href="#">PL-01-04</a>
11:30	Quantum computer innovation in Japan	Kohei Itoh	President, Keio University	<a href="#">PL-01-05</a>
11:50	Break			
14:00-17:50	PL-02. Keynote Speeches			
	Chairperson	Yasunobu Nakamura	General Chair, QI2021 Organizing Committee	
14:00	Novel directions for advancing satellite based quantum communication	Thomas Jennewein	University of Waterloo	<a href="#">PL-02-01</a>
14:40	Towards an experimental demonstration of surface code quantum error correction	Hartmut Neven	Google	<a href="#">PL-02-02</a>
15:20	Break			
15:50	Transportable optical lattice clocks to test and use gravitational redshift	Hidetoshi Katori	The University of Tokyo	<a href="#">PL-02-03</a>
16:30	Quantum technology with spins	Jörg Wrachtrup	University of Stuttgart	<a href="#">PL-02-04</a>
17:10	Towards a quantum internet: status, challenges and progress	Ronald Hanson	QuTech, Delft University of Technology	<a href="#">PL-02-05</a>
17:50	Closing			

## Quantum Computing Track

All the times in the program are **Japan Standard Time**(GMT+9)

8 Dec (Wed.)	Session / Presentation	Chairperson / Presenter	Affiliation	Abstract PDF
8:00-9:45	CP-01. Quantum Computing with Atoms and Ions			
	Chairperson	Hiroki Takahashi	OIST	
8:00	Exploring frontiers of quantum science using programmable atom arrays	Mikhail Lukin	Harvard U	<a href="#">CP-01-01</a>
8:35	Quantum simulations and algorithms with ion trap systems	Christopher Monroe	Duke U / IonQ	<a href="#">CP-01-02</a>
9:10	High performance commercial trapped ion quantum computers based on the QCCD architecture	Patty Lee	Honeywell	<a href="#">CP-01-03</a>
9:45	Break			
10:00-11:45	CP-02. Superconducting Quantum Computers			
	Chairperson	Jaw-Shen Tsai	RIKEN	
10:00	Challenges and directions of quantum computing with superconducting qubits	Jerry Chow	IBM	<a href="#">CP-02-01</a>
10:35	Exponential suppression of bit or phase flip errors with cyclic error correction	Julian Kelly	Google	<a href="#">CP-02-02</a>
11:10	Two-dimensional array of superconducting qubits with vertical access	Yasunobu Nakamura	RIKEN	<a href="#">CP-02-03</a>
11:45	Break			
12:45-13:55	CP-03. Photonic Quantum Computers			
	Chairperson	Atsushi Noguchi	RIKEN / UTokyo	
12:45	Silicon photonic quantum computing	Pete Shadbolt	PsiQuantum	<a href="#">CP-03-01</a>
13:20	Large-scale fault-tolerant universal quantum computing with quantum teleportation	Akira Furusawa	UTokyo / RIKEN	<a href="#">CP-03-02</a>
13:55	Break			
14:05-15:15	CP-04. Young Researcher Session			
	Chairperson	Erika Kawakami	RIKEN	
14:05	Superconducting quantum- and digital-hybrid computers - tackling of increasing wirings	Yutaka Tabuchi	RIKEN	<a href="#">CP-04-01</a>
14:40	The hybrid quantum circuits with trapped electrons	Atsushi Noguchi	UTokyo	<a href="#">CP-04-02</a>
15:15	Break			
15:25-16:35	CP-05. Quantum Simulations			
	Chairperson	Takeshi Fukuhara	RIKEN	
15:25	Quantum simulation with ytterbium atoms in optical lattices	Shintaro Taie	Kyoto U	<a href="#">CP-05-01</a>
16:00	Ultrafast and ultracold quantum simulator/computer with attosecond precision	Kenji Ohmori	IMS	<a href="#">CP-05-02</a>
16:35	Break			
16:45-18:30	CP-06. Semiconductor Quantum Computers			
	Chairperson	Takahiro Mori	AIST	
16:45	Engineering qubits in silicon with atomic precision	Michelle Simmons	Silicon Quantum Computing	<a href="#">CP-06-01</a>
17:20	Quantum computation - spins inside	Lieven Vandersypen	TU Delft	<a href="#">CP-06-02</a>
17:55	Si platform for spin-based quantum computing	Seigo Tarucha	RIKEN	<a href="#">CP-06-03</a>
18:30	Closing			

## Quantum Computing Track

9 Dec (Thu.)	Session / Presentation	Chairperson / Presenter	Affiliation	Abstract PDF
8:00-8:35	CP-07. Quantum Annealing 1			
	Chairperson	Shu Tanaka	Keio U	
8:00	Next-generation quantum annealing testbed	William Oliver	MIT	<a href="#">CP-07-01</a>
8:35	Break			
8:40-9:15	CP-15. Toward FTQC			
	Chairperson	Yuuki Tokunaga	NTT	
8:40	Toward realization of quantum error correction and fault-tolerant quantum computing	Keisuke Fujii	Osaka U / RIKEN / UTokyo	<a href="#">CP-12-01</a>
9:15	Break			
9:20-10:30	CP-08. Toward FTQC (Tutorial)			
	Chairperson	Keisuke Fujii	Osaka U / RIKEN / UTokyo	
9:20	Fault-tolerance with bosonic qubits	Shruti Puri	Yale U	<a href="#">CP-08-01</a>
9:55	Fault-tolerant quantum computation in with 3D cluster states	Robert Raussendorf	UBC	<a href="#">CP-08-02</a>
10:30	Break			
10:40-12:00	CP-09. Beyond NISQ / Toward FTQC Panel Discussion			
	Chairperson	Masato Koashi	UTokyo	<a href="#">CP-09-01</a>
	Panelists	Shruti Puri	Yale U	
		Robert Raussendorf	UBC	
		Keisuke Fujii	Osaka U	
		Kosuke Fukui	UTokyo	
		Kae Nemoto	NII	
		Yasunari Suzuki	NTT	
		Atsushi Noguchi	UTokyo /RIKEN	
		Yutaka Tabuchi	RIKEN	
12:00	Break			
13:00-14:10	CP-10. Quantum Algorithms (Long-term)			
	Chairperson	Hiroshi Imai	UTokyo	
13:00	Provably accurate simulation of gauge theories and bosonic systems	Yuan Su	Google	<a href="#">CP-10-01</a>
13:35	Quantum algorithms for large-scale problems	François Le Gall	Nagoya U	<a href="#">CP-10-02</a>
14:10	Break			
14:20-15:30	CP-11. NISQ Algorithms			
	Chairperson	Seiichiro Tani	NTT	
14:20	Promises and challenges of variational quantum algorithms	Patrick Coles	LANL	<a href="#">CP-11-01</a>
14:55	Development of quantum machine learning algorithms and experimental realization	Kosuke Mitarai	Osaka U	<a href="#">CP-11-02</a>
15:30	Break			
15:35-16:10	CP-12. Quantum Annealing 2			
	Chairperson	Shu Tanaka	Keio U	
15:35	Algorithmic breakeven in quantum annealing	Daniel Lidar	USC	<a href="#">CP-07-02</a>
16:10	Break			
16:20-17:30	CP-13. Quantum Algorithms for Chemistry			
	Chairperson	Wataru Mizukami	Osaka U	
16:20	Break down the high-order tensors of quantum chemistry, for O(N)-depth circuit algorithm	Yuki Kurashige	Kyoto U	<a href="#">CP-13-01</a>
16:55	Quantum computing for chemistry	Markus Reiher	ETH Zurich	<a href="#">CP-13-02</a>
17:30	Break			
17:35-18:10	CP-14. Quantum Annealing 3			
	Chairperson	Shu Tanaka	Keio U	
17:35	Improving adiabatic quantum computing with non-adiabatic methods	Wolfgang Lechner	U Innsbruck	<a href="#">CP-14-01</a>
18:10	Closing			

## Quantum Cryptography & Communication Track

All the times in the program are **Japan Standard Time(GMT+9)**

8 Dec (Wed.)	Session / Presentation	Chairperson / Presenter	Affiliation	Abstract PDF
9:00 - 11:00	CC-01. Quantum Internet 1			
	Chairperson	Kae Nemoto	NII	
9:00 - 9:30	Bringing QKD to real-world digital infrastructures	Michele Mosca	U Waterloo	<a href="#">CC-01-01</a>
9:30 - 10:00	Quantum controlled routers and quantum data centers	Liang Jiang	U Chicago	<a href="#">CC-01-02</a>
10:00 - 10:30	Ion-photon interface for quantum networks	Hiroki Takahashi	OIST	<a href="#">CC-01-03</a>
10:30 - 11:00	Designing tomorrow's quantum internet	William Munro	NTT	<a href="#">CC-01-04</a>
11:00	Break			
15:00-16:00	CC-02. Young Researcher Session			
	Chairperson	Rodney Van Meter	Keio U	
	Facilitator	Mariko Kobayashi	Mercari	
	Panelist	Shota Nagayama	Mercari	
	Panelist	Wojciech Kozlowski	TU Delft	
	Panelist	Toshihiko Sasaki	UTokyo	
	Panelist	Tomoyuki Horikiri	YNU	
16:00	Break			
17:00-20:00	CC-03. Quantum Internet 2			
	Chairperson	Koji Azuma	NTT	
17:00 - 17:30	Quantum Internet: from classical to quantum paths	Angela Cacciapuoti	U Naples Federico II	<a href="#">CC-03-01</a>
17:30 - 18:00	Software and protocol stacks for quantum networks	Wojciech Kozlowski	TU Delft	<a href="#">CC-03-02</a>
18:00 - 18:30	Genuine and optimized entanglement-based quantum networks	Wolfgang Duer	U Innsbruck	<a href="#">CC-03-03</a>
18:30 - 19:00	Quantum physical unclonable functions and their comprehensive cryptanalysis	Elham Kashefi	U Edinburgh / CNRS Sorbonne U	<a href="#">CC-03-04</a>
19:00- 19:30	Entanglement based quantum networking	Siddarth Joshi	U Bristol	<a href="#">CC-03-05</a>
19:30	Break			
21:00-24:30	CC-04. Quantum Cryptography (Up-to-date Technologies of Field and Satellite QKDs) [SIP(cross-ministerial Strategic Innovation promotion Program)]			
	Chairperson	Masahiro Takeoka	Keio U	
21:00	Opening Remarks	Hideyuki Tokuda	NICT	<a href="#">CC-04-01</a>
21:05	OpenQKD use-case demonstrations in Europe	Andreas Poppe	AIT	<a href="#">CC-04-02</a>
21:35	Lessons from the SpooQy-1 satellite	Alexander Ling	NUS	<a href="#">CC-04-03</a>
22:05	High-level concepts and design of commercial satellite-based QKD networks	Manuel Erhard	qtlabs	<a href="#">CC-04-04</a>
22:35	Break			
23:00	Quantum networking research at Los Alamos	Raymond Newell	LANL	<a href="#">CC-04-05</a>
23:30	Fundamentally applied quantum communication	Rob Thew	U Geneva	<a href="#">CC-04-06</a>
24:00	Finite-key security of continuous-variable quantum key distribution	Masato Koashi	UTokyo	<a href="#">CC-04-07</a>
24:30	Closing			

9 Dec (Thu.)	Session / Presentation	Chairperson / Presenter	Affiliation	Abstract PDF
21:00-22:30	CC-05. Challenges for Quantum Technology Platform (QKD Networks, Satellite QKD and Their Integration) [SIP(cross-ministerial Strategic Innovation promotion Program)]			
	Chairperson	Kaoru Kenyoshi	NICT	
21:00	Overview of Japanese project "SIP" and quantum secure cloud technologies	Masahide Sasaki	NICT	<a href="#">CC-05-01</a>
21:15	Secure information society using "Quantum Secure Cloud"	Mikio Fujiwara	NICT	<a href="#">CC-05-02</a>
21:30	Quantum key distribution research and development in NEC	Junich Funada	NEC	<a href="#">CC-05-03</a>
21:45	QKD R&D and field trials in Toshiba	Yoshimichi Tanizawa	Toshiba	<a href="#">CC-05-04</a>
22:00	Quantum communication activities in Canada	Norbert Lütkenhaus	U Waterloo	<a href="#">CC-05-06</a>
22:30	Break			
23:00-24:30	CC-06. Industry Panel Session[SIP(cross-ministerial Strategic Innovation promotion Program)]			
	Chairperson	Masahide Sasaki	NICT	
		Andrew Lord	BT	
		David Williams	ArQIT	
		Diego Lopez	Telephonica	
		Hyung-Soo (Hans) Kim	KT	
		Venkat Josyula	Verizon	
24:30	Closing			

## Quantum Sensing Track

All the times in the program are **Japan Standard Time(GMT+9)**

**8th Dec Sessions are a joint-program with The 4th IFQMS (The 4th International Forum on Quantum Metrology and Sensing).**

8 Dec (Wed.)	Session / Presentation	Chairperson / Presenter	Affiliation	Abstract PDF
8:00-10:10	SE-01. Solid-State Quantum Sensors 1 [4th IFQMS]			
	Chairperson	Takeshi Ohshima	QST	
8:00	Quantum sensing of quantum materials using NV center microscopy	Amir Yacoby	Harvard U	<a href="#">SE-01-01</a>
8:40	Current status and prospects of solid-state quantum sensors for Quantum-LEAP	Mutsuko Hatano	Tokyo Tech	<a href="#">SE-01-02</a>
9:10	Nanoscale vector AC magnetometry with a single nitrogen-vacancy center in diamond	Paola Cappellaro	MIT	<a href="#">SE-01-03</a>
9:40	Planetary magnetic field sensing via electrical readout of quantum centers in SiC	Corey Cochrane	JPL Caltech	<a href="#">SE-01-04</a>
10:10	Break			
10:30-12:10	SE-02. Quantum Sensors for Life Sciences [4th IFQMS]			
	Chairperson	Hiroshi Yukawa/Kensuke Osada	QST	
10:30	Production of color centers in nanodiamond	Olga Shenderova	Adámas Nanotechnologies	<a href="#">SE-02-01</a>
11:10	Nitrogen-vacancy centers in nanodiamonds as temperature sensors and immunoassay reporters	Huan-Cheng Chang	Academia Sinica	<a href="#">SE-02-02</a>
11:40	Treatment responses to immune checkpoint inhibitor therapy evaluated by MRI	Shun Kishimoto	NIH	<a href="#">SE-02-03</a>
12:10	Break			
13:10-16:10	SE-03A. Short Presentations by Young Researchers on SE-01, 04, 06, 07 Topics [4th IFQMS]			<a href="#">SE-03A</a>
	Break-out Sessions			
13:10-16:10	SE-03B. Short Presentations by Young Researchers on SE-02, 05 Topics [4th IFQMS]			<a href="#">SE-03B</a>
16:10	Break			
17:00-18:40	SE-04. Solid-State Quantum Sensors 2 [4th IFQMS]			
	Chairperson	Takayuki Iwasaki	Tokyo Tech	
17:00	Quantum sensing enabled by spin qubits in diamond	Fedor Jelezko	Ulm U	<a href="#">SE-04-01</a>
17:40	Programmable quantum simulators based on spins in diamond	Tim Taminiu	TU Delft	<a href="#">SE-04-02</a>
18:10	Development and optimisation of diamond for quantum technologies	Matthew Markham	Element Six	<a href="#">SE-04-03</a>
18:40	Break			
19:00-21:10	SE-05. Quantum Sensors and Quantum Life Sciences [4th IFQMS]			
	Chairperson	Ryuji Igarashi	QST	
19:00	Quantum biology: an Introduction	Johnjoe McFadden	U Surrey	<a href="#">SE-05-01</a>
19:40	Avian magnetoreception – a radical sense of direction	Peter Hore	U Oxford	<a href="#">SE-05-02</a>
20:10	Surface chemistry of diamond for quantum applications	Anke Krüger	U Stuttgart	<a href="#">SE-05-03</a>
20:40	Diamond-based quantum sensors: technology and applications in physics and biology	Christian Degen	ETH Zurich	<a href="#">SE-05-04</a>
21:10	Closing			

9 Dec (Thu.)	Session / Presentation	Chairperson / Presenter	Affiliation	Abstract PDF
9:20-12:00	SE-06. Atom Interferometers			
	Chairperson	Takashi Mukaiyama	Osaka U	
9:20	Tests of quantum mechanics and gravity with atom interferometry	Mark Kasevich	Stanford U	<a href="#">SE-06-01</a>
10:00	Classical and quantum sensing for precise inertial navigation	Mikio Kozuma	Tokyo Tech	<a href="#">SE-06-02</a>
10:40	Rotation sensing with the BIGTOP gyroscope	Cass Sackett	U Virginia	<a href="#">SE-06-03</a>
11:20	Development of transportable atomic gravimeters for field applications	Ken'ichi Nakagawa	UEC	<a href="#">SE-06-04</a>
12:00	Break			
17:00-19:40	SE-07. Atom/Ion Clocks			
	Chairperson	Masao Takamoto	RIKEN	
17:00	A Lu+ optical clock	Murray Barrett	NUS	<a href="#">SE-07-01</a>
17:40	Optical clocks based on multi-ion systems	Kazuhiro Hayasaka	NICT	<a href="#">SE-07-02</a>
18:20	Strontium lattice clocks at PTB: transportable and in the lab	Christian Lisdat	PTB	<a href="#">SE-07-03</a>
19:00	Lattice clock as a frequency standard for JST and UTC	Tetsuya Ido	NICT	<a href="#">SE-07-04</a>
19:40	Closing			

## Quantum Sensing Track : Short Presentations by Young Researchers

### SE-03A. Short Presentations by Young Researchers on SE-01, 04, 06, 07 Topics [4th IFQMS]

\*Note: Depending on the program, the order of presentations may change within the same group.  
All the times in the program are **Japan Standard Time**(GMT+9)

8 Dec (Wed.)	Session / Presentation	Mentor / Presenter	Affiliation	Abstract PDF
13:10-16:10	SE-03A. Short Presentations by Young Researchers on SE-01, 04, 06, 07 Topics [4th IFQMS]			
	Break-out Sessions			
13:10-14:30	<b>SE-03A-α1</b>			
	Mentor	Fedor Jelezko	Ulm U	
	Mentor	Takeshi Ohshima	QST	
	Mentor	Masaki Sekino	U Tokyo	
	Mentor	Takayuki Iwasaki	Tokyo Tech	
	Chair	Motofumi Fushimi	U Tokyo	
	Co-chair	Chikara Shinei	NIMS	
	Exploring NV center formation condition for high Econv and charge-state ratio of NV- and NV0 centers	Chikara Shinei	NIMS	SE-03A-α1-01
	Sensitive atomic magnetometer beyond the standard quantum limit	Kosuke Shibata	Gakushuin U	SE-03A-α1-02
	Imaging hydrodynamic flow in WTe <sub>2</sub> using cryogenic quantum magnetometry	Uri Vool	Harvard U	SE-03A-α1-03
	Toward on-board magnetoencephalography with wearable magnetometers and active noise canceler	Xinyu Cao	U Tokyo	SE-03A-α1-04
	Continuous-wave temperature sensing using RF-dressed states of nitrogen-vacancy centers in diamond	Hibiki Tabuchi	Keio U	SE-03A-α1-05
	High-quality lead-vacancy centers in diamond by high-pressure and high-temperature annealing	Peng Wang	Tokyo Tech	SE-03A-α1-06
	Magnetocardiography imaging of living rats using NV centers in Diamond	Ryoma Matsuki	Tokyo Tech	SE-03A-α1-07
13:10-14:30	<b>SE-03A-β1</b>			
	Mentor	Satoshi Yamasaki	Kanazawa U	
	Mentor	Tokuyuki Teraji	NIMS	
	Mentor	Toshiharu Makino	AIST	
	Mentor	Akimichi Nakazono	YAZAKI	
	Chair	Hiroki Morishita	Kyoto U	
	Co-chair	Moriyoshi Haruyama	AIST	
	Probing correlated phenomena in 2D materials with diamond quantum sensors	Mark Ku	U Delaware	SE-03A-β1-01
	Electroluminescence observation of NV center in diamond lateral p-i-n diode	Moriyoshi Haruyama	AIST	SE-03A-β1-02
	Synthesis of HPHT diamond with controlled nitrogen concentration	Masashi Miyakawa	NIMS	SE-03A-β1-03
	Formation of diamond film containing perfectly aligned NV center ensembles at a high growth rate by high-power density plasma CVD	Takeyuki Tsuji	Tokyo Tech	SE-03A-β1-04
	High dynamic range current detection using a diamond quantum sensor	Yuta Shigenobu	Tokyo Tech	SE-03A-β1-05
	Vector DC magnetic field sensing with the reference microwave field using nitrogen vacancy centers in diamond	Takuya Isogawa	Keio U	SE-03A-β1-06
	Thermal effects on generation of spin defects in hexagonal boron nitride	Tetta Suzuki	Saitama U / QST	SE-03A-β1-07
13:10-14:30	<b>SE-03A-γ1</b>			
	Mentor	Keiichi Edamatsu	Tohoku U	
	Mentor	Ryosuke Shimizu	UEC	
	Mentor	Hirohisa Terai	NICT	
	Mentor	Ryo Okamoto	Kyoto U	
	Chair	Fumihiko China	NICT	
	Co-chair	Le Bin Ho	Tohoku U	
	Error-disturbance uncertainty relations in faraday measurements	Le Bin Ho	Tohoku U	SE-03A-γ1-01
	Hydrogen annealing effect on silicon optical waveguide	Yixin Wang	Tohoku U	SE-03A-γ1-02
	Wavelength-tunable broadband infrared quantum absorption spectroscopy in the mid-infrared region 2-5 μm	Masaya Arahata	Kyoto U	SE-03A-γ1-03
	Evaluation of superconducting nanowire single photon detectors for mid-infrared wavelengths	Yuki Gama	Kyoto U	SE-03A-γ1-04

Dec (Wed.)	Session / Presentation	Mentor / Presenter	Affiliation	Abstract PDF
	Phase retrieval of joint spectral amplitude	Kemeng Chen	UEC	<a href="#">SE-03A-y1-05</a>
	Temporal shaping of an entangled-photon wave packet by fourier optical synthesis	Hiroki Oshima	UEC	<a href="#">SE-03A-y1-06</a>
13:10-14:30	<b>SE-03A-δ1</b>			
	Mentor	Takuya Hirano	Gakushuin U	
	Mentor	Takashi Mukaiyama	Osaka U	
	Mentor	Masaki Ando	U Tokyo	
	Mentor	Tadashi Sakai	Tokyo Tech	
	Chair	Kiyotaka Aikawa	Tokyo Tech	
	Co-chair	Satoru Takano	U Tokyo	
	Cryogenic monolithic interferometer for sensing gravity gradient	Satoru Takano	U Tokyo	<a href="#">SE-03A-δ1-01</a>
	Suspension noise measurements of cryogenic torsion pendulums with crystalline fibrifibres	Ching Pin Ooi	U Tokyo	<a href="#">SE-03A-δ1-02</a>
	Angular sensor with a coupled cavity for gravity gradient sensing	Yuka Oshima	U Tokyo	<a href="#">SE-03A-δ1-03</a>
	Towards sensitive accelerometers with levitated single nanoparticles	Kiyotaka Aikawa	Tokyo Tech	<a href="#">SE-03A-δ1-04</a>
	Interferometric gyroscope using slow and continuous atomic beam	Tomoya Sato	Tokyo Tech	<a href="#">SE-03A-δ1-05</a>
	Development of a quantum gyroscope based on a single ion trapping techniques	Ryoichi Saito	Osaka U	<a href="#">SE-03A-δ1-06</a>
	Exponentially enhanced quantum metrology by quenching superradiant light-matter systems beyond the critical point	Karol Gietka	OIST	<a href="#">SE-03A-δ1-07</a>
14:50-16:10	<b>SE-03A-α2</b>			
	Mentor	Fedor Jelezko	Ulm U	
	Mentor	Takeshi Ohshima	QST	
	Mentor	Masaki Sekino	U Tokyo	
	Mentor	Takayuki Iwasaki	Tokyo Tech	
	Chair	Chikara Shinei	NIMS	
	Co-chair	Motofumi Fushimi	U Tokyo	
	Three-layered magnetically shielded room for ultrahigh-sensitivity quantum sensing of biomagnetic signals	Motofumi Fushimi	U Tokyo	<a href="#">SE-03A-α2-01</a>
	Super-resolution in nanoscale NMR	Nicolas Staudenmaier	Ulm U	<a href="#">SE-03A-α2-02</a>
	Sensitivity of weight imaging using a hybrid system based on piezoactive magnetic material and diamond quantum sensor	Ryota Kitagawa	Tokyo Tech	<a href="#">SE-03A-α2-03</a>
	Study on electron spin control method for high-sensitivity diamond quantum sensor	Hiroyoshi Tomioka	Tokyo Tech	<a href="#">SE-03A-α2-04</a>
	Optically detected magnetic resonance spectra of silicon vacancies in 4H-SiC with different temperatures	Shu Motoki	QST / Saitama U	<a href="#">SE-03A-α2-05</a>
	High efficiency formation of NV center inside diamond by femtosecond laser	Ryusei Yanoshita	Kyoto U	<a href="#">SE-03A-α2-06</a>
14:50-16:10	<b>SE-03A-β2</b>			
	Mentor	Satoshi Yamasaki	Kanazawa U	
	Mentor	Tokuyuki Teraji	NIMS	
	Mentor	Toshiharu Makino	AIST	
	Mentor	Akimichi Nakazono	YAZAKI	
	Chair	Moriyoshi Haruyama	AIST	
	Co-chair	Hiroki Morishita	Kyoto U	
	AC magnetic field sensing with ensemble NV centers using electrical detection methods	Hiroki Morishita	Kyoto U	<a href="#">SE-03A-β2-01</a>
	OPuS-MAGNM - miniaturized optically pumped solid state quantum magnetometers for space applications	Hannes Kraus	NASA	<a href="#">SE-03A-β2-02</a>
	Development of phthalocyanine ion beam for creation of multiple NV centers.	Kosuke Kimura	QST, Gunma U	<a href="#">SE-03A-β2-03</a>

Dec (Wed.)	Session / Presentation	Mentor / Presenter	Affiliation	Abstract ID
	Fabrication of diamond protective film using microwave plasma CVD towards high-quality quantum emitters	Kazuki Hirokawa	Tokyo Tech	<b>SE-03A-β2-04</b>
	A compact quantum sensor head with side excitation of CVD diamond	Yuki Nishio	Tokyo Tech	<b>SE-03A-β2-05</b>
	Hybrid integration of Si <sub>3</sub> N <sub>4</sub> grating structure on diamond NV substrate for efficient photon extraction	Ryota Katsumi	Toyohashi Tech	<b>SE-03A-β2-06</b>
14:50-16:10	<b>SE-03A-γ2</b>			
	Mentor	Keiichi Edamatsu	Tohoku U	
	Mentor	Kenichi Nakagawa	UEC	
	Mentor	Ryosuke Shimizu	UEC	
	Mentor	Hiroataka Terai	NICT	
	Chair	Le Bin Ho	Tohoku U	
	Co-chair	Fumihiko China	NICT	
	Superconducting nanostrip single-photon detectors with dielectric multilayer cavities	Fumihiko China	NICT	<b>SE-03A-γ2-01</b>
	Estimation of the quantum efficiency of the up-conversion system based on injection-locked dual oscillators	Masayuki Hojo	Kyoto U	<b>SE-03A-γ2-02</b>
	Selective measurement of biexciton luminescence by photon correlation spectroscopy	Hiroya Seki	UEC	<b>SE-03A-γ2-03</b>
	Towards optical manipulation of gold-nanoparticles for efficient single photon sources	Rui Sun	Tohoku U	<b>SE-03A-γ2-04</b>
	Single photon emission from a quantum-dot-gold-nanostar coupled sYining Xuan	Yining Xuan	Tohoku U	<b>SE-03A-γ2-05</b>
	Focusing constraints on coupling efficiency of collinear type-I degenerated SPDC photon pairs into a single-mode fiber	Nicolas Schwaller	Kyoto U	<b>SE-03A-γ2-06</b>

## Quantum Sensing Track : Short Presentations by Young Researchers

### SE-03B. Short Presentations by Young Researchers on SE-02, 05 Topics [4th IFQMS]

\*Note: Depending on the program, the order of presentations may change within the same group.  
All the times in the program are **Japan Standard Time(GMT+9)**

8 Dec (Wed.)	Session / Presentation	Mentor / Presenter	Affiliation	Abstract ID
13:10-16:10	SE-03B. Short Presentations by Young Researchers on SE-02, 05 Topics [4th IFQMS]			
	<b>SE-03B-01</b>			
	Mentor	Johnjoe McFadden	U Surrey	
	Mentor	Tanaka Shigenori	Kobe U	
	Mentor	Maeda Kiminori	Saitama U	
	Chair	Yahata Noriaki	QST	
	Co-chair	Yokoya Akinari	QST	
	Intracellular thermal conductivity determined by dual-functionalized diamond nanosensor	Suzuki Madoka	Osaka U	SE-03B-01-01
	Label-free analysis of diffusion constant in lipid bilayers using nanoscale diamond magnetometry	Ishiwata Hitoshi	QST	SE-03B-01-02
	Temperature sensing using silicon vacancy centers in detonation nanodiamonds	Fujiwara Masanori	Kyoto U	SE-03B-01-03
	Quantum-inspired machine learning for exponentially big neural data analysis	Majima Kei	QST	SE-03B-01-04
	Empirical verification of the violation of the temporal Bell inequality in bistable perception	Aizawa Yasunori	QST	SE-03B-01-05
	Tracking radiation damage induction pathway following core-hole creation of DNA molecules in aqueous solution	Kumagai Yoshiaki	TUAT	SE-03B-01-06
13:10-14:30	<b>SE-03B-02</b>			
	Mentor	Peter Hore	U Oxford	
	Mentor	Ishizaki Akihito	IMS	
	Mentor	Shigeta Yasuteru	U Tsukuba	
	Chair	Takakusagi Yoichi	QST	
	Co-chair	Imaoka Tatsuhiko	QST	
	High-resolution structure of an electron-transfer protein by neutron crystallography	Hanazono Yuya	TMDU	SE-03B-02-01
	Fabrication of a quantum sensor to reveal a topic in thermal physiology	Ishii Shuya	QST	SE-03B-02-02
	Investigation of irradiation induced nitrogen-vacancy centers in 5-nanometer-sized detonation nanodiamonds	So Kit	Kyoto U	SE-03B-02-03
	Formation of flavin anion and tyrosine radicals in avian Cryptochrome4	Otsuka Hiroaki	Waseda U	SE-03B-02-04
	Do neural activities of binocular rivalry follow a quantum probability model? A test of temporal Bell inequalities	Hirao Takahiro	QST	SE-03B-02-05
	X-ray absorption spectroscopy of a silicon phthalocyanine derivative, IR700, for X-ray excited photoimmunotherapy	Izumi Yudai	QST	SE-03B-02-06
	Magnetically sensitive radical pairs in avian cryptochrome 4 proteins	Xu Jingjing	U Oldenburg	SE-03B-02-07

# Abstract

Tracks

## PL

### Plenary Sessions

Contents / Topics

Welcome from Organizing Committee and Hosting Ministries, Plenary Talks, Keynote Speeches

Tracks

## CP

### Quantum Computing Track

Contents / Topics

Quantum Computing with Atoms and Ions, Superconducting Quantum Computers(QC), Photonic QC, Young Researcher Session, Quantum Simulations, Semiconductor QC, Quantum Annealing Toward FTQC(Tutorial), Beyond NISQ/Toward FTQC Panel Discussion, Quantum Architecture, Quantum Algorithms, NISQ Algorithms, Quantum Algorithms for Chemistry

Tracks

## CC

### Quantum Cryptography & Communication Track

Contents / Topics

Quantum Internet, Quantum Cryptography(Up-to-date Technologies of Field and Satellite QKDs), Challenges for Quantum Technology Platform (QKD Networks, Satellite QKD and their integration), Industry Panel, Young Researcher Session  
\*\*CC-04 on 8th and CC-05, CC-06 on 9th Dec are supported by SIP (cross-ministerial Strategic Innovation promotion Program).

Tracks

## SE

### Quantum Sensing Track

Contents / Topics

Solid-State Quantum Sensors, Quantum Sensors for Life Sciences, Quantum Sensors and Quantum Life Sciences, Atom Interferometer, Cold Atom, Atomic/Ion Clocks, Short Presentations by Young Researchers  
\*8th Dec Sessions are a joint-program with The 4th IFQMS (The 4th International Forum on Quantum Metrology and Sensing).

## Quantum technology innovation for Society 5.0

**Makoto Gonokami**

*Graduate School of Science, the University of Tokyo, Japan*

---

### Abstract

We are facing major global challenges such as global warming and pandemic. Both are caused by human behavior, and cross-border cooperation is essential. Appropriate use of data in cyberspace to encourage behavioral change is the key to solutions.

With recent DX, the integration of the real world and cyberspace is accelerating. Digital technologies connect people in remote places, and reduce disparities across age, ability, gender, race, or location. In Japan, all sectors including the government, industry and academia are working together to realize this ideal future, which we call Society 5.0. In order to realize Society 5.0, it is crucial to secure trust in the cyberspace.

Nature is driven by physical, chemical, and biological mechanisms, but humanity has not yet fully unveiled and utilized them. Emerging quantum technology is one of them, and the unused principles of quantum mechanics are about to be utilized. We should continue basic research to expand our wisdom. Fostering next generation is further important. Under this situation, I believe the role of the academia that have diverse knowledge is becoming more and more important. The daily collaboration among top scientists transcending countries is indispensable.

---

PL-01-04

## **Introduction of quantum business creation consortium Q-STAR**

**Taro Shimada**

*Toshiba SVP Chief Digital Officer*

---

### **Abstract**

2021 was year of Quantum Business Consortium around world. In Europe and Asia many countries and relation started Business creation Consortium. In Japan 9/1/2021 Q-STAR was formed. This consortium started with already 24 member leading companies and ventures, but expands in rapidly. At this session mission and scope and ambition of Q-STAR will be explained. Also how it' s fit to existing organization and accelerate entire Quantum activity in Japan towards Quantum Transformation namely QX.

PL-01-05

## Quantum computer innovation in Japan

**Kohei Itoh**

*Keio University*

---

### **Abstract**

Quantum technology is expected to advance the basis of entire current information technology. This talk overview a variety of research and development in Japan towards realization of useful quantum computers.

PL-02-01

## **Novel directions for advancing satellite based quantum communication**

**Thomas Jennewein**

*Institute for Quantum Computing, University of Waterloo, Canada*

---

### **Abstract**

Extending today' s internet, the Quantum Internet will readily transfer quantum bits, rather than classical bits, between users near and far and over multiple different channels and could be used for secure communications, quantum computer networks and metrological applications. I will discuss recent advances on implementations and tools useful for generating and distributing photonic quantum entanglement over large distances using satellites. I will present some recent research on quantum channel advancements including time-bin encoding, reference-frame-free protocols and single-photon emitters. I will also present an overview of the upcoming Canadian quantum communication satellite QEYSSAT.

## Towards an experimental demonstration of surface code quantum error correction

Hartmut Neven

*Google*

---

### Abstract

The Quantum AI team is working on experimentally demonstrating that surface code error correction reduces the logical error rate as one moves from smaller to larger grids of data qubits. To achieve this multiple sources of error have to be reduced simultaneously. Besides 1- and 2-qubit gate errors and readout errors, idling errors, crosstalk and leakage need to be addressed. While making progress on our roadmap towards an error corrected quantum computer we are also designing quantum algorithms for our current processors with the goal to compute scientifically or commercially interesting quantities beyond the reach of classical computers. This presentation will describe circuits to i) compute out-of-time-order correlators, ii) study the properties of a realization of time crystals and iii) implement a quantum machine learning algorithm that achieves exponentially reduced sample complexity as compared to classical machine learning techniques.

## Transportable optical lattice clocks to test and use gravitational redshift

**Hidetoshi Katori**

*Department of Applied Physics, Graduate School of Engineering, The University of Tokyo, Bunkyo-ku, Tokyo 113-8656, Japan.*

---

### Abstract

Clocks are devices to share time using ubiquitous oscillatory phenomena in nature. We once relied on astronomical observations, and today we use far regular oscillations of cesium atoms to define the international system of unit (SI) for time, i.e., the SI second. Recent optical atomic clocks have demonstrated more than 100-fold improvement over cesium clocks, leading to a redefinition of the second in the future. This extreme precision, in turn, allows clocks to investigate relativistic spacetime curved by gravity, where clocks serve as gravitational potential sensors. Roles of the clocks are rapidly changing from those supposed previously.

An “optical lattice clock” proposed in 2001 benefits from a low quantum-projection noise by simultaneously interrogating a large number of atoms trapped in optical lattices. About a thousand atoms enable such clocks to achieve  $10^{-18}$  instability in a few hours of operation. This superb stability is especially suitable for relativistic geodesy, where gravitational redshift between the clocks resolves a centimeter height differences.

We overview the progress of optical lattice clocks and address recent topics including 1) transportable optical clocks operated at a broadcasting tower, TOKYO SKYTREE, to test gravitational redshift and 2) an on-vehicle optical clock and its applications.

## Quantum technology with spins

**Jörg Wrachtrup**

*3rd Institute of Physics, Centre for Applied Quantum Technologies  
and IQST, University of Stuttgart, Germany*

---

### Abstract

Spins in wide band gap semiconductors are a leading contender in various areas of quantum technology. Most notably they have been established as a novel tool for nanoscale sensing, major hardware for long distance quantum entanglement, as well as small scale quantum registers for quantum computing. I will present the use of spins in in those areas [1,2,3]. Specifically, I will discuss quantum sensing with spins to investigate magnetism in 2D materials including the investigation domain patterns [4] and Moiré structures in twisted 2D layers. Here the nitrogen vacancy center in diamond is used to probe and image electronic magnetism in mono- and multilayers of materials like CrBr<sub>3</sub>. By using dedicated measurements strategies based on quantum algorithms one can enhance the performance of those quantum sensors to achieve better signal quality and improve the spectral resolution in those measurements. [5].

- [1] T. Oeckinghaus et al., Nano Lett. 20, 463 (2020)
- [2] N. Morioka et al. Nature Com. 2516 (2020)
- [3] N. Chejanovsky et al. Nature Mat. 20, 1079 (2021)
- [4] Qi-Chao Sun et al. Nature Com. 12, 1989 (2021)
- [5] V. Vorobyov et al., arxiv2104.04507.(2021)

## **Towards a quantum internet: status, challenges and progress**

**Ronald Hanson**

*QuTech, Delft University of Technology, The Netherlands*

---

### **Abstract**

Future quantum networks [1] may harness the unique features of entanglement in a range of exciting applications such as blind quantum computation in the cloud, secure communication and enhanced metrology. To fulfill these promises, a strong worldwide effort is ongoing to gain precise control over the full quantum dynamics of multi-particle nodes and to wire them up using quantum-photon channels.

Here I will briefly introduce the field of entanglement-based quantum networks and discuss some of the current status and challenges. I will then give an overview of our latest work on the realization of a multi-node network in the lab including first protocols and teleportation [2,3], on increasing the distance between nodes to metropolitan scales, on development of next-generation devices with improved quantum spin-photon interfaces, and on the development of a quantum network control stack.

[1] Quantum internet: A vision for the road ahead, S.D.C. Wehner, D. Elkouss, R. Hanson, *Science* 362, eaam9288 (2018).

[2] Realization of a multi-node quantum network of remote solid-state qubits, M. Pompili, S.L.N. Hermans, S. Baier et al., *Science* 372, 259 (2021)

[3] Qubit teleportation between non-neighboring nodes in a quantum network, S.L.N. Hermans, M. Pompili et al., arXiv:2110.11373 (2021).

# Abstract

Tracks

## PL

### Plenary Sessions

Contents / Topics

Welcome from Organizing Committee and Hosting Ministries, Plenary Talks, Keynote Speeches

Tracks

## CP

### Quantum Computing Track

Contents / Topics

Quantum Computing with Atoms and Ions, Superconducting Quantum Computers(QC), Photonic QC, Young Researcher Session, Quantum Simulations, Semiconductor QC, Quantum Annealing Toward FTQC(Tutorial), Beyond NISQ/Toward FTQC Panel Discussion, Quantum Architecture, Quantum Algorithms, NISQ Algorithms, Quantum Algorithms for Chemistry

Tracks

## CC

### Quantum Cryptography & Communication Track

Contents / Topics

Quantum Internet, Quantum Cryptography(Up-to-date Technologies of Field and Satellite QKDs), Challenges for Quantum Technology Platform (QKD Networks, Satellite QKD and their integration), Industry Panel, Young Researcher Session  
\*\*CC-04 on 8th and CC-05, CC-06 on 9th Dec are supported by SIP (cross-ministerial Strategic Innovation promotion Program).

Tracks

## SE

### Quantum Sensing Track

Contents / Topics

Solid-State Quantum Sensors, Quantum Sensors for Life Sciences, Quantum Sensors and Quantum Life Sciences, Atom Interferometer, Cold Atom, Atomic/Ion Clocks, Short Presentations by Young Researchers  
\*8th Dec Sessions are a joint-program with The 4th IFQMS (The 4th International Forum on Quantum Metrology and Sensing).

## Exploring frontiers of quantum science using programmable atom arrays

**Mikhail Lukin**

*Department of Physics, Harvard University, United States*

---

### Abstract

We will discuss the recent advances involving programmable, coherent manipulation of quantum many-body systems using neutral atom arrays excited into Rydberg states, allowing the control over 200 qubits in two-dimensional arrays. Recent results involving the realization of exotic phases of matter, study of quantum phase transitions and exploration of their non-equilibrium dynamics will be presented. In particular, we will report realization and probing of quantum spin liquid states - the exotic states of matter have thus far evaded direct experimental detection. Finally, most recent progress involving testing quantum optimization algorithms and realization of novel architecture based on dynamically reconfigurable entanglement will be described. Prospects for scaling up these techniques, including realization of large-scale quantum processors and quantum simulators will be discussed.

## Quantum simulations and algorithms with ion trap systems

**Christopher Monroe**

*Duke University Depts of ECE and Physics and IonQ, Inc.*

---

### Abstract

Laser-cooled trapped atomic ions are well-established as possessing the highest performance of any platform for quantum computing. But as importantly, the path to scaling trapped ion quantum computers involves well-defined architectural plans, from shuttling ions between quantum processor unit (QPU) cores and modular photonic interconnects between multiple QPUs to gradual error-correction strategies. Full-stack ion trap quantum computers have thus moved away from the physics of qubits and gates and toward the engineering of optical control signals, quantum gate compilation for algorithms, and high level system design considerations. I will summarize the state-of-the-art in these quantum computers, covering recent algorithms and quantum simulations of physical processes, and speculate on how they might be used in the future.

---

## High performance commercial trapped ion quantum computers based on the QCCD architecture

**Patty Lee**

*Honeywell Quantum Solutions*

---

### Abstract

Honeywell Quantum Solutions launched its first commercial trapped-ion quantum computer in 2020, designed around the quantum charge-coupled device (QCCD) architecture. By applying fast transport operations to reorder and position ion qubits across multiple trapping zones simultaneously on the device, the QCCD architecture creates a fully-connected, high fidelity, and scalable quantum computer. These systems offer the unique capability of performing conditional quantum operations dependent on mid-circuit measurement outcomes, and qubits can be re-used in the same circuit after measurements. This feature allows users to perform efficient quantum simulations and execute repeated cycles of quantum error correction, which was demonstrated for the first time on System Model H1. Recently, the system became the first quantum computer to pass the quantum volume 1024 benchmark, the largest quantum volume ever measured on a commercial quantum computer. Future generation systems will incorporate new technologies such as 2D trap architectures and integrated photonics, in order to scale the number of physical qubits and further increase system performance.

## Challenges and directions of quantum computing with superconducting qubits

**Jerry Chow**

*IBM Quantum*

---

### Abstract

The field of quantum computing has evolved into a large interdisciplinary community that includes experts from all domains including industry, government, and academia. As a result, we have seen accelerated progress towards understanding the scope of quantum computing, pushing its hardware and software technology, developing applications, and advancing error mitigation/correction protocols. In this talk, I would like to present a view on how to progress technologies for quantum computing systems using key metrics - scale, quality, speed that indicate the level of performance of a quantum computer. I will overview the recent development of superconducting quantum computing systems and the scientific advances by IBM that enabled to scale superconducting qubits to 27-qubit and 65-qubit processors. As quantum computing is becoming a research tool, I will discuss how we harness the computational power of a quantum computer in machine learning and chemistry by integrating with classical computing resources and using error mitigation. Exploiting classical resources will allow us to extend the computational capacity that the current limits of the quantum hardware can offer.

## Exponential suppression of bit or phase flip errors with cyclic error correction

**Julian Kelly**

*Hardware Lead: System Control, Google Quantum AI*

---

### Abstract

Many promising practical applications using quantum computers will require error rates below  $1e-10$ , but state-of-the-art hardware features physical error rates near  $1e-3$ . Quantum error correction theoretically promises to bridge this divide by combining physical qubits into logical qubits, and exponentially reducing error rates according to the number of physical qubits used. In this work, we run distance 3-11 repetition codes and distance 2 surface codes in the Sycamore superconducting qubit architecture. Using repetition codes, we demonstrate exponential suppression of bit or phase errors with 100x reduction in error rate from  $d=3$  to  $d=11$ , even after 50 rounds of measurement. We also show that our device is well described by a simple depolarizing error model, allowing us to project the performance of larger codes. The exponential suppression of error and validation of theoretical assumptions about the behavior of errors provides further evidence that surface codes with superconducting qubits are a viable path towards a fault tolerant quantum computer.

## Two-dimensional array of superconducting qubits with vertical access

**Yasunobu Nakamura**

*RIKEN Center for Quantum Computing*

---

### Abstract

Superconducting circuits are one of the most promising platforms for quantum computing. With the rapidly improving fidelities of the control gates and readouts, more and more advanced computation becomes achievable. There are a few different architectures under intensive studies, roughly classified with tunable-frequency or fixed-frequency qubits and with tunable or fixed couplings. The less tunability tends to lead the longer coherence and less demands for wiring. On the other hand, the system could be vulnerable to the device parameter fluctuations in the fabrication as well as the energy coincidences with two-level fluctuators and the residual interactions between neighboring qubits, causing a trade-off. In this talk, we introduce our approach with a square lattice of fixed-frequency transmon qubits directly coupled with their nearest neighbors via capacitors. The circuit is controlled and read out only through microwave signals. To realize a tile-able design and mitigate the wiring issues in the planar approaches, we bring the control and readout lines vertically to the chip. We report the progress on the design and characterization of the chips and discuss the possible improvements and limitations.

## Silicon photonic quantum computing

**Pete Shadbolt**

*PsiQuantum*

---

### Abstract

PsiQuantum is building the world's first useful quantum computer using silicon photonic chips to process quantum information with single photons. This linear optical approach to quantum computing offers highly coherent qubits, high fidelity single qubit gates, and probabilistic entangling operations that can be implemented using well-known quantum optical methods. PsiQuantum's fusion-based quantum computing (FBQC) architecture based on these operations has a very low optical depth and extremely high tolerance to optical loss. The key advantage of photonic quantum computing is the fact that the required silicon photonic chips can be mass manufactured in semiconductor fabrication facilities, allowing scaling to achieve large-scale error correction. In this talk, we will show how unique technology in the areas of silicon photonics and quantum system architecture enable the path to large-scale, fault-tolerant, general-purpose quantum computing.

# Large-scale fault-tolerant universal quantum computing with quantum teleportation

**Akira Furusawa**

*The University of Tokyo and RIKEN*

---

## Abstract

Time-domain multiplexed one-way quantum computing based on quantum teleportation is a method to overcome various problems for the realization of practical quantum computers, such as scalability, fault-tolerance, and universality. I will talk about our recent progress to this direction.

---

## **Superconducting quantum- and digital-hybrid computers - tackling of increasing wirings**

**Yutaka Tabuchi**

*RIKEN Center for Quantum Computing*

---

### **Abstract**

Quantum computing gains intensive attention to broad fields of researchers, people in the industry, governments, and many scientific fans all over the world. In RIKEN Center for Quantum Computing, we research superconducting quantum computers by developing the quantum computers themselves. Whereas we know that fundamental elements in hardware include superconducting circuits fabricated on a silicon substrate, packaging enclosure, wiring inside a cryostat, control electronics, and signal processing circuits, a scalable organization of the elements for quantum computers are in the research stage. Here, I focus on the I/O interface between a chip and control electronics and discuss the scalable wiring architecture for a future goal. Having reconsidered current bottlenecks, we find that the uniformity of devices and quantum gates, exploits of translation symmetry in the surface code, and wiring hierarchization lead to I/O bandwidth reduction. I will lastly introduce a stacked heterogeneous quantum module structure as an organization of quantum computers.

## The hybrid quantum circuits with trapped electrons

**Atsushi Noguchi**

*Komaba Institute for Science, The Univ. of Tokyo, Japan*

---

### Abstract

Electrons trapped in a vacuum by a Paul trap have the wonderful features of a quantum system: fast operation, isolation from the environment, and a perfect two-level system. It is also possible to efficiently connect the different traps using superconducting wires. The electron Paul traps have recently been reported in room temperature system. On the other hand, the floating electrons have no internal degrees of freedom to interact with light, and cannot be controlled like ion trap systems, and have not yet been cooled to the ground state. In this talk, we will introduce our efforts to realize the electron Paul trap quantum system.

## Quantum simulation with ytterbium atoms in optical lattices

**Shintaro Taie**

*Department of Physics, Kyoto University, Japan*

---

### Abstract

Ultracold atoms in optical lattices have been attracted much interest for its application to quantum simulation. For their defect-free periodic potentials, highly controllable kinetic and interaction energies and experimental access to various physical quantities, optical lattices provide a unique opportunity to simulate strongly correlated solid electrons, especially those described by the Hubbard model.

The  $SU(N)$  Hubbard model which is a simple extension of the spin  $SU(2)$  symmetry in the Hubbard model to general  $SU(N)$ . The  $SU(N)$  Hubbard model has long history of theoretical study such as large- $N$  approach for deeper understanding of the physically important  $SU(2)$  case, and simple models for transition metals with orbital degeneracy. Recently  $SU(N)$  physics gained much more practical interests due to the possibility of its quantum simulation with laser-cooled alkaline-earth-metal atoms, which possess natural  $SU(N)$  spin symmetry due to the decoupling of nuclear spin from inter-atomic interactions.

In this talk, we present our experimental progress on simulating the  $SU(N)$  Hubbard model with ultracold ytterbium atoms. Especially, we focus on short-range antiferromagnetic behavior observed in optical lattices and thermometry performed by the detailed comparison with state-of-the-art many-body theory.

## **Ultrafast and ultracold quantum simulator/ computer with attosecond precision**

**Kenji Ohmori**

*Institute for Molecular Science, National Institutes of Natural Sciences*

---

### **Abstract**

Many-body correlations govern a variety of important quantum phenomena including the emergence of superconductivity and magnetism in condensed matter as well as chemical reactions in liquids. Understanding quantum many-body systems is thus one of the central goals of modern sciences and technologies. Here we demonstrate a new pathway towards this goal by generating a strongly correlated ultracold Rydberg gas with a broadband ultrashort laser pulse. We have applied our ultrafast coherent control with attosecond precision [1] to a strongly correlated Rydberg gas in an optical dipole trap, and have successfully observed and controlled its ultrafast many-body electron dynamics [2-4]. This new approach is now applied to an atomic BEC, Mott insulator lattice, and arbitrary array assembled with optical tweezers to develop into a pathbreaking platform for quantum simulation and computation on the ultrafast timescale [5-7].

This project is in progress in tight collaboration with Hamamatsu Photonics K.K..

---

## References

- [1] H. Katsuki et al., *Acc. Chem. Res.* 51, 1174 (2018).
- [2] N. Takei et al., *Nature Commun.* 7, 13449 (2016).  
Highlighted by *Science* 354, 1388 (2016); *IOP PhycisWorld.com* (2016).
- [3] C. Sommer et al., *Phys. Rev. A* 94, 053607 (2016).
- [4] C. Liu et al., *Phys. Rev. Lett.* 121, 173201 (2018).
- [5] M. Mizoguchi et al., *Phys. Rev. Lett.* 124, 253201 (2020).
- [6] Patents (US: 3rd. Nov. 2020 and JAPAN: 27th Apr. 2021)  
“Quantum simulator and quantum simulation method” ,  
H. Sakai (Hamamatsu Photonics K.K.), K. Ohmori (NINS) et al.
- [7] UC Boulder / NIST Quantum Technology Website : CUbit Quantum Initiative  
<https://www.colorado.edu/initiative/cubit/newsletter/newsletter/june-2020>  
“A metal-like quantum gas: A pathbreaking platform for quantum simulation”

## Engineering qubits in silicon with atomic precision

**Michelle Simmons**

*Silicon Quantum Computing, Sydney Australia*

---

### Abstract

The realisation of a large-scale error corrected quantum computer relies on our ability to reproducibly manufacture qubits that are fast, highly coherent, controllable and stable. The promise of achieving this in a highly manufacturable platform such as silicon requires a deep understanding of the materials issues that impact device operation. In this talk I will demonstrate our progress to engineer every aspect of device behaviour in atomic qubits in silicon. This will cover the use of atomic precision lithography to achieve fast, controllable exchange coupling, qubit initialisation and read-out; high quality epitaxial growth to create all epitaxial gate structures allowing for highly stable qubits; and unique imaging and modelling techniques that provide a deep understanding of the impact of the solid state environment on qubit designs and operation.

## Quantum computation - spins inside

**Lieven M.K. Vandersypen**

*QuTech and Kavli Institute of Nanoscience, Delft University of Technology*

---

### Abstract

Quantum computation has captivated the minds of many for almost two decades. For much of that time, it was seen mostly as an extremely interesting scientific problem. In the last few years, we have entered a new phase as the belief has grown that a large-scale quantum computer can actually be built. Quantum bits encoded in the spin state of individual electrons in silicon quantum dot arrays, have emerged as a highly promising direction. In this talk, I will present our vision of a large-scale spin-based quantum processor, and ongoing work to realize this vision. This includes two-qubit gate fidelities of more than 99.5%, universal control of up to six qubits, and the coherent coupling of spin qubits at a distance. Finally, in close collaboration with Intel, we have fabricated and measured quantum dots using all-optical lithography on 300 mm wafer, using industry-standard processing, demonstrating excellent qubit performance. When combined, the progress along these various fronts can lead the way to scalable networks of high-fidelity spin qubit registers for computation and simulation.

## Si platform for spin-based quantum computing

**Seigo Tarucha**

*Riken Center for Quantum Computing & Center for Emergent Matter Science*

---

### Abstract

Silicon is a promising platform for making spin qubits in quantum dots (QDs), on the grounds of several advantages of a long intrinsic decoherence time, a possible high-temperature operation, and compatibility in device fabrication with industrial technology. One of the challenges in development of Si quantum computing is to improve the control fidelities of single- and two-qubits beyond the quantum error correction threshold, 99 % in the surface code. For the single qubits the fidelity higher than 99.9% has been achieved but yet limited to 98 % for the two-qubits. But very recently a couple of reports on the two-qubit gate fidelity above 99% have appeared on arXiv.

In this work we use Si/SiGe triple quantum dots (TQDs) to operate two and three spin qubits with high fidelities. We apply a micro-magnet technique to increase the single qubit drive and exchange control for two qubits in two QDs of the TQD and finally achieve the two-qubit gate fidelity above 99 %. Based on this result we develop three qubit operations for implementing quantum error correction. We use the TQD to generate a three-spin entangled state, called GHZ state, and a Toffoli gate and then demonstrate the three-qubit phase error correction.

## Next-generation quantum annealing testbed

**William Oliver**

*EECS, Physics, and Lincoln Laboratory, MIT, USA*

---

### Abstract

Quantum annealers based on superconducting flux qubits have generated significant interest as a tool for solving complex optimization problems. However, a demonstration of improved performance over the best known classical algorithms has remained elusive on existing quantum annealing hardware. Hardware improvements such as longer qubit coherence times and enhanced access to key control parameters may be central to achieving a computational advantage. Under DARPA's Reversible Quantum Machine Learning and Simulation (RQMLS) program, MIT Lincoln Laboratory is responsible for operating a state-of-the-art quantum annealing testbed. This flexible testbed is fabricated using a 3D-integrated three-tier architecture. It contains 25 high-coherence flux qubits with high-bandwidth individual flux controls (100 MHz) and high-fidelity readout. In this presentation, we will provide an overview of the testbed design and operation.

This research was funded in part by the Office of the Director of National Intelligence (ODNI), Intelligence Advanced Research Projects Activity (IARPA) and the Defense Advanced Research Projects Agency (DARPA) under Air Force Contract No. FA8702-15-D-0001. The views and conclusions contained herein are those of the authors and should not be interpreted as necessarily representing the official policies or endorsements, either expressed or implied, of the ODNI, IARPA, DARPA, or the U.S. Government.

---

## Algorithmic breakeven in quantum annealing

**Daniel Lidar**

*Departments of Electrical and Computer Engineering, Chemistry,  
and Physics, University of Southern California, USA*

---

### Abstract

As quantum computing proceeds from perfecting physical qubits towards testing logical qubits and small scale algorithms an urgent question being confronted is how to decide that critical milestones and thresholds have been reached. Typical criteria are gates exceeding the accuracy threshold for fault tolerance logical qubits with higher coherence than the constituent physical qubits and logical gates with higher fidelity than the constituent physical gates. In this talk I will argue in favor of a different criterion I call "quantum algorithmic breakeven" which focuses on demonstrating an algorithmic scaling improvement in an error-corrected setting over the uncorrected setting. I will present evidence that current experiments with commercial quantum annealers have already crossed this threshold. I will also discuss our latest evidence for a "limited quantum speedup" with such devices, and the need to explore alternatives to the traditional setting of adiabatic, "forward" quantum annealing.

### References:

- T. Albash, D. Lidar, PRX 8, 031016 (2018)
- A. Pearson, A. Mishra, I. Hen, D. Lidar npjQI 5 107 (2019)
- E.J. Crosson, D. Lidar, Nat. Rev. Phys. (2021)

## Fault-tolerance with bosonic qubits

**Shruti Puri**

*Yale University*

---

### Abstract

Recently a new paradigm of quantum computing has gained momentum in which a qubit is encoded in non-classical states of a quantum oscillator. Such qubits are known as continuous-variable or bosonic qubits and their primary advantage is that they can be made robust against certain sources of noise by design or by active error correction directly to the physical oscillator mode. I will discuss recent advances in the development of bosonic qubits in the circuit-QED platform and show how their inherent properties can be leveraged for hardware-efficient fault-tolerant quantum computation.

## **Fault-tolerant quantum computation in with 3D cluster states**

**Robert Raussendorf**

*University of British Columbia, Canada*

---

### **Abstract**

I discuss fault-tolerant quantum computation in the presence of geometric constraints, specifically fault-tolerant measurement-based quantum computation on 3D cluster states, and its two-dimensional circuit counterpart based on the surface code. After reviewing some background on measurement-based quantum computation and fault-tolerance, I discuss the inherent quantum error-correction capability of 3D cluster states, and its topological origin. I then describe how to implement topologically protected quantum gates in this setting. I conclude with a description of recent advances on the theory frontier, and a summary of the status of experiment.

## Beyond NISQ / Toward FTQC Panel Discussion

**Masato Koashi**

*Univ. of Tokyo*

---

### Abstract

While we are about to enter the era of quantum computers with a few hundreds of qubits with Noisy Intermediate-Scale Quantum (NISQ) technology, it is also necessary to endeavor after fault-tolerant (FT) architecture in order to build a quantum computer of much larger scale and to benefit from the full potential of quantum computation. The panel will discuss future directions of research to achieve such a goal of FTQC technology.

## Provably accurate simulation of gauge theories and bosonic systems

Yuan Su

*Google*

---

### Abstract

Quantum many-body systems involving bosonic modes or gauge fields have infinite-dimensional local Hilbert spaces which must be truncated to perform simulations of real-time dynamics on classical or quantum computers. To analyze the truncation error, we develop methods for bounding the rate of growth of local quantum numbers such as the occupation number of a mode at a lattice site, or the electric field at a lattice link. Our approach applies to various models of bosons interacting with spins or fermions, and also to both abelian and non-abelian gauge theories. We show that if states in these models are truncated by imposing an upper limit  $\Lambda$  on each local quantum number, and if the initial state has low local quantum numbers, then an error at most  $\epsilon$  can be achieved by choosing  $\Lambda$  to scale polylogarithmically with  $1/\epsilon$ , an exponential improvement over previous bounds based on energy conservation. For the Hubbard-Holstein model, we numerically compute a bound on  $\Lambda$  that achieves accuracy  $\epsilon$ , obtaining significantly improved estimates in various parameter regimes. We also establish a criterion for truncating the Hamiltonian with a provable guarantee on the accuracy of time evolution. Building on that result, we formulate quantum algorithms for dynamical simulation of lattice gauge theories and of models with bosonic modes; the gate complexity depends

---

almost linearly on spacetime volume in the former case, and almost quadratically on time in the latter case. We establish a lower bound showing that there are systems involving bosons for which this quadratic scaling with time cannot be improved. By applying our result on the truncation error in time evolution, we also prove that spectrally isolated energy eigenstates can be approximated with accuracy  $\varepsilon$  by truncating local quantum numbers at  $\Lambda = \text{polylog}(1/\varepsilon)$ .

# Quantum algorithms for large-scale problems

**François Le Gall**

*Graduate School of Mathematics, Nagoya University, Japan*

---

## Abstract

In view of the significant progress made on the hardware side of quantum computing, unravelling the potential of large-scale quantum computers, and especially discovering compelling applications that can justify the huge amount of effort, time and investments needed in the next decades for their development, is a pressing issue. In this talk I will give an overview of the vibrant research field of quantum algorithms for large-scale quantum computers. I will in particular discuss exciting recent developments, such as quantum algorithms for string problems with potential applications to bioinformatics, quantum algorithms for graph problems with potential applications to big data, and quantum algorithms for algebraic problems such as matrix multiplication and eigenvalue estimation.

## Promises and challenges of variational quantum algorithms

**Patrick Coles**

*LANL*

---

### Abstract

Beyond finding ground states, new applications have recently emerged for Variational Quantum Algorithms (VQAs). These include dynamical simulation, metrology, solving linear systems, and principal component analysis, among others. Moreover, new tools are making VQAs more feasible, such as quantum-aware optimizers and error mitigation methods. VQAs also exhibit an intriguing resilience to certain types of noise. These signs point to VQAs soon providing quantum advantage for practically interesting problems. On the flip side, new analytical results have studied the gradient scaling for VQAs. These results paint a concerning picture, and show that barren plateaus in the training landscape will emerge if care is not taken. Barren plateaus are caused by lack of structure or simply by the presence of noise. Avoiding barren plateaus has now become a crucial area of research. This talk will review both the exciting and challenging nature of VQAs for near-term quantum computing.

## Development of quantum machine learning algorithms and experimental realization

**Kosuke Mitarai**

*Graduate School of Engineering Science, Osaka University/  
QIQB Center, Osaka University/ JST PRESTO*

---

### **Abstract**

Applying quantum computers to machine learning tasks is an exciting new area of research. In this talk, I will first present our experimental demonstration of a quantum machine learning algorithm called quantum kernel method. Using an NMR quantum simulator, we successfully employed ~25 qubits for machine learning tasks. Secondly, I will present an algorithm called a quantum recurrent neural network, which is an extension of the classical recurrent neural network to a quantum setting. Its algorithm details and properties will be discussed.

---

# Toward realization of quantum error correction and fault-tolerant quantum computing

**Keisuke Fujii**

*Graduate School of Engineering Science, Osaka Univ., Japan*

---

## Abstract

Now that 50-100 qubit scale quantum computers have been realized, then an experimental demonstration of quantum error correction is becoming a reality. In this talk, I will present a result of simulation of quantum error correction on the scale of 50 qubits under a realistic noise model. Specifically, we will discuss what physical conditions are required to extend the lifetime of logical qubits against the coherence time of physical qubits. In the post-NISQ era, it is required to evaluate the performance of quantum error correction on the scale of 1000 qubits. For such a situation, we will show that it is possible to simulate quantum error correction over 1000 qubits by using a quasi-probability method, taking advantage of the fact that most of the quantum circuits employed in quantum error correction are Clifford. Furthermore, by applying quantum error mitigation, which was developed as a method to overcome the noise problem in NISQ devices, to quantum error correction, the number of required physical qubits can be greatly reduced. We expect that these researches will make an important contribution to the evolution from the NISQ era to the FTQC era closing their gap.

---

## Break down the high-order tensors of quantum chemistry, for $O(N)$ -depth circuit algorithm

**Yuki Kurashige**

*Department of Chemistry, Graduate School of Science, Kyoto University*

---

### Abstract

Quantum chemistry is gaining more attention as a promising field of application of quantum computers because of its high affinity to the qubit representations and universal gate operations. Even so, the status is far from real-world applications. One of the reasons is that high-order tensors that describe electron interaction or correlation, e.g., the two-electron molecular integrals or double-excitation cluster amplitudes, need to be processed in quantum chemical calculations, which will be interpreted by at least  $O(N^4)$  quantum gates in the circuits, thereby making it infeasible on current and near-term quantum computers. Here, we present an efficient tensor decomposition for the above high-order tensors, and a new ansatz for the variational quantum eigensolver. The method is able to be implemented with  $O(N)$ -depth quantum circuit and at the same time considerably reduce the required number of measurements.

## Quantum computing for chemistry

**Markus Reiher**

*Lab. f. Phys. Chem., ETH Zurich, Switzerland*

---

### Abstract

Five years ago, we discussed whether and how quantum computing may contribute to the solution of actual chemical problems that are hard to tackle with traditional means at the example of the nitrogenase enzyme [PNAS 114 (2017) 7555]. We have recently updated that study at another example (a carbon dioxide fixation catalyst), considering latest estimates for hardware timings and algorithmic advances [Phys. Rev. Res. 3 (2021) 033055]. A main result of these efforts, which always target the exact many-particle wave function, has been that quantum computing may indeed become a game changer in the not too distant future. Accordingly, we proceeded to present a more general discussion of a potential quantum advantage in the molecular sciences in a perspective article [arXiv:2102.10081], which ponders the many aspects of a quantum computation in comparison to competing traditional methods (see, e.g., the density matrix renormalization algorithm as an example [J. Chem. Phys. 152 (2020) 040903]). Apart from error-controlled exact-diagonalization solutions, more approximate parametrization obtained, for example, with the variational quantum eigensolver are also advantageous (see, for instance, our contribution to this field regarding vibrational spectroscopy [Chem. Sci. 11 (2020) 6842]). In my talk, I will review our work of the past years and present an outlook to future work.

## Improving adiabatic quantum computing with non-adiabatic methods

**Wolfgang Lechner**

*University of Innsbruck*

---

### Abstract

The speed of adiabatic processes, and thus adiabatic quantum computing is fundamentally limited by the adiabatic theorem. Counter-diabatic driving is a method that introduces additional time-dependent Hamiltonian terms in order to suppress diabatic transitions. However, these terms are highly non-local in many-body systems and thus not practical for near term applications. Recently, approximations for counter-diabatic terms have been introduced which offer a trade-off between complexity of the implementation and gain in ground-state fidelity. I will discuss the simplest approximations of single and two-body counter-diabatic terms.

# Abstract

Tracks

## PL

### Plenary Sessions

Contents / Topics

Welcome from Organizing Committee and Hosting Ministries, Plenary Talks, Keynote Speeches

Tracks

## CP

### Quantum Computing Track

Contents / Topics

Quantum Computing with Atoms and Ions, Superconducting Quantum Computers(QC), Photonic QC, Young Researcher Session, Quantum Simulations, Semiconductor QC, Quantum Annealing Toward FTQC(Tutorial), Beyond NISQ/Toward FTQC Panel Discussion, Quantum Architecture, Quantum Algorithms, NISQ Algorithms, Quantum Algorithms for Chemistry

Tracks

## CC

### Quantum Cryptography & Communication Track

Contents / Topics

Quantum Internet, Quantum Cryptography(Up-to-date Technologies of Field and Satellite QKDs), Challenges for Quantum Technology Platform (QKD Networks, Satellite QKD and their integration), Industry Panel, Young Researcher Session  
\*\*CC-04 on 8th and CC-05, CC-06 on 9th Dec are supported by SIP (cross-ministerial Strategic Innovation promotion Program).

Tracks

## SE

### Quantum Sensing Track

Contents / Topics

Solid-State Quantum Sensors, Quantum Sensors for Life Sciences, Quantum Sensors and Quantum Life Sciences, Atom Interferometer, Cold Atom, Atomic/Ion Clocks, Short Presentations by Young Researchers  
\*8th Dec Sessions are a joint-program with The 4th IFQMS (The 4th International Forum on Quantum Metrology and Sensing).

## Bringing QKD to real-world digital infrastructures

**Michele Mosca**

*evolutionQ, and IQC, University of Waterloo, Canada*

---

### Abstract

For the advent of large-scale fault-tolerant quantum computers to represent a positive milestone in human history, we must first evolve critical digital infrastructures to be safe from quantum-enabled attacks.

However, the current status quo in cryptography is already not good enough anymore. With connected industrial devices, driverless cars, 5G, and more, the stakes are already far higher than they were a decade or more ago, and they keep getting higher.

The emerging “quantum internet” further amplifies the positive impacts of quantum computation and quantum sensing, and also offers a fundamentally new suite of tools for protecting digital platforms from a range of cyber attacks. Quantum key establishment (known as Quantum Key Distribution, QKD) is one such tool that is already commercially available and will continue to improve as quantum technologies continue to advance.

It is already time to design QKD into real-world digital infrastructures, alongside other quantum-safe methods. I will overview our work facilitating robust scalable real-world deployment of QKD.

## Ion-photon interface for quantum networks

**Hiroki Takahashi**

*Okinawa Institute of Science and Technology*

---

### Abstract

The complementary benefits of trapped ions and photons as carriers of quantum information make it appealing to interface them via cavity QED. In particular a quantum register made of a string of ions and interfaced efficiently with optical photons provides an excellent platform for quantum repeaters and quantum networks. With this objective in mind, we have been working on the integration of micro optical cavities in ion traps. In the talk, we will present our achievements so far and future prospects.

## Designing tomorrow' s quantum internet

**William John Munro**

*NTT Basic Research Laboratories, Japan*

---

### Abstract

Tomorrow' s quantum internet will rely on the transmission of quantum signals over long distances that can be used to support many tasks including quantum communication, quantum remote sensing and even distributed quantum computation. The performance of such a long-distance network will be severely affected by channel losses between the network' s users. Quantum repeaters are one solution to this issue but a key question is how to generate the required long-range entanglement efficiently. In this talk we will take a top-down architectural approach to explore how the various kinds of quantum repeaters may operate in the future and estimate their performance in a network environment. We will show that the architectural network design will have a profound impact on the network' s performance highlighting how it is critical that both the quantum and classical signals are integrated together. Further we will explore circuit, packet and quantum switched networks discussing what constraints they put on the form of the quantum repeaters noting that not all repeater designs allow all the network modes.

## Quantum Internet: from classical to quantum paths

**Angela S. Cacciapuoti**

*Department of Electrical Engineering and Information Technology,  
University of Naples Federico II, Italy*

---

### Abstract

Generally, in a quantum network, the information carriers are treated quantum mechanically, but the paths through which they propagate are still classical, obeying the laws of classical causality. But this assumption can be generalized such as, not only the information or the channels, but also the placement of the channels – i.e., the paths along with the carriers propagate – can be quantum. This unconventional placement of channels has been theoretically and experimentally verified, and it has been proven to be able to describe powerful setups for the transmission of both classical and quantum information. This genuine quantum phenomenon plays a paramount role for achieving unprecedented information transfer capacities, and it must be fully understood and harnessed for the Quantum Internet design.

## Software and protocol stacks for quantum networks

**Wojciech Kozlowski**

*QuTech, Delft University of Technology, the Netherlands*

---

### Abstract

The second quantum revolution brings with it the promise of a quantum internet. As research efforts move beyond basic demonstrations of fundamental physics new challenges emerge in the field of system design and implementation of quantum networks. For example, scaling current quantum communication experiments to a global quantum internet will also require platform-independent programmability and robust automation capabilities. A new – quantum – software and network protocol stack need to be developed for this purpose. In this talk I will present our efforts on the first ever implementation of a link and physical layer protocol on state-of-the-art solid-state quantum networking nodes. The physical layer protocol provides a best-effort service for entanglement generation attempts and the link layer protocol abstracts that into a robust and platform-independent entanglement generation service. We evaluate our implementation by running a full state tomography of the delivered entangled states, as well as preparation of a remote qubit state on a server by its client. Our results mark a clear transition from physics experiments to quantum communication systems, which will enable the development and scaling of future quantum networks.

## Genuine and optimized entanglement-based quantum networks

**Wolfgang Duer**

*University of Innsbruck, Austria*

---

### Abstract

We consider entanglement-based quantum networks, where pre-shared multipartite entangled states -that can be generated prior to any network request- serve as a resource to fulfill general network requests on demand. This offers new possibilities and features such as speeding up network requests, and network optimization independent of the underlying physical structure. The main challenge is to identify suitable resource states shared between network devices that can be stored, and then modified by local means such that the desired output state (and hence the desired network functionality) can be guaranteed. This minimizes generation times for target states, and allows for optimizing network structures that are independent of the underlying physical network topology. We show how to design and optimize such entanglement-based networks, and demonstrate a storage advantage when using multipartite entangled states. Finally, we discuss how to make quantum networks genuine quantum by providing them with the possibility of handling superposed tasks and superposed addressing via a quantum control register. This allows one e.g. to prepare superposition of different target states, or to send information among a superposition of different paths.

# Quantum physical unclonable functions and their comprehensive cryptanalysis

**Elham Kashefi**

*CNRS Sorbonne Université and University of Edinburgh*

---

## Abstract

A Physical Unclonable Function (PUF) is a device with unique behaviour that is hard to clone due to the imperfections and natural randomness during the manufacturing procedure, hence providing a secure fingerprint. A variety of PUF structures and PUF-based applications have been explored theoretically as well as being implemented in practical settings. Recently, the inherent unclonability of quantum states has been exploited to derive the quantum analogue of PUF as well as new proposals for the implementation of PUF. In this talk, we present the first comprehensive study of quantum Physical Unclonable Functions (qPUFs) with quantum cryptographic tools, introducing a new quantum learning attack that can explore the vulnerabilities of quantum and certain classical PUFs leading to general no-go results on the unforgeability of qPUFs. On the other hand, we prove that a large family of qPUFs (called unitary PUFs) can provide quantum selective unforgeability which is the desired level of security for most PUF-based applications. Moreover, we elaborate on the connection between qPUFs as hardware assumptions, and computational assumptions such as quantum pseudorandomness in order to establish the link between these two relatively new fields of research.

## Entanglement based quantum networking

**Siddarth K. Joshi**

*University of Bristol*

---

### Abstract

Quantum communication is inherently a two party point to point protocol. Its information theoretically perfect security depends on the physical impossibility of exactly duplicating individual quantum states. However, this very property also makes long distance and network based implementations very difficult. This is because information cannot be read and then resent without compromising the security of the quantum network.

Multiplexed distribution of entanglement allows the simple and scalable distribution of bipartite entangled states to all pairs of multiple users. The users can then perform measurements on these states to implement many protocols including Quantum Key Distribution, Anonymous protocols, Digital Signatures, Secure Initial Authentication Transfer and network flooding. We present the experimental implementation of all these protocols on our 8-user city wide quantum network using deployed telecom infrastructure. Lastly we present preliminary data on how we can extend this type of quantum network over even longer fibre distances of up to 50km.

CC-04-02

## OpenQKD use-case demonstrations in Europe

**Andreas Poppe**

*Center for Digital Safety & Security, AIT Austrian Institute of Technology, Austria*

---

### Abstract

In this talk I will briefly update the status of the ongoing European initiative to bring QKD to the field. Testbeds will be installed at 18 different sites distributed over EU, Switzerland and UK with more than 25 commercial QKD-systems involved. Thereby deployments relevant to future use-cases have already been demonstrated and I will also point to some future work of the 38 partners.

## Lessons from the SpooQy-1 satellite

**Alexander Ling**

*Centre for Quantum Technologies, National University of Singapore, Singapore*

---

### Abstract

SpooQy-1 was a nanosatellite developed by the Centre for Quantum Technologies (Singapore) to demonstrate entanglement generation in space, as a pathfinder for more ambitious satellite to ground experiments. The satellite was deployed in June 2019, and spent 28 months fully operational in low Earth orbit before burning up on re-entry. I will review some of the major results and data that have been collected over the lifetime of the satellite and discuss how it will guide future in-orbit demonstrations and experiments.

# High-level concepts and design of commercial satellite-based QKD networks

**Manuel Erhard**

*Quantum Technology Laboratories [qtlabs] GmbH, Austria*

---

## Abstract

Quantum Key Distribution (QKD) is a fast-growing scientific but today primarily commercial field. Governments and private businesses seek enhanced security solutions that can withstand future hacking attacks directed against public key encryption systems. Today, many different QKD protocols claim to offer “unconditional” security. However, looking in more detail, many subtleties lead to different security levels, or in worst-case scenarios, to no security at all. Thus, it is essential to appropriately select and design QKD protocols and networks suitable for intercontinental long-distance satellite-based QKD networks. This talk presents and compares different QKD protocols concerning their security, key-rate performance, and applicability, especially for satellite-based QKD networks. Our focus lies in high-level mission planning parameters, such as orbital height, number of satellites per orbit, and realistically achievable secret key rates with various QKD protocols and technologies. Finally, we present simulation results of various case studies ranging from European to intercontinental use-cases.

## Quantum networking research at Los Alamos

**Raymond Newell**

*Los Alamos National Laboratory, USA*

---

### Abstract

The value of a classical network, defined as the number of unique connections possible, scales as the square of the number of connected users (Metcalfe's law). In contrast, for quantum networks with quantum resources, such as computers and sensors, the computational power of the network scales exponentially in the number of connected nodes, making a quantum network of quantum devices much more capable than a classical network of the same size.

Quantum networks will require efficient sources of indistinguishable single photons on demand to create ancilla photons for quantum error correction of multi-qubit quantum error correcting codes. Existing technologies currently face several challenges: output photons are often easily distinguishable; wavelengths are often not compatible with standard telecom optical fiber; and emission is often omnidirectional, making it difficult to couple into fiber. We will review our efforts to create defects in single-wall carbon nanotubes (SWCNT) via covalent chemical functionalization to emit a stream of single photons at a telecom wavelengths. Our existing SWCNT devices yield 79% photon indistinguishability and we have realized telecommunications C-band photon emission as well as high-efficiency coupling into fiber. We plan to develop these devices for integration with quantum communication links in support of large-scale quantum networks.

---

# Fundamentally applied quantum communication

**Rob Thew**

*University of Geneva*

---

## Abstract

We present several aspects of our work on quantum communication ranging from next generation quantum repeaters and multipartite systems to QRNG and QKD development. We will touch on the connection between fundamental research and applied development of quantum communication devices and systems, in particular, exploiting concepts from Bell and nonlocality to make these “better” , as well as the importance of integrated photonics.

# Finite-key security of continuous-variable quantum key distribution

**Masato Koashi**

*Univ. of Tokyo*

---

## Abstract

The security of quantum key distribution is often proved in the asymptotic regime, but in order to establish security for an actual implementation, one needs to prove it in the finite-key regime where the communication time is finite. Although a conventional approach to the security using phase errors in qubits excels in dealing with finite-size statistics, the use of qubits limited its use to discrete-variable QKD protocols with photon detectors until recently. Here I will explain how we can apply this approach to a two-state continuous-variable QKD protocol with homodyne/heterodyne detection to prove its finite-key security against general attacks.

## **Overview of Japanese project “SIP” and quantum secure cloud technologies**

**Masahide Sasaki**

*Quantum ICT Collaboration Center, NICT, Japan*

---

### **Abstract**

We present quantum secure cloud technologies which protect critical data securely for a long time with high availability, and provide near optimal computing services with quantum-classical hybrid solvers in a secure manner.

To realize these functions, we have integrated QKD, secret sharing, post-quantum cryptography, secret computing, as well as codesign middleware for getting various quantum and classical computers work together. We overview current status of deployment and standardization of quantum secure cloud.

## Secure information society using "Quantum Secure Cloud"

**Mikio Fujiwara**

*Quantum ICT Laboratory, Advanced ICT Research Institute,  
National Institute of Information and Communications Technology, Japan*

---

### Abstract

We have developed a system that implements a secret sharing protocol on a quantum cryptography network and enables secure transmission, storage, and secondary use of data. We named the system as "a Quantum Secure Cloud". We are promoting a proof of concept (POC) in various fields. This system not only handles electronic medical record data and genome analysis data as data that requires confidentiality for a long period of time, but is also expanding into the financial field. We have developed an exclusive OR-based high-speed secret sharing and high-speed OTP cryptographic transmission system to support distributed backup of large volumes of data. We were able to complete a distributed backup of a large volume of 80GB of genomic data within 36 hours. Furthermore, regarding the secondary use of secure data (genomic data), a secret calculation system assuming a trusted server is installed in the quantum secure cloud, and the trusted server restores the data only at the time of calculation and encrypts the system at the time of input / output. developed. This system is also equipped with a filtering function to prevent unnecessary leakage of personal information. We will introduce other POCs as well.

## Quantum key distribution research and development in NEC

**Junichi Funada**

*NEC Technology Synergy Creation Division*

---

### Abstract

Quantum cryptography is a cryptographic method that can protect information in the ultra-long term without the risk of being deciphered in the future, and is expected to be applied to many important mission-critical systems. NEC is engaged in various research and development toward the commercialization of quantum key distribution.

This presentation first shows overview of NEC's QKD related activities, then introduction of CV-QKD research and field trials of QKD. CV-QKD method can be used over existing optical fibers and is expected to be inexpensively implemented. NEC and the partners are developing CV-QKD prototype and proceed evaluation. NEC and the partners also conduct field trials of QKD in some important application areas.

## **QKD R&D and field trials in Toshiba**

**Yoshimichi Tanizawa**

*Corporate R&D Center, Toshiba Corporation, Japan*

---

### **Abstract**

Quantum key distribution (QKD) provides a means for exchanging cryptographic keys, the security of which makes no assumptions about an adversary's computing power or technological capability. This presentation shows R&D activities including high speed, long distance, and stable operation of QKD, as well as a key delivery API for the QKD network environment. It also shows various kinds of field trials of QKD system and QKD network conducted by Toshiba and the partners.

## Quantum communication activities in Canada

**Norbert Lütkenhaus**

*Institute for Quantum Computing and Department of Physics and Astronomy,  
University of Waterloo, Canada*

---

### Abstract

Canada has a strong background in quantum communication. In addition to the experimental activities (see presentation of Thomas Jennewein) there is a broad theory landscape in Canada that covers researchers in places like Montreal, Ottawa, Toronto, Waterloo and Calgary. The theory research deals with groundwork of handling side-channels of QKD, QKD networks and also applications beyond QKD. We are also leading a number of open source platforms, including a project for post-quantum cryptography ([openquantumsafe.org](http://openquantumsafe.org)), QKD network stack ([openQKDnetwork.ca](http://openQKDnetwork.ca)) and the numerical security evaluation of QKD ([openQKDsecurity.org](http://openQKDsecurity.org)). The spectrum of activities range from academia to industry, with the quantum industry coming together in the Quantum Industry Canada consortium.

# Abstract

Tracks

## PL

### Plenary Sessions

Contents / Topics

Welcome from Organizing Committee and Hosting Ministries, Plenary Talks, Keynote Speeches

Tracks

## CP

### Quantum Computing Track

Contents / Topics

Quantum Computing with Atoms and Ions, Superconducting Quantum Computers(QC), Photonic QC, Young Researcher Session, Quantum Simulations, Semiconductor QC, Quantum Annealing Toward FTQC(Tutorial), Beyond NISQ/Toward FTQC Panel Discussion, Quantum Architecture, Quantum Algorithms, NISQ Algorithms, Quantum Algorithms for Chemistry

Tracks

## CC

### Quantum Cryptography & Communication Track

Contents / Topics

Quantum Internet, Quantum Cryptography(Up-to-date Technologies of Field and Satellite QKDs), Challenges for Quantum Technology Platform (QKD Networks, Satellite QKD and their integration), Industry Panel, Young Researcher Session  
\*\*CC-04 on 8th and CC-05, CC-06 on 9th Dec are supported by SIP (cross-ministerial Strategic Innovation promotion Program).

Tracks

## SE

### Quantum Sensing Track

Contents / Topics

Solid-State Quantum Sensors, Quantum Sensors for Life Sciences, Quantum Sensors and Quantum Life Sciences, Atom Interferometer, Cold Atom, Atomic/Ion Clocks, Short Presentations by Young Researchers  
\*8th Dec Sessions are a joint-program with The 4th IFQMS (The 4th International Forum on Quantum Metrology and Sensing).

SE-01-01

## Quantum sensing of quantum materials using NV center microscopy

**Amir Yacoby***Harvard University*

---

### Abstract

The magnetic fields generated by spins and currents provide a unique window into the physics of correlated-electron materials and devices. Proposed only a decade ago, magnetometry based on the electron spin of nitrogen-vacancy (NV) defects in diamond is emerging as a platform that is exceptionally suited for probing condensed matter systems. It can be operated from cryogenic temperatures to above room temperature, has a dynamic range spanning from DC to GHz, and allows sensor-sample distances as small as a few nanometers. As such, NV magnetometry provides access to static and dynamic magnetic and electronic phenomena with nanoscale spatial resolution. While pioneering work focused on proof-of-principle demonstrations of its nanoscale imaging resolution and magnetic field sensitivity, now experiments are starting to probe the correlated-electron physics of magnets and superconductors and to explore the current distributions in low-dimensional materials. In this talk, I will review some of our recent work that uses NV center magnetometry to image skyrmions in thin magnetic films, measure the spin chemical potential in magnetic insulators, and image hydrodynamic electron flow in layered materials. In addition I will describe the use of NV centers in a new scattering platform that uses spin waves as the probing excitation.

---

SE-01-02

## **Current status and prospects of solid-state quantum sensors for Quantum-LEAP**

**Mutsuko Hatano***Tokyo Institute of Technology*

---

### **Abstract**

Solid-state quantum sensors using diamond and SiC are expected to have various applications due to their principle possibilities such as wide-field dynamic range, operating temperature range, and high special resolution down to the atomic level.

In the MEXT Q-LEAP Quantum Solid-state Flagship Project, five companies, five academia, and two national research institutes have teamed up to develop a solid-state quantum sensor from basic science and technologies such as materials and quantum protocols to sensor modules and application prototypes.

In this talk, I would like to introduce the latest research topics of Q-LEAP, such as high precision simultaneous measurement of current and temperature in EV batteries, high-resolution magnetocardiographic imaging of rats, probing into living cells by tip-type NV sensor. In addition, expectations for a future "quantum leap" society based on quantum solid-state sensor technology will be discussed.

This work was supported by MEXT Quantum Leap Flagship Program (MEXT Q-LEAP) Grant Number JPMXS0118067395.

SE-01-03

## **Nanoscale vector AC magnetometry with a single nitrogen-vacancy center in diamond**

**Paola Cappellaro**

*Nuclear Science and Engineering, Physics Departments,  
Massachusetts Institute of Technology, USA*

---

### **Abstract**

Detection of AC magnetic fields at the nanoscale is critical in applications ranging from fundamental physics to materials science. Isolated nitrogen-vacancy centers in diamond can achieve the desired spatial resolution with high sensitivity. Still, vector AC magnetometry currently relies on using different orientations of an ensemble of sensors, with degraded spatial resolution. Here I will present a novel protocol that exploits a single NV to reconstruct the vectorial components of an AC magnetic field, by tuning a continuous driving to distinct resonance conditions. As an experimental proof-of-principle, I'll show how to map the spatial distribution of an AC field generated by a copper wire on the surface of the diamond.

The proposed protocol combines high sensitivity, broad dynamic range, and sensitivity to both coherent and stochastic signals, with broad applications in condensed matter physics.

---

SE-01-04

## Planetary magnetic field sensing via electrical readout of quantum centers in SiC

**Corey J. Cochrane**

*Jet Propulsion Laboratory, California Institute of Technology, United States*

---

### Abstract

The most widely used magnetometers for scientific missions to space are fluxgate and optically-pumped atomic-gas instruments due to their high sensitivity, reliability, and proven performance. Fluxgates are simple and robust while the atomic-gas designs are highly accurate and stable. However, it is very difficult to include all of these desired specifications in a single package with adequate size and power constraints for smaller scientific missions that involve cubesats. This opens the door for infusion of next-generation magnetometer technologies. In this work, we report on the development of a silicon carbide magnetometer, promising to be a low complexity, lightweight, low power, and inexpensive alternative to these heritage technologies. It measures magnetic field induced changes in spin dependent recombination (SDR) current within a pn junction. The change in SDR current arises from the interaction of external magnetic fields with the atomic-scale defects in the SiC semiconductor. This change in current can be detected electrically via magnetoresistance caused by zero-field level crossings or low-field electrically-detected magnetic resonance, thereby giving the instrument the ability to self-calibrate, a significant advantage in the remoteness of space. The material properties of SiC, namely radiation and temperature hardness, are also very attractive for space applications in harsh environments.

---

SE-02-01

## Production of color centers in nanodiamond

**Olga A. Shenderova**

*Adamas Nanotechnologies, United States*

---

### Abstract

Diamond particles containing fluorescent color centers provide combination of outstanding photostability, sensitivity of fluorescence to external stimuli and excellent biocompatibility attractive for life science applications. Until recently, however, the fluorescent color palette of N-based centers was restricted to particles emitting only in red or green, based on NV centers produced in type Ib synthetic diamond, or NVN centers produced in type Ia natural diamond, correspondingly. Limited color options impacts applications of fluorescent nanodiamonds (FND) in multiplexed biological imaging. Here we report on a breakthrough method of production of multicolor diamond particulates using ultra-high temperature annealing (>1500 °C), which generates conditions for the formation of one-, two- and three-atom nitrogen complexes with vacancies in electron irradiated type Ib synthetic diamond, providing vibrant luminescence in the red (NV), green (NVN) and blue (N<sub>3</sub> centers) spectral ranges, correspondingly. Remarkably, the ultra-high temperature treated particles containing NV centers demonstrated improved magneto-optical properties and open routes for multiplexed labeling combined with sensing when NV centers coexist with NVN or N<sub>3</sub> centers within individual particles. Moreover, enhanced <sup>13</sup>C optical hyperpolarizability of the treated particles was also observed, which advocates a new paradigm in dual-mode fluorescence/magnetic resonance imaging enabled by diamond contrast agents.

---

SE-02-02

## **Nitrogen-vacancy centers in nanodiamonds as temperature sensors and immunoassay reporters**

**Huan-Cheng Chang**

*Institute of Atomic and Molecular Sciences, Academia Sinica, Taiwan*

---

### **Abstract**

The negatively charged nitrogen-vacancy (NV<sup>-</sup>) center in fluorescent nanodiamonds (FNDs) is a point defect with unique magneto-optical properties. It has found wide applications in frontier areas of science and many new innovations are emerging. Here, we present two new applications of this quantum sensor: (1) FNDs embedded in polymer films as temperature sensing devices and (2) FNDs conjugated with antibodies as immunodiagnostic reagents. In the first task, we closely examined the temperature dependence of the peak positions and heights of the zero phonon line of NV<sup>-</sup> centers in poly(2-hydroxyethyl methacrylate) films from 35 to 120 °C. A measurement sensitivity of better than 0.5 K Hz<sup>-1/2</sup> was achieved over this temperature range. In the second task, we magnetically modulated the fluorescence intensities of NV<sup>-</sup> centers in FNDs. We achieved selective detection of 100 nm FNDs on a highly fluorescent nitrocellulose membrane at a particle density of 0.04 ng/mm<sup>2</sup> (or  $\sim 2 \times 10^4$  particles/mm<sup>2</sup>). The utility and versatility of these techniques were demonstrated with a study for the energy transfer kinetics of a resistively heated gold microwire embedded in the films as well as an application to background-free detection of FNDs as reporters for lateral flow immunoassays.

SE-02-03

## Treatment responses to immune checkpoint inhibitor therapy evaluated by MRI

**Shun Kishimoto**

*Radiation Biology Branch, NCI, USA*

---

### Abstract

Although immune checkpoint blockade (ICB) therapy has been widely used as a promising treatment option, the evaluation for its efficacy relies on the change in tumor size, which can delay the clinical decision-making because strong immune response often causes temporary tumor swelling called pseudo-progression. Thus, developing new imaging approach to evaluate the early physiological changes inside of the treated tumor is of great importance. Our laboratory is equipped with Electron Paramagnetic Resonance (EPR) scanner and hyperpolarized  $^{13}\text{C}$  MRI capable of in vivo oximetry and metabolic imaging, respectively. By using these imaging modalities as well as conventional  $^1\text{H}$  MRI, we identified useful functional/metabolic imaging biomarkers for early detection of the therapeutic effect of ICB therapy.

Anti-cancer effect in parts of the body that were not the direct target of local therapy is called abscopal effect. Although abscopal effect induced by local radiation therapy is rarely observed, the occurrence is much higher when combined with ICB treatment. We are investigating functional/metabolic factors affecting the occurrence of abscopal effect by ICB+radiation therapy in an ongoing study. The results from this study will also be presented.

SE-04-01

## Quantum sensing enabled by spin qubits in diamond

**Fedor Jelezko***Institute of Quantum Optics, Ulm University*

---

### Abstract

Single nitrogen vacancy (NV) color centers in diamond currently have sufficient sensitivity for detecting single external nuclear spins and resolve their position within a few angstroms. The ability to bring the sensor close to biomolecules by implantation of single NV centers and attachment of proteins to the surface of diamond enabled the first proof of principle demonstration of proteins labeled by paramagnetic markers and label-free detection of the signal from a single protein. Single-molecule nuclear magnetic resonance (NMR) experiments open the way towards unraveling dynamics and structure of single biomolecules. However, for that purpose, NV magnetometers must reach performance comparable to that of conventional solution state NMR. We will discuss new techniques allowing to combine high spectral resolution and sensitivity in nanoscale NMR. The ability to sense nuclear spins by NV centers also enables the transfer of polarization from optically polarized spins of NV centers to external nuclear spins. Such diamond based techniques for dynamic nuclear spin polarization are very promising for the enhancement of sensitivity of conventional MRI imaging.

SE-04-02

## Programmable quantum simulators based on spins in diamond

**Tim Taminiau***QuTech and Kavli Institute of Nanoscience, Delft University of Technology, the Netherlands*

---

### Abstract

Spins associated to optically active defects in diamond provide a versatile platform for quantum science and technology. In this talk, I will discuss our recent advances in realizing programmable quantum simulators based on individually controllable carbon-13 nuclear spins in diamond. I will present how one can use a single nitrogen-vacancy (NV) centre to sense, characterize and control a large number of spins in its environment [1,2,3]. By controlling the interactions between the spins it becomes possible to create a variety of many-body Hamiltonians with tunable parameters. As an example, I will discuss our investigation of a discrete-time crystal stabilized by many-body localization, a new out-of-equilibrium phase of matter [4].

[1] M. H. Abobeih et al., *Nature* 576, 411 (2019)

[2] C. E. Bradley et al., *Phys. Rev. X* 9, 031045 (2019)

[3] M. J. Degen et al., *Nature Commun.* 12, 3470, 2021 (2021)

[4] J. Randall et al., arXiv:2107.00736 (2021)

SE-04-03

## Development and optimisation of diamond for quantum technologies

**Matthew Markham**

*Element Six*

---

### Abstract

Quantum technologies is attracting significant investment due to the range of potential applications, but behind any new technology are the enabling materials. Diamond is one such material and ensembles of negatively-charged nitrogen-vacancy (NV-) centres constitutes a promising platform for sensing applications utilizing the quantum properties of this defect. However, the sensitivity of present NV-ensemble devices and the need for diamond material with reproducible properties has the potential to hinder progress toward many envisioned commercial-scale applications. The work covered in this presentation will address the material-related challenges associated with the development of diamond materials with reproducible properties for diamond quantum technologies.

SE-05-01

## Quantum biology: an Introduction

**Johnjoe McFadden**

*Faculty of Health and Medical Sciences, University of Surrey, Guildford, United Kingdom*

---

### Abstract

Quantum mechanics and molecular biology were the two revolutionary scientific disciplines that grew out of the twentieth century: quantum mechanics and molecular biology. Quantum biology can be said to have been initiated by a physicist, Erwin Schrödinger, in his lecture, essay and book entitled “What in Life” (published in 1944) in which he proposed that that heredity was based on non-trivial aspects of quantum mechanics. The book was very influential to molecular biology pioneers, such as James Watson and Francis Crick, who went on to discover the double-helical structure of DNA. Thereafter the field of quantum biology largely languished. However, the twenty-first century has seen a revival of quantum biology with the arrival of new experimental evidence of quantum mechanical effects in a range of biological phenomena such as photosynthesis and enzyme action. In this talk I will provide an introduction to quantum biology, returning to Schrödinger’s original insight that quantum phenomena may be found in biological processes that involve very numbers of molecules including photosynthesis, enzyme action, avian navigation and mutation.

SE-05-02

## Avian magnetoreception – a radical sense of direction

**Peter Hore**

*Department of Chemistry, University of Oxford, UK*

---

### Abstract

Small migratory songbirds travel spectacular distances each year, navigating by a variety of means most of which are poorly understood. Among them is a remarkable ability to perceive the direction of the Earth's magnetic field. Despite more than 50 years of research, the biophysical mechanism of this extraordinary sense remains obscure. In this lecture, I will discuss the proposal that the birds' magnetic compass relies on light-dependent chemical reactions in their eyes. Specifically, the unique quantum mechanical properties of photochemically formed radical pairs in cryptochrome proteins could allow detection of magnetic interactions six orders of magnitude weaker than previously thought possible. I will outline the basis of the radical pair mechanism, present some of the evidence for the involvement of cryptochrome, and comment on the fundamentally quantum nature of this hypothesis.

---

SE-05-03

## Surface chemistry of diamond for quantum applications

**Anke Krüger**

*Institute for Organic Chemistry, Stuttgart University, Germany*

---

### Abstract

The surface of diamond plays an important role for its properties. Not only is the surface itself the origin of characteristics such as zeta potential, wettability, aggregation behaviour etc., also lattice defects such as the NV or the SiV center can be influenced in their charge states by the nature of the surface termination or the attachment of larger functional groups. The latter can be also exploited for sensing applications using lattice defects as luminescent or spin sensors.

It is thus of utmost importance to properly control the surface groups and to develop methods for the efficient and highly reproducible functionalization of diamond materials.

In this presentation, methods for the initial termination of diamond with different atoms such as H, O and F will be presented. Further, the attachment of larger surface groups applicable as sensors, for the prevention of non-specific interactions and other applications will be shown. Additionally, highly sensitive methods for the quantitative assessment of surface groups will be presented.

SE-05-04

## **Diamond-based quantum sensors: technology and applications in physics and biology**

**Christian Degen**

*Department of Physics and Quantum Center, ETH Zurich, Switzerland*

---

### **Abstract**

Diamond has emerged as a unique material for a variety of applications, both because it is very robust and because it has defects with interesting properties. One of these defects, the nitrogen-vacancy center (NV center), has a single spin associated with it that shows quantum behavior up to room temperature. Our group is harnessing the properties of single NV centers for high resolution magnetic sensing applications.

In this talk, I will introduce the basic technology and concepts and emerging applications of diamond-based quantum sensors. I will discuss the challenges in the fabrication of high-quality diamond probes, and present some illustrative examples of applications in nanoscale imaging, including the imaging of antiferromagnetic domains and domain walls, the flow of current in graphene devices, and magnetic resonance imaging (MRI) of nuclear spins with atomic spatial resolution.

SE-06-02

## **Classical and quantum sensing for precise inertial navigation**

**Mikio Kozuma***Institute of Innovative Research, Tokyo Institute of Technology, Japan*

---

### **Abstract**

Inertial navigation is a technique to estimate self-position without the help of external signals such as electromagnetic waves from GPS satellites. Such a technique is essential, especially for controlling the position of the autonomous underwater vehicle since radio waves do not reach the deep sea. The current performance of the inertial navigation is the order of kilometers for 10 hours, which is not enough for various applications such as marine resource exploration and data acquisition under Arctic sea ice. An ultra-precise inertial navigation system can, in principle, be constructed by an accelerometer, gyroscope, and gravity gradiometer. Among them, the gyroscope and gravity gradiometer are key components to get high performance. I will talk about our experimental efforts to improve the precision of inertial navigation using both classical and quantum sensors.

SE-06-03

## Rotation sensing with the BIGTOP gyroscope

**Cass Sackett***University of Virginia*

---

### Abstract

Precision rotation sensing is useful for navigation, geophysics, and tests of fundamental physics. Atom interferometers provide, by some measures, the most sensitive method for rotation sensing achieved to date. However, the best performance requires freely falling atoms in a large experimental apparatus. Many applications, such as navigating a vehicle, will benefit from a more compact geometry. One method to achieve this is by using trapped atoms that are suspended against gravity. BIGTOP (Bragg Interferometer Gyroscope in a Time-Orbiting Potential) implements such an interferometer. It has been used to measure a rotation rates comparable to that of the Earth, and recent improvements provide an enclosed area approaching 10 mm<sup>2</sup>.

SE-06-04

## Development of transportable atomic gravimeters for field applications

**Ken'ichi Nakagawa**

*Institute for Laser Science, University of Electro-Communications, Japan*

---

### Abstract

Atomic interferometers are promising technology for precision measurements of gravity and inertial forces. Atomic gravimeters based on atomic interferometry are expected to be high-precision gravimeters for geodesy, metrology, and geophysics. Transportable atomic gravimeters are required in the field applications such as seismology, gravity mapping. We have developed a transportable atomic gravimeter for the field applications. Our atomic gravimeter is based on an atomic interferometer with cold  $87\text{Rb}$  atoms. We have developed a compact sensor head for the  $87\text{Rb}$  atomic interferometer using a small glass cell. The sensor head has a height of 60cm and a diameter of 24 cm. We have also developed a compact laser system based on fiber optics and frequency doubling of diode lasers at 1560 nm. Fast frequency switching of diode lasers enables to produce the lasers for cooling, Raman transition, and detection. In our preliminary experiment, we could measure the interferometer fringe signal and determine the gravity acceleration  $g$  with a precision of about  $dg/g = 10^{-5}$ . By optimizing the system, the sensitivity is expected to be improved by more than two orders. We will discuss the further investigation toward the realization of practical transportable atomic gravimeters for the field applications.

SE-07-01

## A Lu<sup>+</sup> optical clock

**Murray D Barrett**

*Center for Quantum Technologies, Singapore*

---

### **Abstract**

We give an overview of the Lu<sup>+</sup> optical clock system developed in Singapore. We outline the favorable properties and advantages this system affords as a high performance frequency standard. Supporting data demonstrating high accuracy performance of a Lu<sup>+</sup> frequency standard will also be presented.

## Optical clocks based on multi-ion systems

**Kazuhiro Hayasaka**

*Advanced ICT Research Institute, National Institute of Information  
and Communications Technology, Japan*

---

### Abstract

The most successful implementations of the optical clock are single-ion clocks and optical lattice clocks. In contrast to the large signal to noise ratio with many atoms in the latter that of the former is limited by single ion. However, in most of the ion clocks a single ion in a Paul trap has been used. In this presentation we discuss our experimental studies to overcome inhomogeneous frequency shifts of the ions, which hinder extension to multi-ion systems. The one of the major shifts is the electric quadrupole shift associated with the electric field. In the first strategy we use ion species with null electric quadrupole moment.  $^{115}\text{In}^+$  ions in a linear trap realize the extension to a multi-ion clock. The second strategy is to engineer the trapping potential to suppress the quadrupole shift inhomogeneity. We have found that  $^{40}\text{Ca}^+$  ions in the 'iso-spacing potential' implemented with planar surface traps can be extended to the multi-ion clock. The last strategy uses the macroscopic coherence of  $\text{Ca}^+$  ions prepared in the iso-spacing potential. We found that coherent radiation by superradiance might be observed when more than 1000  $\text{Ca}^+$  ions with the suppressed quadrupole-shift inhomogeneity are coupled to an optical cavity.

SE-07-03

## **Strontium lattice clocks at PTB: transportable and in the lab**

**Christian Lisdat**

*Physikalisch-Technische Bundesanstalt, Germany*

---

### **Abstract**

I will present our developments in the field optical lattice clocks for applications in the laboratory and as transportable devices. The talk will address a new laboratory clock with the capability of cryogenic interrogation. I will present a new transportable interrogation laser system with below  $2\text{E-}16$  fractional frequency instability and our plans for a new transportable strontium lattice clock that targets  $1\text{E-}18$  uncertainty. Furthermore, I will discuss our progress concerning chip-based traps for strontium.

SE-07-04

## Lattice clock as a frequency standard for JST and UTC

**Tetsuya Ido***Space-Time Standards Laboratory, NICT, Japan*

---

### Abstract

The recent development of optical clocks inspires the expectation of a wide variety of potential applications. But the results have been still in the realm of proof of principle experiments. However, in recent years, optical lattice clocks have finally achieved a social implementation. At NICT, the optical lattice clock is operated intermittently to build a timescale with its scale interval adjusted to the one second provided by an optical lattice clock. The obtained data is also sent to the International Bureau of Weights and Measures (BIPM), where BIPM adjusts the frequency of UTC with reference to those data in addition to those from Cesium primary standards. I will talk about the details of the optically-steered timescale and also discuss possible redefinition of the SI second which may happen in ten years.

# Abstract

Tracks

## PL

### Plenary Sessions

Contents / Topics

Welcome from Organizing Committee and Hosting Ministries, Plenary Talks, Keynote Speeches

Tracks

## CP

### Quantum Computing Track

Contents / Topics

Quantum Computing with Atoms and Ions, Superconducting Quantum Computers(QC), Photonic QC, Young Researcher Session, Quantum Simulations, Semiconductor QC, Quantum Annealing Toward FTQC(Tutorial), Beyond NISQ/Toward FTQC Panel Discussion, Quantum Architecture, Quantum Algorithms, NISQ Algorithms, Quantum Algorithms for Chemistry

Tracks

## CC

### Quantum Cryptography & Communication Track

Contents / Topics

Quantum Internet, Quantum Cryptography(Up-to-date Technologies of Field and Satellite QKDs), Challenges for Quantum Technology Platform (QKD Networks, Satellite QKD and their integration), Industry Panel, Young Researcher Session  
\*\*CC-04 on 8th and CC-05, CC-06 on 9th Dec are supported by SIP (cross-ministerial Strategic Innovation promotion Program).

Tracks

## SE

### Quantum Sensing Track Short Presentations by Young Researchers

**SE-03A, 03B**

# 4<sup>th</sup> IFQMS

The 4th International Forum  
on Quantum Metrology and Sensing

## PROCEEDINGS

Short Presentations by Young Researchers  
Part 1: SE-03A

December 8th, 2021  
Online Conference (Zoom)

## Quantum Sensing Track : Short Presentations by Young Researchers

### SE-03A. Short Presentations by Young Researchers on SE-01, 04, 06, 07 Topics [4th IFQMS]

\*Note: Depending on the program, the order of presentations may change within the same group.

All the times in the program are Japan Standard time (GMT+9)

Dec 8 (Wed.)	Session / Presentation	Mentor / Presenter	Affiliation	ID
13:10-14:30	<b>SE-03A-<math>\alpha</math>1</b>			
	Mentor	Fedor Jelezko	Ulm U	
	Mentor	Takeshi Ohshima	QST	
	Mentor	Masaki Sekino	U Tokyo	
	Mentor	Takayuki Iwasaki	Tokyo Tech	
	Chair	Motofumi Fushimi	U Tokyo	
	Co-chair	Chikara Shinei	NIMS	
	Exploring NV center formation condition for high Econv and charge-state ratio of NV- and NV0 centers	Chikara Shinei	NIMS	SE-03A- $\alpha$ 1-01
	Sensitive atomic magnetometer beyond the standard quantum limit	Kosuke Shibata	Gakushuin U	SE-03A- $\alpha$ 1-02
	Imaging hydrodynamic flow in WTe <sub>2</sub> using cryogenic quantum magnetometry	Uri Vool	Harvard U	SE-03A- $\alpha$ 1-03
	Toward on-board magnetoencephalography with wearable magnetometers and active noise canceler	Xinyu Cao	U Tokyo	SE-03A- $\alpha$ 1-04
	Continuous-wave temperature sensing using RF-dressed states of nitrogen-vacancy centers in diamond	Hibiki Tabuchi	Keio U	SE-03A- $\alpha$ 1-05
	High-quality lead-vacancy centers in diamond by high-pressure and high-temperature annealing	Peng Wang	Tokyo Tech	SE-03A- $\alpha$ 1-06
	Magnetocardiography imaging of living rats using NV centers in Diamond	Ryoma Matsuki	Tokyo Tech	SE-03A- $\alpha$ 1-07
13:10-14:30	<b>SE-03A-<math>\beta</math>1</b>			
	Mentor	Satoshi Yamasaki	Kanazawa U	
	Mentor	Tokuyuki Teraji	NIMS	
	Mentor	Toshiharu Makino	AIST	
	Mentor	Akimichi Nakazono	YAZAKI	
	Chair	Hiroki Morishita	Kyoto U	
	Co-chair	Moriyoshi Haruyama	AIST	
	Probing correlated phenomena in 2D materials with diamond quantum sensors	Mark Ku	U Delaware	SE-03A- $\beta$ 1-01
	Electroluminescence observation of NV center in diamond lateral p-i-n diode	Moriyoshi Haruyama	AIST	SE-03A- $\beta$ 1-02
	Synthesis of HPHT diamond with controlled nitrogen concentration	Masashi Miyakawa	NIMS	SE-03A- $\beta$ 1-03
	Formation of diamond film containing perfectly aligned NV center ensembles at a high growth rate by high-power density plasma CVD	Takeyuki Tsuji	Tokyo Tech	SE-03A- $\beta$ 1-04
	High dynamic range current detection using a diamond quantum sensor	Yuta Shigenobu	Tokyo Tech	SE-03A- $\beta$ 1-05
	Vector DC magnetic field sensing with the reference microwave field using nitrogen vacancy centers in diamond	Takuya Isogawa	Keio U	SE-03A- $\beta$ 1-06
	Thermal effects on generation of spin defects in hexagonal boron nitride	Tetta Suzuki	Saitama U, QST	SE-03A- $\beta$ 1-07

Dec 8 (Wed.)	Session / Presentation	Mentor / Presenter	Affiliation	ID
13:10-14:30	SE-03A-γ1			
	Mentor	Keiichi Edamatsu	Tohoku U	
	Mentor	Ryosuke Shimizu	UEC	
	Mentor	Hiroataka Terai	NICT	
	Mentor	Ryo Okamoto	Kyoto U	
	Chair	Fumihiko China	NICT	
	Co-chair	Le Bin Ho	Tohoku U	
	Error-disturbance uncertainty relations in faraday measurements	Le Bin Ho	Tohoku U	SE-03A-γ1-01
	Hydrogen annealing effect on silicon optical waveguide	Yixin Wang	Tohoku U	SE-03A-γ1-02
	Wavelength-tunable broadband infrared quantum absorption spectroscopy in the mid-infrared region 2-5 μm	Masaya Arahata	Kyoto U	SE-03A-γ1-03
	Evaluation of superconducting nanowire single photon detectors for mid-infrared wavelengths	Yuki Gama	Kyoto U	SE-03A-γ1-04
	Phase retrieval of joint spectral amplitude	Kemeng Chen	UEC	SE-03A-γ1-05
	Temporal shaping of an entangled-photon wave packet by fourier optical synthesis	Hiroki Oshima	UEC	SE-03A-γ1-06
13:10-14:30	SE-03A-δ1			
	Mentor	Takuya Hirano	Gakushuin U	
	Mentor	Takashi Mukaiyama	Osaka U	
	Mentor	Masaki Ando	U Tokyo	
	Mentor	Tadashi Sakai	Tokyo Tech	
	Chair	Kiyotaka Aikawa	Tokyo Tech	
	Co-chair	Satoru Takano	U Tokyo	
	Cryogenic monolithic interferometer for sensing gravity gradient	Satoru Takano	U Tokyo	SE-03A-δ1-01
	Suspension noise measurements of cryogenic torsion pendulums with crystalline fibrifibres	Ching Pin Ooi	U Tokyo	SE-03A-δ1-02
	Angular sensor with a coupled cavity for gravity gradient sensing	Yuka Oshima	U Tokyo	SE-03A-δ1-03
	Towards sensitive accelerometers with levitated single nanoparticles	Kiyotaka Aikawa	Tokyo Tech	SE-03A-δ1-04
	Interferometric gyroscope using slow and continuous atomic beam	Tomoya Sato	Tokyo Tech	SE-03A-δ1-05
	Development of a quantum gyroscope based on a single ion trapping techniques	Ryoichi Saito	Osaka U	SE-03A-δ1-06
	Exponentially enhanced quantum metrology by quenching superradiant light-matter systems beyond the critical point	Karol Gietka	OIST	SE-03A-δ1-07
14:50-16:10	SE-03A-α2			
	Mentor	Fedor Jelezko	Ulm U	
	Mentor	Takeshi Ohshima	QST	
	Mentor	Masaki Sekino	U Tokyo	
	Mentor	Takayuki Iwasaki	Tokyo Tech	
	Chair	Chikara Shinei	NIMS	
	Co-chair	Motofumi Fushimi	U Tokyo	
	Three-layered magnetically shielded room for ultrahigh-sensitivity quantum sensing of biomagnetic signals	Motofumi Fushimi	U Tokyo	SE-03A-α2-01
	Super-resolution in nanoscale NMR	Nicolas Staudenmaier	Ulm U	SE-03A-α2-02
	Sensitivity of weight imaging using a hybrid system based on piezoactive magnetic material and diamond quantum sensor	Ryota Kitagawa	Tokyo Tech	SE-03A-α2-03
	Study on electron spin control method for high-sensitivity diamond quantum sensor	Hiroyoshi Tomioka	Tokyo Tech	SE-03A-α2-04
	Optically detected magnetic resonance spectra of silicon vacancies in 4H-SiC with different temperatures	Shu Motoki	QST, Saitama U	SE-03A-α2-05
	High efficiency formation of NV center inside diamond by femtosecond laser	Ryusei Yanoshita	Kyoto U	SE-03A-α2-06

Dec 8 (Wed.)	Session / Presentation	Mentor / Presenter	Affiliation	ID
14:50-16:10	<b>SE-03A-β2</b>			
	Mentor	Satoshi Yamasaki	Kanazawa U	
	Mentor	Tokuyuki Teraji	NIMS	
	Mentor	Toshiharu Makino	AIST	
	Mentor	Akimichi Nakazono	YAZAKI	
	Chair	Moriyoshi Haruyama	AIST	
	Co-chair	Hiroki Morishita	Kyoto U	
	AC magnetic field sensing with ensemble NV centers using electrical detection methods	Hiroki Morishita	Kyoto U	SE-03A-β2-01
	OPuS-MAGNM - miniaturized optically pumped solid state quantum magnetometers for space applications	Hannes Kraus	NASA	SE-03A-β2-02
	Development of phthalocyanine ion beam for creation of multiple NV centers.	Kosuke Kimura	QST, Gunma U	SE-03A-β2-03
	Fabrication of diamond protective film using microwave plasma CVD towards high-quality quantum emitters	Kazuki Hirokawa	Tokyo Tech	SE-03A-β2-04
	A compact quantum sensor head with side excitation of CVD diamond	Yuki Nishio	Tokyo Tech	SE-03A-β2-05
	Hybrid integration of Si <sub>3</sub> N <sub>4</sub> grating structure on diamond NV substrate for efficient photon extraction	Ryota Katsumi	Toyohashi Tech	SE-03A-β2-06
14:50-16:10	<b>SE-03A-γ2</b>			
	Mentor	Keiichi Edamatsu	Tohoku U	
	Mentor	Kenichi Nakagawa	UEC	
	Mentor	Ryosuke Shimizu	UEC	
	Mentor	Hirohiko Terai	NICT	
	Chair	Le Bin Ho	Tohoku U	
	Co-chair	Fumihiko China	NICT	
	Superconducting nanostrip single-photon detectors with dielectric multilayer cavities	Fumihiko China	NICT	SE-03A-γ2-01
	Estimation of the quantum efficiency of the up-conversion system based on injection-locked dual oscillators	Masayuki Hojo	Kyoto U	SE-03A-γ2-02
	Selective measurement of biexciton luminescence by photon correlation spectroscopy	Hiroya Seki	UEC	SE-03A-γ2-03
	Towards optical manipulation of gold-nanoparticles for efficient single photon sources	Rui Sun	Tohoku U	SE-03A-γ2-04
	Single photon emission from a quantum-dot-gold-nanostar coupled system on an optical nanofiber	Yining Xuan	Tohoku U	SE-03A-γ2-05
	Focusing constraints on coupling efficiency of collinear type-I degenerated SPDC photon pairs into a single-mode fiber	Nicolas Schwaller	Kyoto U	SE-03A-γ2-06

## Exploring NV center formation condition for high $E_{\text{conv}}$ and charge-state ratio of $\text{NV}^-$ and $\text{NV}^0$ centers

Chikara Shinei<sup>1</sup>, Masashi Miyakawa<sup>1</sup>, Shuya Ishii<sup>2</sup>, Seiichi Saiki<sup>2</sup>, Shinobu Onoda<sup>2</sup>,

Kenji Watanabe<sup>1</sup>, Takashi Taniguchi<sup>1</sup>, Takeshi Ohshima<sup>2</sup> and Tokuyuki Teraji<sup>1</sup>

<sup>1</sup>National Institutes for Materials Science

<sup>2</sup>National Institutes for Quantum Science

SHINEI.Chikara@nims.go.jp

### Introduction

Negatively-charged NV center ( $\text{NV}^-$ ) is promising color centers for high sensitivity magnetometer due to its long coherence time ( $\sim 2$  ms) and clear Rabi and Ramsey contrast due to spin dependent fluorescence<sup>1</sup>. Weak DC magnetic signal detection such as detection of single-neuron action potential<sup>2</sup>, malarial hemozoin<sup>3</sup>, biological tissue<sup>4</sup>, and paleomagnetic in rocks<sup>5</sup>, has been demonstrated using ensemble of  $\text{NV}^-$  center. For the weak DC magnetic signal detection, diamond with  $[\text{N}^{\text{T}}]$  ranged from 1 to 30 ppm and  $[\text{NV}^-]$  ranged from 0.1 – 4 ppm is empirically suitable. Assuming that the detected volume of diamond is constant, the magnetic sensitivity is proportional to  $[\text{NV}^-]$  which corresponds to the number of elements of the magnetometer. Increasing of  $[\text{NV}^-]$  is the most important for improving the magnetic sensitivity. Generally, the conversion efficiency ( $E_{\text{conv}}$ ) from substitutional nitrogen ( $\text{N}_s^0$ ) to  $\text{NV}^-$  center,  $[\text{NV}^-]/[\text{N}_s^0]$ , must be increased in order to achieve higher  $[\text{NV}^-]$ <sup>6</sup>.

$\text{NV}^-$  centers has also neutral charged state ( $\text{NV}^0$ ) which shows no spin dependent fluorescence. Since  $\text{NV}^-$  and  $\text{NV}^0$  often coexist, fluorescence of  $\text{NV}^0$  becomes background and reduces fluorescence contrast of  $\text{NV}^-$ . Thus, suppression of  $\text{NV}^0$  formation while increasing  $E_{\text{conv}}$  (or  $[\text{NV}^-]$ ) is important for improving the sensitivity.

### Method and Result

Diamond single crystals used in this study were grown using either HPHT synthesis or CVD method. Substitutional nitrogen concentration was controlled by tuning concentration of Ti in the metal solvent for the former while by changing flow rate of nitrogen gas for the later. After the nitrogen doped diamond growth, an electron beam irradiation was applied with the total fluence of  $10^{17}$ - $10^{18}$   $\text{cm}^{-2}$  to create vacancies in the diamond. it was followed by vacuum annealing at  $1000^\circ\text{C}$  for 2h to form NV center in the diamond crystals. The number density ratio of  $\text{NV}^-$  to  $\text{NV}^0$  is estimated from the intensity ratio of their ZPL. The  $[\text{NV}^-]$  and  $[\text{N}^{\text{T}}]$  was estimated using EPR method at room temperature.  $[\text{N}^{\text{T}}]$  is equal to sum of  $[\text{NV}^-]$  and  $[\text{NV}^0]$ .

In FIG. 1, the relationship between  $[\text{NV}^-]/[\text{N}^{\text{T}}]$  and  $[\text{NV}^{\text{T}}]/[\text{N}^{\text{T}}]$  measured by EPR and PL is presented. Circles and squares respectively show synthesis method of HPHT and CVD. The color scale indicates substitutional nitrogen concentration  $[\text{N}^{\text{T}}]$  which was measured before electron beam irradiation process. The solid line shows the case in which  $[\text{NV}^-]$  is equal to  $[\text{NV}^{\text{T}}]$ , indicating all NV center is negative charge state. The rate of increase of  $[\text{NV}^-]/[\text{N}^{\text{T}}]$  with respect to  $[\text{NV}^{\text{T}}]/[\text{N}^{\text{T}}]$  becomes smaller when  $[\text{NV}^{\text{T}}]/[\text{N}^{\text{T}}]$  is larger than 20 – 30%. The result indicate that the NV centers were fully negatively charged when  $[\text{NV}^{\text{T}}]/[\text{N}^{\text{T}}]$  was up to about 20%. in our diamond samples. In the presentation, we will discuss physical picture of charge state of NV center depending on  $[\text{NV}^{\text{T}}]/[\text{N}^{\text{T}}]$ : equilibrium equation.

### Reference

<sup>1</sup> John F. Barry *et al.* *Rev. Mod. Phys.* **92**, 015004 (2020).

<sup>2</sup> J. F. Barry *et al.* *Proc. Natl. Acad. Sci. U.S.A.* **113**, 14133 (2016).

<sup>3</sup> I. Fescenko *et al.* *Phys. Rev. Applied* **11**, 034029 (2019).

<sup>4</sup> H. C. Davis *et al.* *Nat. Commun.* **9**, 131 (2018).

<sup>5</sup> D. R. Glenn *et al.* *Geochem. Geophys. Geosyst.* **18**, 3254 (2017).

<sup>6</sup> J. F. Barry *et al.* *Rev. Mod. Phys.* **92**, 015004 (2020).

This work was supported by MEXT Q-LEAP (JPMXS0118068379 and JPMXS0118067395). T. Teraji acknowledges the support of, JST CREST (JPMJCR1773), MIC R&D for construction of a global quantum cryptography network (JPMI00316), JSPS KAKENHI (Nos. 20H02187, 20H05661 and 19H02617). T. Teraji and S. Onoda acknowledge the support of JST Moonshot R&D (JPMJMS2062).

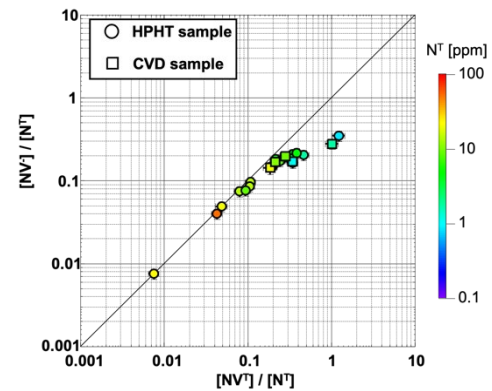


FIG. 1. The relationship  $[\text{NV}^-]/[\text{NT}]$  and  $[\text{NV}^-]/[\text{NV}^- + \text{NV}^0]$

## Sensitive atomic magnetometer beyond the standard quantum limit

Kosuke Shibata, Naota Sekiguchi, Aki Torii, Junnosuke Takai, and Takuya Hirano

*Department of Physics, Faculty of Science, Gakushuin University*

*shibata@go.phys.gakushuin.ac.jp*

### Introduction

Atoms can be used for sensitive magnetometry. While vapor magnetometers have achieved sub fT Hz<sup>-1/2</sup> sensitivities [1,2], cold atom gases may work as sensitive and spatially-resolved magnetometers due to small thermal diffusion. Magnetic field sensitivities in the state-of-art atomic magnetometers are limited by the so-called standard quantum limit (SQL), which results from quantum noises. Reduction of the quantum noises below the SQL has attracted attentions as a tool for enhancing performance of a magnetometer.

We have constructed a sensitive magnetometer using a Bose-Einstein condensate (BEC) of rubidium atoms [3]. Our BEC magnetometer sensitivity is already almost limited by quantum noises, consisting of the photon shot noise at detection and atomic spin shot noise. We aim to squeeze both of them to realize a sensitive magnetometer surpassing the classical ones.

### Method

We probe a BEC exhibiting the Larmor precession using a two-polarization phase contrast imaging. This imaging setup detects difference in phase shifts of orthogonal circular components of an off-resonant probe at 795 nm, which is proportional to the spin projection along the probe propagation axis and gives the information on the precession phase or a magnetic field at the atom position. The photon shot noise, which naturally appears in this difference detection, can be reduced by adding a squeezed light to the probe. We have successfully generated a squeezed light at the probe wavelength using waveguides and are now constructing a new squeezed light source near the BEC experiment machine. The two-polarization phase contrast detection will introduce spin squeezing on the basis of quantum nondemolition (QND) measurement of an atomic spin variable. We expect that planar squeezed state, which has quantum noise smaller than that in the coherent (classical) spin state in the plane of the Larmor precession [4,5], should be generated in our experiment. The planar squeezed state will improve the magnetic field sensitivity. We have conducted experiments to measure the atomic spin shot noise level and the spin squeezing. I will present on the details of these topics and our recent status.

This work was supported by MEXT Q-LEAP Grant Number JPMXS0118070326.

### Reference

- <sup>1</sup>I.K. Kominis, T. W. Kornack, J. C. Allred, and M. V. Romalis, *Nature (London)*, **422**, 596-599 (2003).
- <sup>2</sup>S.-K. Lee, K. L. Sauer, S. J. Seltzer, O. Alem, and M. V. Romalis, *Applied Phys. Lett.*, **89**, 214106596-599 (2006).
- <sup>3</sup>N. Sekiguchi, K. Shibata, A. Torii, H. Toda, R. Kuramoto, D. Fukuda, and T. Hirano, *Phys. Rev. A*, **104**, L041306 (2021).
- <sup>4</sup>Q. Y. He, Shi-Guo Peng, P. D. Drummond, and M. D. Reid, *Phys. Rev. A*, **84**, 022107 (2011).
- <sup>5</sup>G. Puentes, G. Colangelo, R. J. Sewell, and M. W. Mitchell, *New. J. Phys.*, **12**, 053007 (2013).

SE-03A- $\alpha$ 1-03**Imaging hydrodynamic flow in  $WTe_2$  using cryogenic quantum magnetometry**

Uri Vool<sup>1,2</sup>, Assaf Hamo<sup>2</sup>, Georgios Varnavides<sup>3,4,5</sup>, Yaxian Wang<sup>3</sup>, Tony X. Zhou<sup>2,3</sup>, Nitesh Kumar<sup>6</sup>, Yuliya Dovzhenko<sup>2</sup>, Ziwei Qiu<sup>2,3</sup>, Christina A. C. Garcia<sup>3</sup>, Andrew T. Pierce<sup>2</sup>, Johannes Gooth<sup>2,6,7</sup>, Polina Anikeeva<sup>4,5</sup>, Claudia Felser<sup>3,6</sup>, Prineha Narang<sup>3</sup>, and Amir Yacoby<sup>2,3</sup>.

<sup>1</sup>John Harvard Distinguished Science Fellows Program, Harvard University

<sup>2</sup>Department of Physics, Harvard University

<sup>3</sup>John A. Paulson School of Engineering and Applied Sciences, Harvard University

<sup>4</sup>Department of Materials Science and Engineering, Massachusetts Institute of Technology

<sup>5</sup>Research Laboratory of Electronics, Massachusetts Institute of Technology

<sup>6</sup>Max-Planck-Institut für Chemische Physik Fester Stoffe, Dresden

<sup>7</sup>Institut für Festkörper- und Materialphysik, Technische Universität Dresden

Hydrodynamic electron flow, where electrons in a conductor flow collectively - akin to a fluid, is a unique signature of strong electron interactions in a material. This effect has been observed in 2D materials, but observations in bulk materials are intriguing as high-carrier density should screen the interactions. In this talk, I will discuss a recent measurement of hydrodynamic flow in the semimetal  $WTe_2$ , allowing us to gain insight into the microscopic origin of its electron interactions<sup>1</sup>.

We image the spatial profile of the electric current by using a nitrogen-vacancy scanning tip. Using coherent quantum sensing, we obtain magnetic field resolution of  $\sim 10$  nT and spatial resolution of  $\sim 100$  nm. The current pattern we observe differs substantially from the flat profile of a normal metal and indicates correlated flow through the semimetal. The pattern also shows non-monotonic temperature dependence, with hydrodynamic effects peaking at  $\sim 20$  K.

We compare our results to a model which combines ab initio electron scattering rates and the electronic Boltzmann transport equation. The model shows quantitative agreement with our measurement, allowing us to extract the strength of electron-electron interactions in our material. Furthermore, we conclude that electron interactions are phonon-mediated. This result opens a path for hydrodynamic flow and strong interactions in a variety of new materials.

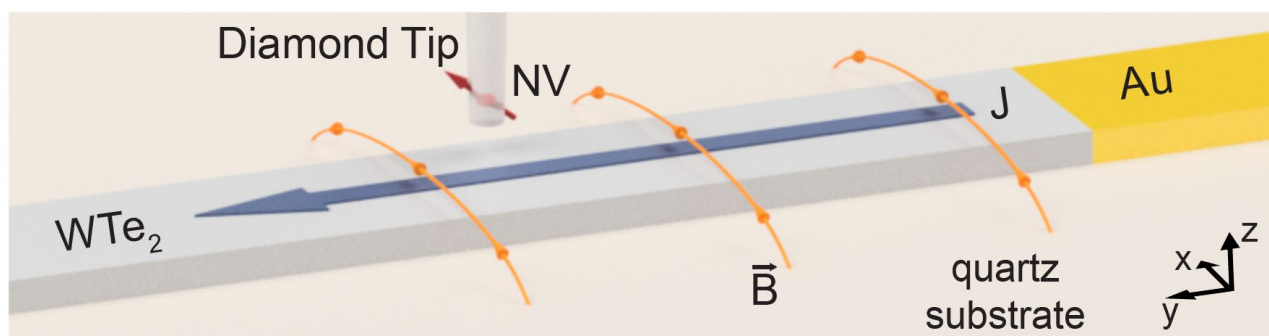


FIG. 1. Measurement technique: imaging local current flow by the effect of its induced magnetic field on a nitrogen-vacancy sensor in a diamond tip.

**Reference**

<sup>1</sup>U. Vool, A. Hamo, G. Varnavides, Y. Wang *et. al.* *Nature Physics* 17 1216-1220 (2021)

## Toward on-board magnetoencephalography with wearable magnetometers and active noise canceler

Xinyu Cao<sup>1</sup>, Zonghao Xin<sup>1</sup>, Akihiro Kuwahata<sup>2</sup>, Motofumi Fushimi<sup>1</sup>, Shinichi Chikaki<sup>1</sup>, Kazuhiro Oyama<sup>3</sup>, Yuki Anno<sup>3</sup>, Teppei Yoshida<sup>3</sup>, Takayuki Shibata<sup>3</sup>, Yuichiro Shirota<sup>4</sup>, Masato Yumoto<sup>4</sup>, Hiromasa Sawamura<sup>4</sup>, Mutsuko Hatano<sup>5</sup>, Takashi Yatsui<sup>6</sup>, and Masaki Sekino<sup>1</sup>

<sup>1</sup>Graduate School of Engineering, The University of Tokyo

<sup>2</sup>Graduate School of Engineering, Tohoku University

<sup>3</sup>DENSO Corporation

<sup>4</sup>Graduate School of Medicine, The University of Tokyo

<sup>5</sup>Department of Electrical and Electronic Engineering, Tokyo Institute of Technology

<sup>6</sup>Graduate School of Engineering, Toyohashi University of Technology

caoxinyu@g.ecc.u-tokyo.ac.jp

### Introduction

Magnetoencephalography (MEG) is a non-contact biosignal measurement with high temporal and spatial resolution, which has the potential to replace electroencephalogram (EEG) in various application scenarios. This study investigated the feasibility of using wearable magnetometers for applications in on-board MEG. The results provide guidance information for the development of MEG on-board measurement.

### Methods

In this study, we proposed the potential application of wearable sensors in on-board MEG measurement, as shown in Figure 1. The steady state visually evoked response (SSVER) signals were measured with superconducting quantum interference devices (SQUIDs), and the signal distribution at potential on-scalp sensor positions were reconstructed with spherical head model [1] and minimum norm estimation (MNE) method [2]. The magnetic fields inside a real car were measured. Noise reduction strategies based on active noise canceler for on-board applications were proposed.

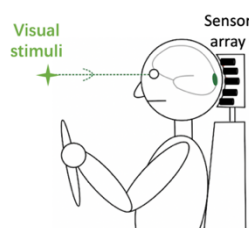


FIG. 1. Schematic diagram of on-board MEG measurement based on wearable sensors.

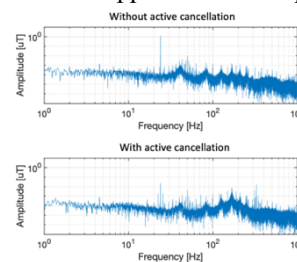


FIG. 2. The FFT of recorded magnetic field without/with active cancellation. Note the change of the peak at 24 Hz.

### Results and Discussion

The signal of the simulated wearable sensors is about 3 times that of the SQUID signal in this experiment. After the engine was started, the AC magnetic field inside a gasoline car in an urban environment is about 7 times larger in the vertical direction than in the horizontal direction. The piston movement of the internal combustion engine and the engine fan may be two of the main causes of the magnetic field noise in the car. The highest signal-to-noise ratio of SSVER is -110 dB in this case. A 350 mm 20-turn active cancel coil can attenuate noise by about 28 dB at the target frequency, as shown in Figure 2.

### Acknowledgements

This work was supported by MEXT Q-LEAP Grant Number JPMXS0118067395.

### References

- <sup>1</sup>J. C. Mosher, R. M. Leahy and P. S. Lewis, *IEEE Trans. Biomed. Eng.*, **46**, 245-259(1999).
- <sup>2</sup>S. Baillet, J. C. Mosher and R. M. Leahy, *IEEE Signal Process Mag.*, **18**, 14-30(2001).

## Continuous-Wave Temperature Sensing using RF-Dressed States of Nitrogen-Vacancy Centers in Diamond

Hibiki Tabuchi<sup>1,2</sup>, Yuichiro Matsuzaki<sup>3</sup>, Noboru Furuya<sup>1</sup>, Yuta Nakano<sup>4</sup>, Hideyuki Watanabe<sup>3</sup>,  
Norio Tokuda<sup>4,5</sup>, Norikazu Mizuochi<sup>6</sup>, and Junko Ishi-Hayase<sup>1,2</sup>

<sup>1</sup>School of Fundamental and Technology, Keio University, Japan

<sup>2</sup>Center for Spintronics Research Network, Keio University, Japan

<sup>3</sup>National Institute of Advanced Industrial Science and Technology (AIST), Japan

<sup>4</sup>Graduate School of Natural Science and Technology, Kanazawa University, Japan

<sup>5</sup>Nanomaterials Research Institute, Kanazawa University, Japan

<sup>6</sup>Institute for Chemical Research, Kyoto University, Japan

hibiade0914@keio.jp

### Introduction

Nowadays, there is a growing need to measure temperature with high sensitivity and special resolution to investigate the properties of cells or nanodevices. A nitrogen-vacancy (NV) center in diamond is a promising candidate to realize a sensitive temperature sensor with a high sensitivity and a special resolution. The temperature sensing using continuous-wave optically-detected magnetic resonance (CW-ODMR) has advantages because this can be simply implemented by continuous applications of a green laser and a microwave field. However, the temperature sensitivity with CW-ODMR is typically worse than that with pulsed-ODMR. Here, we propose a novel way to improve the sensitivity of temperature sensing using CW-ODMR with a quantum state dressed by radio-frequency (RF) fields under the transverse magnetic fields.

### Method

Under applying the transverse magnetic fields with respect to the NV axis, the ground electronic spin states of NV center are composed of  $|B\rangle = (|+1\rangle + |-1\rangle)/\sqrt{2}$ ,  $|D\rangle = (|+1\rangle - |-1\rangle)/\sqrt{2}$ . The transition between  $|D\rangle$  and  $|B\rangle$  can be occurred by applying the resonant RF fields, which results in splitting into quantum states dressed by the RF fields as shown in Fig. 1(a). As the temperature increases, the resonant frequency of RF-dressed state shifts due to the change in the zero-field splitting -  $74.2 \text{ K}/\sqrt{\text{Hz}}$ . Therefore, a temperature change can be estimated by measuring the temperature shift of RF-dressed state observed in CW-ODMR spectra. The CW-ODMR spectra were measured by simultaneous application of continuous-wave of laser, MW, and RF fields as shown in Fig. 1 (b).

### Results and Discussion

Fig. 1(c) shows the observed CW-ODMR spectra with the RF fields under the application of the transverse magnetic fields. It is found the 4 peaks are clearly observed, which confirms the creation of RF-dressed states. The estimated sensitivity of the temperature sensing is calculated to be  $73.0 \text{ mK}/\sqrt{\text{Hz}}$  under the optimal conditions for the laser power, MW and RF field intensities, and this value is 6 times better than that with the conventional scheme. This is because the linewidth becomes narrower by suppressing the effect of the strain variations with increasing RF intensity. Moreover, the sharp dip structure observed in the CW-ODMR contributes to improving the sensitivity.

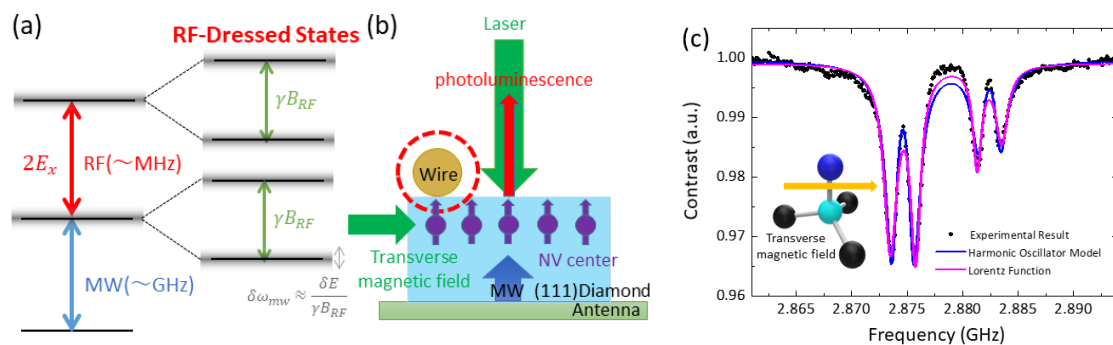


FIG. 1. (a) The energy diagram of our system (b) Experimental setup to measure the CW-ODMR (c) Experimental Result

This work was supported by MEXT Q-LEAP (No. JPMXS0118067395), MEXT KAKENHI (No. 18H01502), and CSRN, Keio University. This work was also supported by Leading Initiative for Excellent Young Researchers MEXT Japan and JST presto (Grant No. JPMJPR1919) Japan.

### Reference

- <sup>1</sup>T. Yamaguchi, *et al.*, Jpn. J. Appl. Phys., **58**, 100901 (2019). <sup>2</sup>Y. Matsuzaki, *et al.*, J. Phys. Condens. Matt., **28**, 275302 (2016).  
<sup>3</sup>K. Hayashi, *et al.*, Phys. Rev. Appl., **10**, 034009 (2018). <sup>4</sup>S. Saijo, *et al.*, Appl. Phys. Lett., **113**, 082405 (2018).

## High-quality lead-vacancy centers in diamond by high-pressure and high-temperature annealing

Peng Wang<sup>1</sup>, Takashi Taniguchi<sup>2</sup>, Yoshiyuki Miyamoto<sup>3</sup>, Mutsuko Hatano<sup>1</sup> and Takayuki Iwasaki<sup>1</sup>

<sup>1</sup>Department of Electrical and Electronics Engineering, School of Engineering, Tokyo Institute of Technology

<sup>2</sup>International Center for Materials Nanoarchitectonics, NIMS, Japan

<sup>3</sup>Research Center for Computational Design of Advanced Functional Materials, AIST, Japan

wang.p.ac@m.titech.ac.jp

### Introduction

Color centers in diamond have aroused great interests nowadays: especially heavy group-IV vacancy centers in diamond are expected to possess sharp Zero phonon lines (ZPLs) and predicted long spin coherence times<sup>1</sup>, serving as promising candidates for quantum network. However, the heavy atom (such as lead atom) suffers from difficulty in introducing into the diamond lattice during ion implantation, resulting in strong strained environment around lead vacancy (PbV) center. Such strained environment resulted in broad florescent emission, making it difficult to investigate properties of the PbV center. In order to observe its energetic structure and move forward to wavelength tuning or spin measurement, there is an urgent demand for high quality PbV whose fine structure could be clearly demonstrated, which requires an efficient approach to release the strain and recover defects formed during ion implantation.

### Method and Results

For the fabrication of high-quality PbV centers in diamond, we adopted high-pressure and high-temperature (HPHT) annealing after Pb ion implantation, at 2100°C under 7.7 GPa. Such a high temperature is considered to reduce the strain and recover defects in diamond, while the high-pressure condition maintains the stable phase of diamond. The same procedure has been proved to reduce inhomogeneous distribution of tin-vacancy center in diamond<sup>1,2</sup>.

We show a sharp and clear spectrum of single PbV at around 6 K, in which the linewidth of C-transition was limited to the spectrometer<sup>3</sup>. By recording Hanbury Brown-Twiss (HBT) measurement at varying excitation powers, the single configuration was confirmed by antibunching, and we were able to estimate the excited state lifetime according to time correlation<sup>4</sup>, ~3.7 ns, as shown in Fig. 1. Besides, our major concern is the strained environment around PbVs, which can be evaluated by their spectral distribution. We depicted the inhomogeneous distribution of the C-transition, which turned out a linewidth of 155 GHz, as shown in Fig. 2. Compared with former reported distribution of 10 nm with 950°C annealing<sup>5</sup>, our experimental results indicated that the inhomogeneous energetic distribution of PbVs were suppressed by HPHT annealing. Such narrow distribution is of vital importance for further research on photon indistinguishability.

This work was supported by Toray Science Foundation and MEXT Q-LEAP Grant Number JPMXS0118067395.

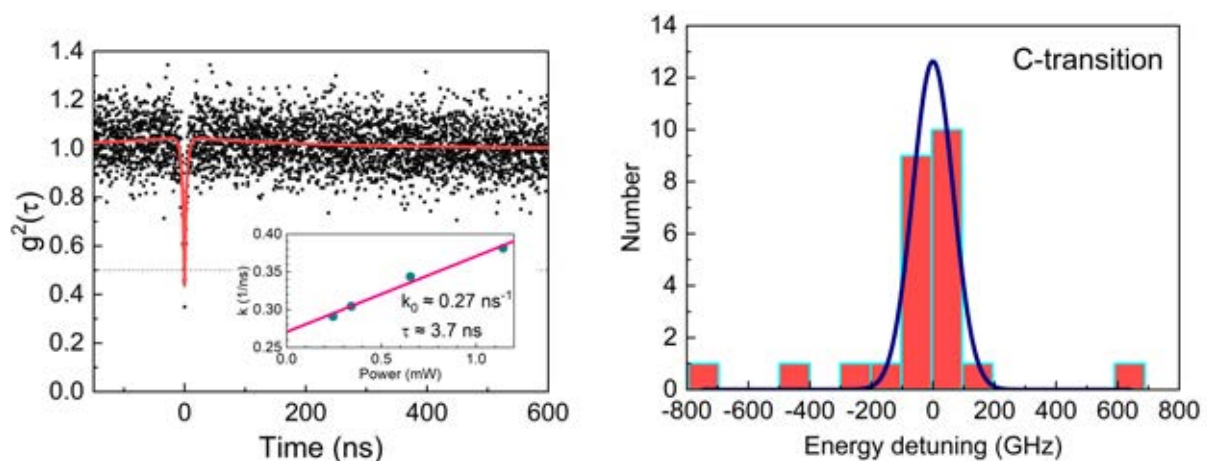


Fig.1 Estimated excited state lifetime of a single PbV

### Reference

1. Iwasaki, T. *et al.* Tin-Vacancy Quantum Emitters in Diamond. *Phys. Rev. Lett.* **119**, 253601 (2017).
2. Goertzt, J. *et al.* Spectroscopic investigations of negatively charged tin-vacancy centres in diamond. *New J. Phys.* **22**, 013048 (2020).
3. Wang, P., Taniguchi, T., Miyamoto, Y., Hatano, M. & Iwasaki, T. Low-Temperature Spectroscopic Investigation of Lead-Vacancy Centers in Diamond Fabricated by High-Pressure and High-Temperature Treatment. *ACS Photonics* **8**, 2947–2954 (2021).
4. Khalid, A. *et al.* Lifetime Reduction and Enhanced Emission of Single Photon Color Centers in Nanodiamond via Surrounding Refractive Index Modification. *Sci. Rep.* **5**, 11179 (2015).
5. Fröch, J. E. *et al.* Versatile direct-writing of dopants in a solid state host through recoil implantation. *Nat. Commun.* **11**, 5039 (2020).

## Magnetocardiography imaging of living rats using NV centers in Diamond

Ryoma Matsuki<sup>1</sup>, Keigo Arai<sup>1,2</sup>, Akihiro Kuwahata<sup>3</sup>, Daisuke Nishitani<sup>1</sup>, Ikuya Fujisaki<sup>1</sup>, Yuki Nishio<sup>1</sup>, Zonghao Xin<sup>3</sup>, Xinyu Cao<sup>3</sup>, Yuji Hatano<sup>1</sup>, Shinobu Onoda<sup>4</sup>, Chikara Shinei<sup>6</sup>, Masashi Miyakawa<sup>6</sup>, Takashi Taniguchi<sup>6</sup>, Masatoshi Yamazaki<sup>7,8</sup>, Tokuyuki Teraji<sup>5</sup>, Takeshi Ohshima<sup>4</sup>, Mutsuko Hatano<sup>1,4</sup>, Masaki Sekino<sup>3</sup>, and Takayuki Iwasaki<sup>1</sup>

<sup>1</sup>Department of Electrical and Electronics Engineering, School of Engineering, Tokyo Institute of Technology

<sup>2</sup>Japan Science and Technology PRESTO, Saitama, 332-0012, Japan

<sup>3</sup>Graduate School of Engineering, The University of Tokyo, Tokyo, 113-8656, Japan

<sup>4</sup>National Institutes for Quantum and Radiological Science and Technology, Takasaki, 370-1292, Japan

<sup>5</sup>Research Center for Functional Materials, National Institute for Materials Science, Tsukuba, 305-0044, Japan

<sup>6</sup>International Center for Materials Nanoarchitectonics, National Institute for Materials Science, Tsukuba, 305-0044, Japan

<sup>7</sup>Department of Cardiology, Nagano Hospital, Soja, 719-1126, Japan

<sup>8</sup>Medical Device Development and Regulation Research Center, The University of Tokyo, Tokyo, 113-8656, Japan  
matsuki.r.aa@m.titech.ac.jp

### Introduction

Diamond quantum sensors based on nitrogen-vacancy (NV) centers have high spatial resolution operated at room temperature even under large background magnetic fields. We constructed a sensor system suitable for bio-magnetic measurement that can take advantage of the ability to bring the NV center closer to the signal source under ambient operating conditions. In this study, we introduce magnetocardiography (MCG) signal, mm-scale MCG imaging, and reconstruction of current in living rats<sup>[1]</sup>.

### Experimental procedures and Results

We constructed a compact sample holder that allows the distance between a live rat heart and a diamond sample to be as close as about 1 mm as shown Fig.1(a), and measured MCG of living rats. Moreover, we conducted MCG imaging at  $11 \times 11 = 121$  measurement points over 30 mm by automatically moving the XY stage with rats on it, and reconstructed the current density using bfieldtools<sup>[2,3]</sup> an open-source Python software suite. As a result, we measured MCG in a living rat at several tens of nT as shown Fig. 1(b), and reconstructed the current density distribution from MCG imaging with mm-scale spatial resolution as shown Fig. 1(c)(d). In addition, we conducted experiments with multiple rats using this sensor system, and confirmed that similar results could be obtained.

### Acknowledgments

This work was supported by MEXT Q-LEAP Grant Number JPMXS0118067395.

### Reference

- [1] K.Arai et al., arxiv:2105.11676(2021).
- [2] Mäkinen, A. J. et al., J. Appl. Phys.128, 063906 (2020)
- [3] Zetter, R. et al., J. Appl. Phys.128, 063905 (2020)

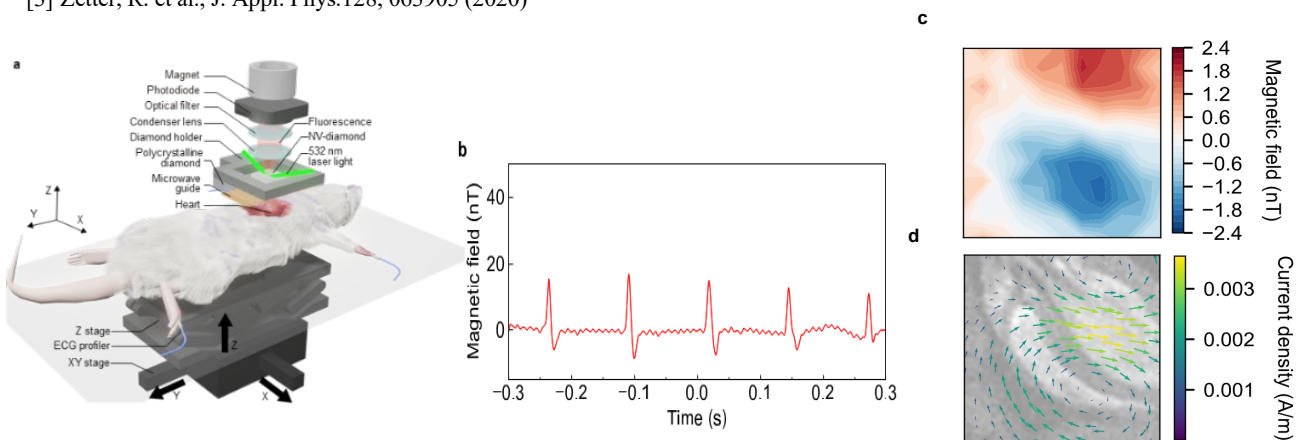


Fig.1 (a) Schematic of the rat MCG setup. (b) MCG signal from a rat. (c) (d) MCG imaging and reconstructed current distribution combined with MRI.

SE-03A- $\beta$ 1-01

## Probing correlated phenomena in 2D materials with diamond quantum sensors

Mark J.H. Ku<sup>1</sup>

<sup>1</sup>*Department of Physics and Astronomy and Department of Materials Science and Engineering, University of Delaware*

*mku@udel.edu*

Understanding correlated spin and charge phenomena presents a rich arena for discovering exotic behaviors in materials and plays a critical role in developing next-generation information processing capabilities. 2D systems realized with van der Waals materials provide particularly interesting platforms for exploring correlated phenomena because of novel effects associated with reduced dimensionality and the opportunity for drastic miniaturization and for creating new functionality. Hence, understanding correlated phenomena in 2D materials is a frontier in condensed matter physics; however, this effort encounters numerous challenges related to measurement techniques, including spatially-varying current or spin distribution, small device dimension, and complex device geometry (e.g. heterostructure). Due to the ability to image magnetic field from current and spins with high spatial resolution over wide temperature range, quantum sensing with nitrogen-vacancy (NV) centers in diamond provides a transformative tool for studying condensed matter phenomena. In this talk, I will discuss two topics in 2D materials probed with NV quantum sensing. We have directly imaged viscous flow of the Dirac electron fluid in graphene via NV magnetic imaging [1]. Understanding of the Dirac fluid presented in this work provides insight into strongly-correlated electrons such as those in high-temperature superconductors. Via NV magnetic imaging, we have also directly established room-temperature ferromagnetism in exfoliated flakes of Fe<sub>5</sub>GeTe<sub>2</sub> (FGT [2] for the first time as well as in Co-doped FGT (Co-FGT). As a step towards detecting magnons (spin excitations in 2D magnets, we have also obtained the first ferromagnetic resonance measurement of Co-FGT bulk crystal. These results contribute towards the applications of 2D magnets in technologies and devices.

### References

- [1] M.J.H. Ku, T.X. Zhou, Q. Li, Y.J. Shin, J.K. Shi, C. Burch, L.E. Anderson, A.T. Pierce, Y. Xie, A. Hamo, U. Vool, H. Zhang, F. Casola, T. Taniguchi, K. Watanabe, M.M. Fogler, P. Kim, A. Yacoby, and R.L. Walsworth, *Nature* **583**, 537 (2020).
- [2] Hang Chen, Shahidul Asif, Matthew Whalen, Jeyson Tamara-Isaza, Brennan Luetke, Yang Wang, Xinhao Wang, Millicent Ayako, Andrew F. May, Michael A. McGuire, Chitrleema Chakraborty, John Q. Xiao, and Mark J.H. Ku, *arXiv:2110.05314* (2021).

## Electroluminescence Observation of NV Center in Diamond Lateral p-i-n Diode

Moriyoshi Haruyama<sup>1</sup>, Hiromitsu Kato<sup>1</sup>, Masahiko Ogura<sup>1</sup>, Yukako Kato<sup>1</sup>, Takayuki Iwasaki<sup>2</sup>,  
Norikazu Mizuochi<sup>3</sup>, and Toshiharu Makino<sup>1</sup>

<sup>1</sup> National Institute of Advanced Industrial Science and Technology

<sup>2</sup> Department of Electrical and Electronics Engineering, School of Engineering, Tokyo Institute of Technology

<sup>3</sup> Institute for Chemical Research, Kyoto University

haruyama.moriyoshi@aist.go.jp

### Introduction

Nitrogen Vacancy (NV) center in diamond is one of the most studied color centers. Especially in negatively charged NV center (NV<sup>-</sup> center), electron spin state initialization and readout can be easily performed by laser irradiation. On the other hand, electrical manipulation of NV center without laser is required for chip-scale quantum device development. In 2013, two papers were reported about electroluminescence of NV center, however electrical excitation of NV<sup>-</sup> center was not realized. It can be expected that charge state of NV<sup>-</sup> center was stabilized by increasing electron concentration around NV center. To realize this, we fabricate high concentration phosphorus doped n layer. In this study, we tried observation of electroluminescence from NV center in the lateral p-i-n diode and investigate the electroluminescence characteristics.

### Method

We fabricated p-i-n diode by using microwave plasma enhanced chemical vapor deposition (CVD) method. The i layer was grown on the (111) Ib high pressure high temperature diamond substrate. The i layer was slightly doped phosphorus to stabilize charge state of NV<sup>-</sup> center (P concentration:  $10^{16}$  cm<sup>-3</sup>). Patterned boron doped p+ and phosphorus doped n+ layer were grown on the i layer. Both of boron and phosphorus concentration in p+ and n+ layer was  $10^{20}$  cm<sup>-3</sup>. After CVD growth, we performed nitrogen ion implantation and post-annealing to create NV center. Acceleration energy, ion fluence and implantation temperature were 350 keV  $5 \times 10^8$  cm<sup>-3</sup> and 600°C, respectively. Post-annealing temperature and time were 850°C, 30 min, respectively. After post-annealing, boiled acid mixture treatment (H<sub>2</sub>SO<sub>4</sub> and HNO<sub>3</sub>) was performed to terminate surface with oxygen. Electrode (Ti / Pt / Au) was created on both p+ layer and n+ layer.

### Results

Figure 1 (a) and (b) shows PL and EL CFM map in i layer. The EL measurement was performed under applied 30V of forward bias. As shown in these figure, isolated luminescent centers were observed at same position. Figure 1 (c) and (d) show PL and EL spectra of luminescence center. Zero phonon line of NV<sup>-</sup> center was detected from PL spectrum, while zero phonon line of NV<sup>0</sup> center was detected from EL spectrum. In these results, we succeed in electroluminescence observation of NV center by using lateral p-i-n diode. In presentation, we will report analysis result about NV<sup>-</sup> component in the EL spectrum.

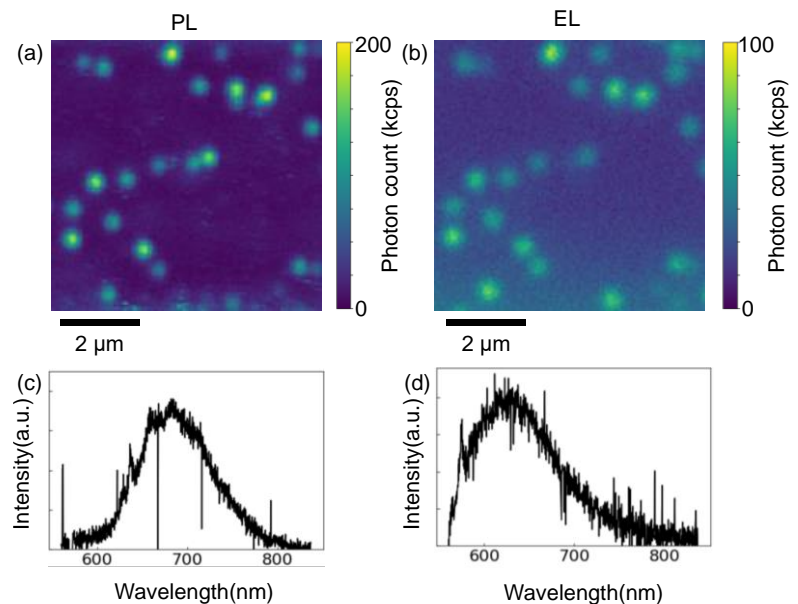


FIG. 1. (a) PL CFM map. (b) EL CFM map. (c) PL spectrum. (d) EL spectrum.

### Acknowledgement

This work was supported by MEXT Q-LEAP Grant Number JPMXS0118067395.

### Reference

- <sup>1</sup>N. Mizuochi et al., *Nature Photonics*, **6**, 299 (2012)
- <sup>2</sup>A. Lohrmann et al., *Applied Physics Letter*, **99**, 251106 (2011)

## Synthesis of HPHT diamond with controlled nitrogen concentration

Masashi Miyakawa<sup>1</sup>, Chikara Shinei<sup>1</sup>, Takashi Taniguchi<sup>2</sup>, and Tokuyuki Teraji<sup>1</sup>

<sup>1</sup> Research Center for Functional Materials, National Institute for Materials Science

<sup>2</sup> International Center for Materials Nanoarchitectonics, National Institute for Materials Science

MIYAKAWA.Masashi@nims.go.jp

### Introduction

For developing quantum sensing devices, it is essential to utilize diamonds containing NV center with desired concentration. The desired concentration of NV centers varies from 1 ppb to 10 ppm, depending on applications in quantum sensing devices. Thus, control of NV center concentration with a wide range is requested in diamond growth method. In case of diamonds grown under high-pressure and high-temperature (HPHT), NV centers are usually formed by electron beam irradiation to nitrogen-doped diamonds followed by post-annealing treatments. Here, precise control of the substitutional nitrogen (P1) center concentration during HPHT growth process with a wide range is a key for the concentration control of NV center. There were reports that nitrogen impurity was reduced to the limit by adding a nitrogen getter of Ti or Al,<sup>1-4</sup> but continuous control of nitrogen concentrations in wide range of the order of 100 to 0.1 ppm was not. In this paper, we will report the controllability of the nitrogen in the HPHT diamond synthesized with Co-Ti and Fe-Co-Ti base solvents by using Ti as a nitrogen getter.

### Method

Single-crystalline diamonds were grown in Co-Ti and Fe-Co-Ti solvents by a temperature-gradient method using a modified belt-type high-pressure apparatus. Graphite and diamond with different boron impurity levels were used as carbon sources. Pressure, temperature, and growth duration were 5.5 GPa and 1350°C for 40~80 h. Concentration of the P1 center was evaluated by electron spin resonance (ESR) measurements using a piece of diamond with (111) faces obtained by cutting parallel to (111) plane.

### Results and discussion

ESR measurements indicated P1 center concentrations were exponentially decreased from 100 ppm to 0.1 ppm with increasing amount of Ti additives in the Co-Ti solvent, which provides the nitrogen concentration in diamond crystals can be controlled by optimizing amount of Ti additive. In the Fe-Co-Ti solvents, P1 concentration was decreased from ~90 ppm to ~0.08 ppm with increasing amount of Ti additive up to 2 wt%, and efficiency of nitrogen gettering by Ti additives was higher compared with the Co-Ti solvents. Moreover, it was found that selection of carbon source became important when the P1 concentration < ~0.2 ppm. The result of SIMS measurements indicated that residual boron concentrations in the grown diamonds were ~0.2 ppm when graphite was used as a carbon source and ~0.02 ppm when CVD diamond was used. Residual boron compensates for the P1 center, leading to an unexpected lower concentration of the P1 centers in the grown diamonds. Therefore, utilizing a high-purity carbon source such as CVD diamonds was found to be efficient for suppressing contamination by boron impurities in the synthesized diamonds with the P1 concentration < ~0.2 ppm.

### Reference

<sup>1</sup>H. Sumiya, S. Satoh, *Diam. Relat. Mater.*, **5**, 1359 (1996).

<sup>2</sup>R.C. Burns, J.O. Hansen, R.A. Spits, M. Sibanda, C.M. Welbourn, D.L. Welch, *Diam. Relat. Mater.*, **8**, 1433 (1999).

<sup>3</sup>H. Kanda, *Braz. J. Phys.*, **30**, 482 (2000).

<sup>4</sup>A. D'Haenens-Johansson, K.S. Katruska, P.J. Moe, W. Wang, *Gems Gemol.*, **51**, 260 (2015).

### Acknowledgements

This work was supported by MEXT Q-LEAP Grant Number JPMXS0118068379.

SE-03A- $\beta$ 1-04

## Formation of diamond film containing perfectly aligned NV center ensembles at a high growth rate by high-power density plasma CVD

Takeyuki Tsuji<sup>1</sup>, Hitoshi Ishiwata<sup>1,2</sup>, Takeharu Sekiguchi<sup>1</sup>, Takayuki Iwasaki<sup>1</sup>, and Mutsuko Hatano<sup>1</sup><sup>1</sup>Department of Electrical and Electronics Engineering, School of Engineering, Tokyo Institute of Technology<sup>2</sup>PRESTO, Japan Science and Technology Agency

tsuji.t.ac@m.titech.ac.jp

Diamond film sensors with large volumes ( $> (0.5 \text{ mm})^3$ ) containing perfectly aligned nitrogen-vacancy (NV) ensembles performing high contrast ( $\approx 30\%$ ) are a promising material for achieving highly sensitive quantum magnetometers such as magnetoencephalography. The step-flow growth mode in which diamonds grow laterally by microwave plasma chemical vapor deposition (MPCVD) is required to realize aligned NV center ensembles. However, the conventional growth rate of aligned NV center ensembles was limited to a low value ( $0.05\sim 0.5 \mu\text{m/h}$ ) because a low gas flow ratio  $\text{CH}_4 / \text{H}_2$  ( $< 0.5\%$ ) is needed for step flow growth [1–3]. In addition, the nitrogen density of the NV center film should be controlled to below 30 ppm to obtain high contrast because the high nitrogen densities shorten the life-time of the excited-state and reduce spin polarization, which leads to decreased the contrast [4].

In this study, we achieved a high growth rate ( $6.6 \mu\text{m/h}$ ) of diamond film containing perfectly aligned NV ensembles with high contrast ( $30\%$ ) by applying high power density plasma ( $103 \text{ W/cm}^2$ ) and precisely controlling the flow rate ratios of  $\text{CH}_4 / \text{H}_2$  and  $\text{N}_2 / \text{CH}_4$ . For introducing high power density plasma, we used an MPCVD with a spherical chamber to reflectively concentrate microwaves on the diamond stage with a microwave antenna, and higher gas pressure up to 30 kPa was introduced to concentrate the plasma on the diamond substrate. The power density was varied as 42, 66,  $103 \text{ W/cm}^2$ , which belongs to the high-density regime ( $> 40 \text{ W/cm}^2$ ) among the previous diamond CVD studies [5]. The growth temperature of  $800^\circ\text{C}$  and growth time of 4 hours are fixed during the CVD growth.

The three-dimensional island growth was observed at the  $\text{CH}_4 / \text{H}_2$  of  $0.32\%$  because of the nucleation formed on the terraces. Then, the hydrogen etching of the nucleation formed on the terraces was induced by decreasing the  $\text{CH}_4 / \text{H}_2$  to below  $0.16\%$  leading to step-flow growth. Fig.1 shows that the growth rate of the diamond films with step flow growth were increased as the power density was increased. It was considered that increasing the power density, which can produce a large amount of carbon precursors while maintaining a low  $\text{CH}_4 / \text{H}_2$  of  $0.16\%$ , realized step-flow growth, leading to a high growth rate ( $6.6 \mu\text{m/h}$ ) with perfectly aligned NV center ensembles. The  $\text{N}_2 / \text{CH}_4$  ratio was also controlled to be lower than  $2.5\%$ , and the nitrogen density in the diamond film was kept below 30 ppm to obtain a high Rabi contrast ( $30\%$ ) as shown in Fig2. Moreover, we measured the  $T_2^*$  of the obtained diamond sensor films by the high growth rate with the Ramsey sequence using a large detection volume of approximately  $8000 \mu\text{m}^3$ . We confirmed that  $T_2^*$  ( $= 210 \text{ ns}$ ) obtained in this study is mainly limited by nitrogen electron spin bath density of the diamond film (24 ppm) [6] and no significant decrease in  $T_2^*$  due to the deterioration of the crystallinity of the diamond film including strain gradients was observed. This result is promising for building material technology for highly sensitive quantum sensors with large sensor volumes.

### Acknowledgment

This work was supported by MEXT Q-LEAP Grant Number JPMXS0118067395. and conducted at (NanofabPF, Tokyo Tech), supported by "Nanotechnology Platform Program" of the Ministry of Education, Culture, Sports, Science and Technology (MEXT), Japan, Grant Number JPMXP09F-21-IT-014.

### Reference

- [1] H. Ozawa, K. Tahara, H. Ishiwata, M. Hatano, and T. Iwasaki, Appl. Phys. Express **10**, 045501 (2017).
- [2] H. Ishiwata, M. Nakajima, K. Tahara, H. Ozawa, T. Iwasaki, and M. Hatano, Appl. Phys. Lett. **111**, 043103 (2017).
- [3] P. Balasubramanian, C. Osterkamp, Y. Chen, X. Chen, T. Teraji, E. Wu, B. Naydenov, and F. Jelezko, Nano Lett. **19**, 6681 (2019).
- [4] K. Mizuno, M. Nakajima, H. Ishiwata, M. Hatano, and T. Iwasaki, Appl. Phys. Express **14**, 032001 (2021).
- [5] T. Teraji, T. Yamamoto, K. Watanabe, Y. Koide, J. Isoya, S. Onoda, T. Ohshima, L. J. Rogers, F. Jelezko, P. Neumann, J. Wrachtrup, and S. Koizumi, Phys. Status Solidi **212**, 2365 (2015).
- [6] E. Bauch, S. Singh, J. Lee, C. A. Hart, J. M. Schloss, M. J. Turner, J. F. Barry, L. M. Pham, N. Bar-Gill, S. F. Yelin, and R. L. Walsworth, Phys. Rev. B Condens. Matter **102**, 134210 (2020).

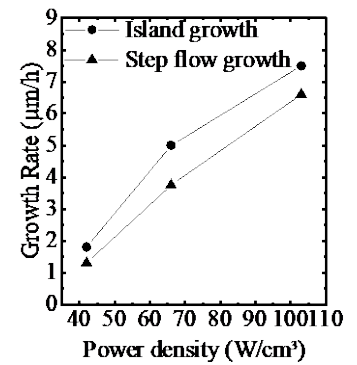


Fig.1. (a) Evolution of the growth rate of the CVD diamond films with island growth (triangular red dots) or the step-flow growth (circle black dots) as a function of the MW power density.

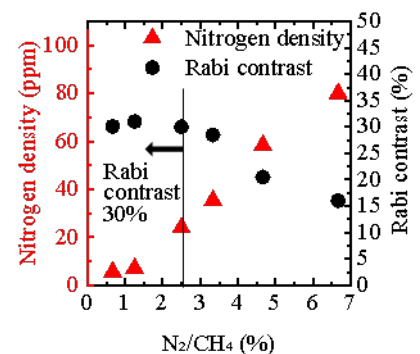


Fig.2. The nitrogen density in the CVD film (circle blue dots) and Rabi contrast (triangular red dots) dependence on  $\text{N}_2 / \text{CH}_4$ . To obtain high contrast ( $\approx 30\%$ ),  $\text{N}_2 / \text{CH}_4$  was controlled to be lower than  $2.5\%$ .

## High dynamic range current detection using a diamond quantum sensor

Yuta Shigenobu<sup>1</sup>, Yuji Hatano<sup>1</sup>, Jaewon Shin<sup>2</sup>, Junya Tanigawa<sup>2</sup>, Akimichi Nakazono<sup>2</sup>,  
Shinobu Onoda<sup>3</sup>, Takeshi Oshima<sup>3</sup>, Keigo Arai<sup>1</sup>, Mutsuko Hatano<sup>1,3</sup>, Takayuki Iwasaki<sup>1</sup>

<sup>1</sup>Department of Electrical and Electronics Engineering, School of Engineering, Tokyo Institute of Technology

<sup>2</sup>Yazaki Corporation,

<sup>3</sup>National Institutes for Quantum Science and Technology

Shigenobu.y.aa@m.titech.ac.jp

### Introduction

High dynamic range current detection is required to estimate the remaining charge in the battery and precisely predict the travelable mileage of EV. The maximum current flowing bus-bars connecting the battery will reach to several hundred amperes. Simultaneously, the measurement with 10 mA accuracy in the well-controlled temperature is required to expand the travelable mileage up to 10 %<sup>1</sup>. Thus, 5-digit dynamic range current sensor is crucial to realize an efficient battery system. In this study, to meet these requirements, we constructed a quantum sensor system using ensemble NV centers in diamond.

### Method

Experimental set-up to measure the bus-bar current with the diamond sensor is shown in FIG.1. The diamond sensor used was a (111) type-Ib HPHT crystal, with a size of  $2.0 \times 2.0 \times 1.0 \text{ mm}^3$  and  $3.0 \times 10^{18} \text{ cm}^{-2}$  EB irradiation. The sensor was attached to one end of a multi-mode fiber to excite by green laser and to collect the red fluorescence from the NV centers. The diamond sensor was placed perpendicular to the bus-bar to coincide the current magnetic field direction with the N-V axis. Since the magnetic field strength in the diamond sensor generated by the 1000 A bus-bar current was estimated to be 9 mT, 15 mT static magnetic field was applied by Nd magnets. The magnetic field was measured as the difference in the lock-in-amplifier (LIA) outputs in the two resonance frequencies generated by the microwave signal generator (SG)<sup>2</sup>.

### Result

The obtained spectrum of the magnetic field noise measured when SG and LIA were modulated by the frequency of  $F_{\text{mod}} = 20 \text{ kHz}$  and the depth of  $F_{\text{dev}} = 3.5 \text{ MHz}$  is shown in FIG.2. The noise floor of the sensor system was less than  $10 \text{ nT}/\sqrt{\text{Hz}}$ . This value is enough to measure the magnetic field generated by the 10 mA around the bus-bar. The current measurement procedure was as follows. The feedback path from LIA through integrator circuit to SG in FIG.1 is always stable if the magnetic field variation caused by the bus-bar current is within a few MHz, which we define as  $D$ , where the slope of CW-ODMR around the resonance frequency is monotonous. For the small range, a current pulse train with changing amplitude from 100 mA to 10 mA was applied and the 10 mA pulse could be detected as the change of the integrator output. Even if the current change was over  $D$ , the feedback was kept stable by repeating the intermittent adjustment of the center frequency of SG when the integrator circuit output reaches a predetermined value below  $D$  (for example,  $D/2$ ). The current was incremented or decremented with 30 A amplitude and 2 s width steps. We confirmed that the feedback path could track the current variation up to  $\pm 1000 \text{ A}$  provided.

This work was supported by MEXT Q-LEAP Grant Number JPMXS0118067395.

### Reference

<sup>1</sup> H. Sugiyama et al., OP2, IFQMS3 (2020)

<sup>2</sup> Y. Hatano et al., Appl. Phys. Lett. 118, 034001 (2021)

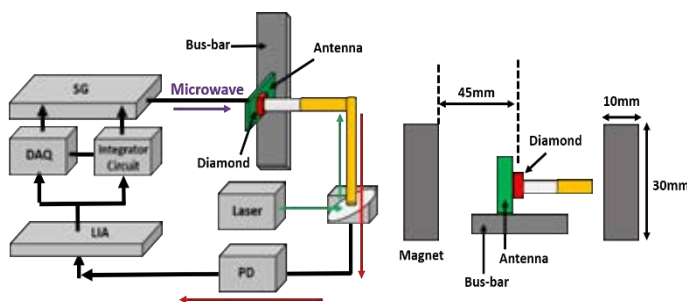


FIG.1 Experimental setup for measuring the bus-bar current with diamond sensor (left) and its expansion around the diamond sensor (right).

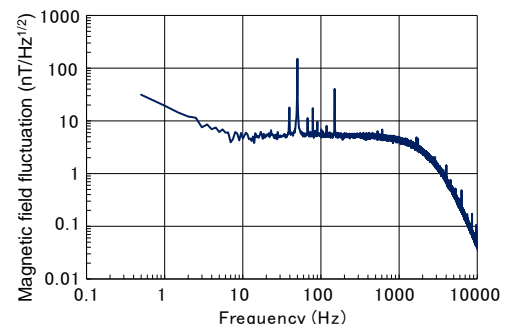


FIG.2 Measured noise spectrum of the diamond sensor at 15 mT magnetic field and 100 mW laser power.

## Vector DC magnetic-field sensing with reference microwave field using a single nitrogen-vacancy center in diamond

Takuya Isogawa<sup>1,\*</sup>, Yuichiro Matsuzaki<sup>2,†</sup>, and Junko Ishi-Hayase<sup>1,‡</sup>

<sup>1</sup>Department of Applied Physics and Physico-Informatics, Keio University, Yokohama 223-8522, Japan

<sup>2</sup>National Institute of Advanced Industrial Science and Technology, Ibaraki 305-8568, Japan

\*tisogawa@keio.jp †matsuzaki.yuichiro@aist.go.jp ‡hayase@appi.keio.ac.jp

### Introduction

The measurement of DC magnetic fields at the nanoscale is important in various fields such as condensed matter physics [1]. In particular, a single nitrogen vacancy (NV) center in diamond is a promising device to achieve high sensitivity and spatial resolution. Recent studies have shown that vector DC magnetic-field sensing using a single NV center provides higher readout contrast and spatial resolution compared to conventional methods using NV center ensembles [2, 3]. However, these methods require the application of a reference DC field that may disturb the target system in order to estimate the azimuthal angle of the target magnetic field with respect to the NV axis. This can be a severe problem for materials that are sensitive to static magnetic fields. Here, we propose a scheme to measure vector DC fields without a reference DC field. The azimuthal angle of the target magnetic field can be measured from the Rabi frequency, using the direction of the microwave field to drive the Rabi oscillation as a reference. The proposed scheme delivers a novel technique for sensitive vector DC magnetic-field sensing with a single NV center.

### Measurement of the azimuthal angle of the target DC magnetic field

The components perpendicular and parallel to the NV axis of the target magnetic field are estimated from the two resonance frequencies. While the azimuthal angle can be determined by applying a reference DC field to the system (Fig. 1a), our method provides a way to determine the azimuthal angle of the target field using the direction of the microwave as a reference (Fig. 1b). The perpendicular component of the target magnetic field tilts the quantization axis from the NV axis. When a linearly polarized resonant microwave is applied, Rabi oscillation occurs at the frequency proportional to the component of the microwave perpendicular to the quantization axis. Therefore, the tilt of the quantization axis can be determined from the Rabi frequency, and the direction of the applied DC magnetic field can be measured. Fig. 1c shows the sensitivity of the conventional scheme and our scheme. The simulation was performed by solving the master equation in the presence of Markovian dephasing. Here, we have used the same decay rate in the calculation of the sensitivity of both schemes. In the actual experiments, we expect that our scheme can achieve higher sensitivity because the coherence time of the Rabi oscillation is usually longer than that of the Ramsey interferometry.

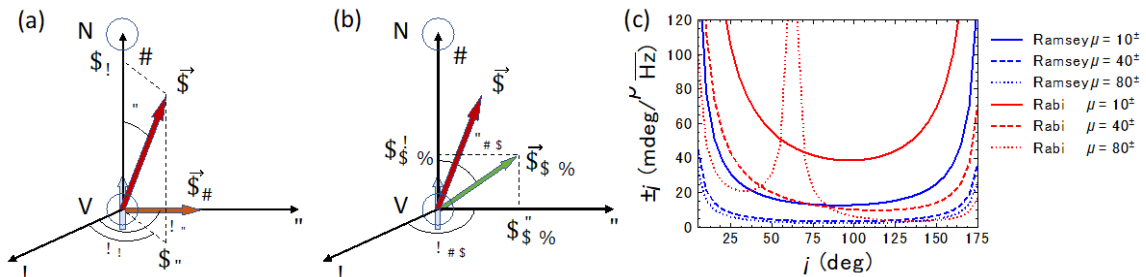


FIG. 1. (a) Configuration of NV axis, the target DC magnetic field, and the reference DC magnetic field. (b) Configuration of NV axis and the reference microwave field. (c) Sensitivity of the conventional scheme (blue) and our scheme (red) as a function of the azimuthal angle  $\phi$  for  $\theta = 10^\circ$  (solid),  $\theta = 40^\circ$  (dashed), and  $\theta = 80^\circ$  (dotted). Here we fix  $B = 8$  mT,  $B_{\text{mw}} = 1$  mT,  $B_r = 1$  mT, and  $\theta_{\text{mw}} = 20^\circ$ . The decay rate is  $1.0 \times 10^6$ .

### Acknowledgements

This work was supported by MEXT Q-LEAP (No. JPMXS0118067395), MEXT KAKENHI (No. 18H01502), and CSRN, Keio University. This work was also supported by Leading Initiative for Excellent Young Researchers MEXT Japan and JST presto (Grant No. JPMJPR1919) Japan.

### Reference

- <sup>1</sup>F. Casola, T. Van Der Sar, and A. Yacoby, Nature Reviews Materials **3**, 1 (2018).
- <sup>2</sup>X.-D. Chen, F.-W. Sun, C.-L. Zou, J.-M. Cui, L.-M. Zhou, and G.-C. Guo, Europhysics letters **101**, 67003 (2013).
- <sup>3</sup>Y.-X. Liu, A. Ajoy, P. Cappellaro, Physical Review Letters **122**, 100501 (2019).

## Thermal effects on generation of spin defects in hexagonal boron nitride

Tetta Suzuki<sup>1,2</sup>, Yuichi Yamazaki<sup>2</sup>, Takashi Taniguchi<sup>3</sup>, Kenji Watanabe<sup>3</sup>,  
Yu-Ichiro Matsushita<sup>4</sup>, Yuta Masuyama<sup>2</sup>, Yasuto Hijikata<sup>1</sup>, Takeshi Ohshima<sup>2</sup>

<sup>1</sup>Saitama Univ, <sup>2</sup>QST, <sup>3</sup>NIMS, <sup>4</sup>Tokyo Tech

t.suzuki.838@ms.saitama-u.ac.jp

### Introduction

There has been a lot of research on quantum sensors based on spin defects in wide gap semiconductors such as nitrogen-vacancy complex defect (known as NV center) in diamond, silicon vacancy in silicon carbide. Recently, hexagonal boron nitride (hBN), a 2D material, has been attracting attention as a new mother material for spin defect<sup>1,2</sup>. Energetic particle (electron, ion and neutron) irradiation is the most typical method to generate spin defects. However, such a method also introduces unnecessary defects degrading spin property of spin defect. Thermal treatment is a useful method to anneal residual defects. The effect after irradiation as well as during irradiation (high temperature irradiation) has been studied<sup>3,4</sup>. In this paper, we investigated the thermal effect on generation of boron vacancy defect ( $V_B$ ) in hBN.

### Method

We used hBN flakes on SiO<sub>2</sub>/Si substrate formed by tape transfer method which is commonly used in graphene research. 40 keV-N<sub>2</sub> ions were irradiated with the optimized fluence of  $1 \times 10^{15}$  cm<sup>-2</sup> at room temperature. Then, the irradiated sample was isochronally annealed up to 800 °C. For comparison, 40 keV-N<sub>2</sub> ion irradiation at elevated temperature up to 800 °C was carried out. The photoluminescence (PL) spectra were measured using a HORIBA LabRAM HR Evolution (laser wavelength: 532 nm, laser power: 0.1 mW). Optically detected magnetic resonance (ODMR) measurements were performed using a home-made confocal microscope. We used a software-based the lock-in detection for the ODMR measurements.

### Result

PL intensity and ODMR signal contrast as a function of treatment temperature were shown in Fig. 1 and 2. In the post-annealing experiment, the PL intensity remained almost the same up to 400 °C and then began to decrease at 500 °C, finally disappeared above 600 °C. ODMR signal contrast showed the similar trend and was maximized on 400 °C annealed sample. On the other hand, for high temperature irradiation, the PL intensity was maintained up to 600 °C, and no PL was shown above 700 °C. The 600 °C irradiated sample showed higher ODMR signal contrast from all other samples. These results concluded that high temperature irradiation is also useful for spin defect in 2D material.

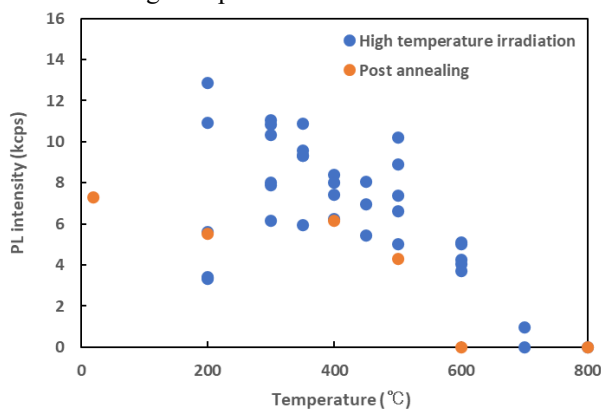


FIG. 1. Change of PL intensity

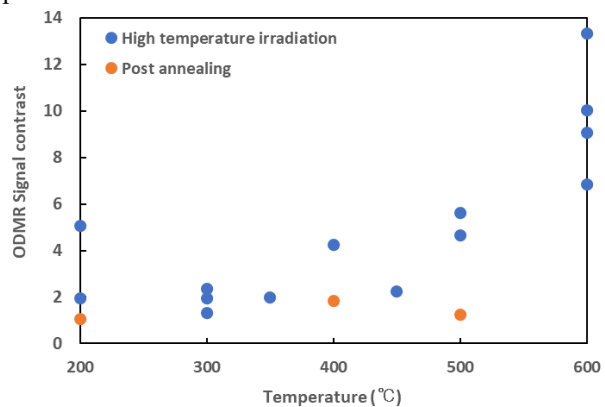


FIG. 2. Change of ODMR signal contrast

### Acknowledgement

This research is supported by QST President's Strategic Grant QST Creative Research and JSPS KAKENHI No. 20K05352.

### Reference

- <sup>1</sup>A.Gottsholl et al., Nat Mater. 19, 540 (2020). <sup>2</sup>M.Kianinia et al., ACS Photonics. 7, 2147 (2020).  
<sup>3</sup>M.Capelli et al., Carbon 143, 714 (2019). <sup>4</sup>Y.Chiba et al., Mater. Sci. Forum 1004, 337 (2020).

## Error-Disturbance uncertainty relations in Faraday measurements

Le Bin Ho<sup>1</sup>, and Keiichi Edamatsu<sup>1</sup>

<sup>1</sup>Research Institute of Electrical Communication, Tohoku University

binho@riec.tohoku.ac.jp

### Introduction

Quantum measurement plays a crucial role in the characterization of physical systems, which elucidate hidden quantum properties to the classical world. One of its important intrinsic properties is the uncertainty relation which is infeasible to measure incompatible observables with arbitrary precision. Heisenberg was first formulated an uncertainty relation between the position and momentum and later generalized by Arthurs and Kelly

$$\epsilon_A \eta_B \geq C_{AB},$$

that we call the Heisenberg-Arthurs-Kelly uncertainty. Here,  $\epsilon_A$  is the error when measuring  $A$  and  $\eta_B$  is the disturbance causes to  $B$  measurement,  $C_{AB} = |\langle \psi | [A, B] | \psi \rangle| / 2$ , where  $|\psi\rangle$  the system state to be measured.

Furthermore, Ozawa [1] and Branciard [2, 3], have considered a rigorous relation reads

$$\epsilon_A^2 \sigma_B^2 + \sigma_A^2 \eta_B^2 + 2\epsilon_A \eta_B \sqrt{\sigma_A^2 \sigma_B^2 - C_{AB}^2} \geq C_{AB}^2,$$

that hereafter we call the Branciard-Ozawa uncertainty, where  $\sigma_\Lambda = \sqrt{\langle \Lambda^2 \rangle - \langle \Lambda \rangle^2}$  represents the standard deviation of  $\Lambda$ .

Recently, Faraday measurements of spin based on an atom-light interface framework have been studied actively. It has contributed to our understating of quantum measurement of spin systems and has various applications in quantum metrology of atoms and spins, quantum information processing, strongly correlated systems, and many-body systems. The Faraday effect causes the rotation of the polarized light by the spin and thus allows indirect measurement of it via the polarized light. Such a measurement contains fundamental limits in the sensitivity caused by the quantum nature of light. Likewise, the back-action of the polarized light perturbs the spin state, which causes disturbance on the subsequent measurements of the spin. In this work, we formulate an atom-light interface scheme for evaluating uncertainty relations.

### Method

The atom is a single spin-1/2 particle interacting with a classical coherent polarized light. In this way, we derive the error and disturbance, and observe the cyclic oscillations as a result of the Faraday rotation and spin rotation as show in Fig. 1. Due to the rotation of the polarized light, the square error first is gradually decreases and then gradually reduces to the minimum at  $g = \pi/4$  and increases again at  $g = \pi/2$ . The behavior is then repeated when increasing  $g$ . Likewise, the square disturbance increases quadratically with the interaction strength and reaches the maximum at  $g = \pi/2$  and then decreases to zero for  $g$  varies from 0 to  $\pi$ . This behavior is the imprint of the back-action effect on the spin system that disturbs (rotates) the spin on its Bloch sphere.

Similarly, we investigate the case of polarization squeezed light using the phase-space approximation for the light, where the squeezing parameter takes place as a measurement strength. Larger squeezed parameter means broader Gaussian shape in the class of the polarization squeezed state, which is equivalent to “weak measurement”, while small squeezed parameter refers to the narrow of Gaussian shape which results in a strong measurement.

We finally formulate the error-disturbance relations in these cases above and provide that the Heisenberg-Arthurs-Kelly uncertainty can be violated while the tight Branciard-Ozawa uncertainty [2] always holds.

In conclusion, we evaluated the error, disturbance and uncertainty relations in quantum measurement in the atom-light interface framework of Faraday measurements. Our analysis would contribute to the understanding of the error and disturbance as well as the uncertainty principle in the spin measurements under the atom-light interface framework.

This work was supported by MEXT Q-LEAP Grant Number MXS0118067581.

### Reference

- <sup>1</sup> M. Ozawa, Error-disturbance relations in mixed states, arXiv:1404.3388 [quant-ph] (2014).
- <sup>2</sup> C. Branciard, Proceedings of the National Academy of Sciences **110**, 6742 (2013).
- <sup>3</sup> C. Branciard, Phys. Rev. A **89**, 022124 (2014).

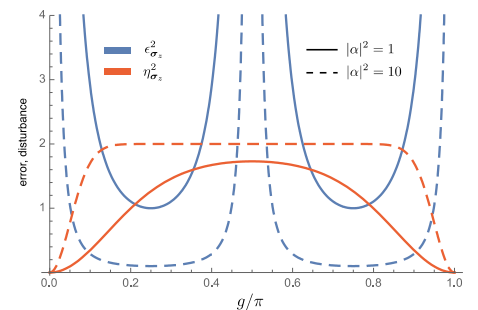


FIG. 1. The plot of the square error and square disturbance as functions of interaction strength.

## Hydrogen Annealing Effect on Silicon Optical Waveguide

Yixin Wang<sup>1</sup>, Kohei Haji<sup>2</sup>, Shunsuke Abe<sup>2</sup>, Takuya Inagaki<sup>2</sup>, Yoshiaki Kanamori<sup>3</sup>,  
Keiichi Edamatsu<sup>1</sup>, Hirohito Yamada<sup>2</sup>, Nobuyuki Matsuda<sup>2</sup>

<sup>1</sup>Research Institute of Electrical Communication, Tohoku University

<sup>2</sup>Department of Communications Engineering, Graduate School of Engineering, Tohoku University

<sup>3</sup>Department of Robotics, Graduate School of Engineering, Tohoku University

wangyixin@quantum.riec.tohoku.ac.jp

### Introduction

In recent years, micro-optical waveguides such as silicon optical waveguides have been attracting attention for large-scale integration of optical circuits. The main cause of propagation loss in silicon optical waveguides is light scattering due to the roughness of the surface of the waveguide core, especially at the side walls [1]. It is expected that the propagation loss of the silicon optical waveguide will be improved by minimizing the roughness of the silicon surface. Hydrogen annealing has been reported as one of the effective techniques for smoothing the silicon surface [2]. In this work, we applied hydrogen annealing to a silicon optical waveguide and evaluated the effect on a silicon optical waveguide.

### Method and Results

The channel waveguides were fabricated in 220-nm silicon on insulator (SOI) substrates. The resist pattern of the waveguides was formed by electron beam lithography. The pattern was transferred to silicon by using inductively-coupled plasma based reactive ion etching. The width of the waveguide was 440 nm, while both facets were designed to be as wide as 3  $\mu\text{m}$  for the effective coupling between a lensed fiber and the waveguide for transverse-electric (TE) mode.

The waveguides chip was then annealed in a hydrogen atmosphere. The temperature, pressure and annealing time were 800  $^{\circ}\text{C}$ , 5 kPa and 2 minutes, respectively. The optical properties of the waveguides were measured with an amplified spontaneous emission (ASE) light source before and after annealing. FIG.1 shows the waveguide insertion loss as a function of the waveguide length. In the measurement the input ASE light was filtered by a 1 nm band-pass filter with the center wavelength of 1550 nm before the waveguide. We see that the propagation loss increased after annealing. By using the cut-back method, we estimate that the propagation loss increased by 14.5 dB/cm while the coupling loss of the waveguide decreased by 1.17 dB/facet. The possible cause of the increase in propagation loss is that silicon may be oxidized at a high temperature [3] due to the presence of oxygen contained in the exposed  $\text{SiO}_2$  layer near the waveguide. FIG.2 shows the transmission spectra of the 1 cm long waveguide before and after annealing. After hydrogen annealing, the insertion loss of the waveguide increased significantly over the whole measurement range. However, the spectral ripple reduced after annealing, which may be due to the low Fabry-Perot interference caused by high propagation loss.

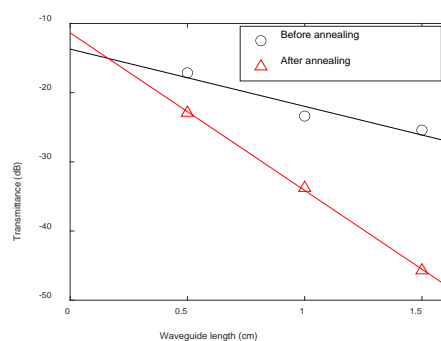


FIG. 1. Insertion loss vs. waveguide length.

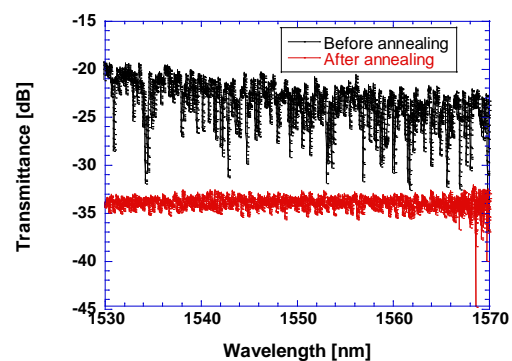


FIG.2. Transmission spectra.

### Acknowledgement

This work was supported by MEXT Q-LEAP Grant Number JPMXS0118067581.

### Reference

- <sup>1</sup> T. Horikawa *et al.*, MRS Communications **6**, 9 (2016).
- <sup>2</sup> T. Okatani *et al.*, Opt. Mater. Express **11**, 189 (2021).
- <sup>3</sup> K. Hofman *et al.*, Appl. Surf. Sci. **30**, 25 (1987).

## Wavelength-tunable broadband infrared quantum absorption spectroscopy in the mid-infrared region 2-5 $\mu\text{m}$

Masaya Arahata<sup>1</sup>, Yu Mukai<sup>1</sup>, Toshiyuki Tashima<sup>1</sup>, Ryo Okamoto<sup>1</sup>, and Shigeki Takeuchi<sup>1</sup>

<sup>1</sup>Department of Electronic Science and Engineering, Kyoto University, Japan

arahata.masaya.34c@st.kyoto-u.ac.jp

### Introduction

Infrared spectroscopy is a powerful technique enabling the noninvasive analysis of the dynamics of the molecular vibration and rotation modes, and an essential tool for material science and life sciences. However, a conventional infrared spectrometer has the problems that infrared light sources have large thermal noise and low directivity and infrared detectors need the cryogenic cooling for the high sensitivity. To overcome these problems, recently, infrared quantum absorption spectroscopy (IRQAS) has been proposed and experimentally demonstrated [1]. IRQAS enables the spectral measurement in the infrared region only with a low-cost and high-performance visible light source and detector using the quantum interference between the generation processes of entangled visible-infrared photon pairs. For the broadband IRQAS, some methods of broadening the generation bandwidths of photon pairs such as the group velocity phase matching were used to the IRQAS measurement [2]. However, the measurable wavelength ranges of IRQAS were limited to less than 1  $\mu\text{m}$  at most. Therefore, there are no IRQAS systems covering the mid-infrared (MIR) region 2-5  $\mu\text{m}$ .

Here, we report a wavelength-tunable IRQAS system covering the MIR region 1.9-5.2  $\mu\text{m}$ . The generation wavelengths of visible-infrared photon pairs can be tuned by rotating a nonlinear crystal with respect to the pump beam to control the phase matching condition [3]. We show the quantum interference is observed in the wavelength region of 2-5  $\mu\text{m}$  just by continuously rotating a crystal without the fine realignment. We also experimentally demonstrate the transmission spectrum measurement of a silica glass sample from the ratio of visibilities of interferogram with and without a sample. Furthermore, we demonstrate the transmittance measurement with a higher resolution with quantum Fourier-transform infrared spectroscopy (QFTIR), which enables the measurement in the whole spectrum of photon pairs from the Fourier analysis of the quantum interferogram [4].

### Method

Figure 1 shows our experimental setup of wavelength-tunable IRQAS system with the continuous crystal rotation. A 0.5-mm-thick type-I MgO:LiNbO<sub>3</sub> crystal with a cut angle of 57.9° is pumped by a CW laser beam with a wavelength of 532 nm. The pump beam is focused into the crystal by a lens ( $f=200$  mm). Signal (visible) photons with a wavelength of 692 nm and idler (infrared) photons with a wavelength of 2300 nm are generated in the case of the normal incidence of the pump beam on the crystal. The SPDC wavelengths can be tuned by rotating the crystal on a rotational stage with respect to the pump beam. When being separated by a dichroic mirror, the signal and pump photons pass through, while the idler photons are reflected. Then, the signal and pump photons are together reflected back to the crystal by a concave mirror ( $f=100$  mm). The idler photons are collimated by a lens ( $f=100$  mm) and then pass through an ultra-violet fused silica glass window with the thickness of 1 mm as a sample and are reflected by a mirror on a high-accurate translation stage with the position repeatability  $\pm 2$  nm. Then, at the crystal, the second SPDC generation process occurs by the reflected pump beam. After being collimated by a lens ( $f=250$  mm) and passing through a long pass filter, an iris as a spatial filter, and a tunable band pass filter on a translation stage to eliminate the residual pump beam and the background light, signal photons are coupled to a multimode fiber and then guided to a Si avalanche photodiode and a photon counter to measure the interference of the single photon counts. In this presentation, we will report on the results of transmittance measurement of the sample with the wavelength-tunable IRQAS system. This work was supported in part by the foundation of MEXT Q-LEAP Grant Number JPMXS0118067634, JST-CREST Grant Number JPMJCR1674, JSPS KAKENHI Grant Number 21H04444, Grant-in-Aid for JSPS Fellows Grant Number 20J23408, and WISE Program, MEXT.

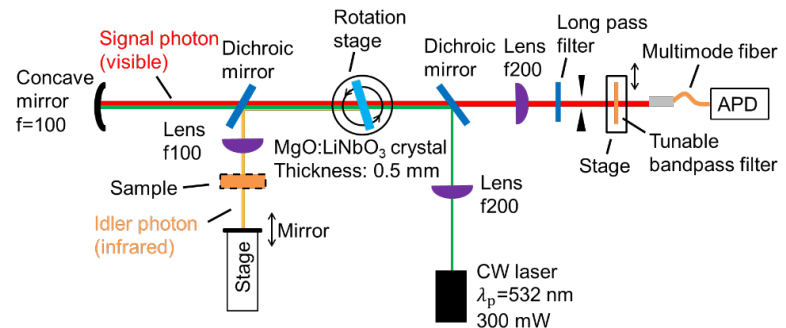


FIG. 1. Schematic of wavelength-tunable IR-QAS system. APD: Avalanche photodetector.

### Reference

- <sup>1</sup>D. Kalashnikov, A. Paterova, S. Kulik, and L. Krivitsky, *Nat. Photonics*, **10**, 98 (2016).
- <sup>2</sup>C. Lindner, J. Kunz, S. J. Herr, S. Wolf, J. Kießling, and F. Kühnemann, *Opt. Express*, **29**, 4035-4047 (2021).
- <sup>3</sup>M. Arahata, Y. Mukai, B. Cao, T. Tashima, R. Okamoto, and S. Takeuchi, *J. Opt. Soc. Am. B*, **38**, 1934-1941 (2021).
- <sup>4</sup>Y. Mukai, M. Arahata, T. Tashima, R. Okamoto, and S. Takeuchi, *Phys. Rev. Applied*, **15**, 034019 (2021).

## Evaluation of superconducting nanowire single photon detectors for mid-infrared wavelengths

Yuki Gama<sup>1</sup>, Toshiyuki Tashima<sup>1</sup>, Masaya Arahata<sup>1</sup>, Yu Mukai<sup>1</sup>, Fumihiro China<sup>2</sup>, Masahiro Yabuno<sup>2</sup>, Satoru Mima<sup>2</sup>, Shigeyuki Miyajima<sup>2</sup>, Shigehito Miki<sup>2</sup>, Hirota Terai<sup>2</sup>, Ryo Okamoto<sup>1</sup>, and Shigeki Takeuchi<sup>1</sup>

<sup>1</sup>Department of Electronic Science and Engineering, Kyoto University

<sup>2</sup>National Institute of Information and Communication Technology

takeuchi@kuee.kyoto-u.ac.jp

### Introduction

Recently, single-photon detection in the mid-infrared spectral region has attracted attention as a fundamental technique for many technologies such as infrared quantum absorption spectroscopy<sup>1,2</sup> and light detection and ranging (LIDAR)<sup>3</sup>. However, the single-photon detectors operating in that region suffers from the limited operating wavelength and low detection efficiency. One of the solutions is to use superconducting nanowire single-photon detector (SNSPD) which possesses single-photon detection ability and low dark count. Some researchers have developed SNSPDs for the mid-infrared spectral region and, for example, Verma *et al.* evaluated the detection performance of SNSPDs fabricated from WSi up to a wavelength of  $10\ \mu\text{m}$ <sup>4</sup>. However, the detection efficiency of such mid-infrared single-photon detectors has not been fully evaluated so far. In this presentation, we report the experimental evaluation of a NbTiN SNSPD working in the mid-infrared spectral region. We evaluated dark count and the linearity of detection count by changing the input photon number and the bias current. We also investigated the detection efficiency and obtained the value of  $1.20 \pm 0.40\%$  at the wavelength of  $4.33\ \mu\text{m}$  with the bias current of  $21.0\ \mu\text{A}$ .

### Method

We developed a NbTiN SNSPD for the mid-infrared single-photon detection. To improve the sensitivity for the mid-infrared single-photons, we fabricated the nanowire with thinner line width of  $50\ \text{nm}$  instead of typical  $80$  to  $100\ \text{nm}$  used for the SNSPD working in visible and telecommunication spectral region. The SNSPD also has a meander structure and the active area of  $15 \times 15\ \mu\text{m}^2$  (see figure 1(a) inset).

The experimental setup for evaluating SNSPD is shown in FIG. 1(a). We used quantum cascade laser (QCL) with a wavelength of  $4.33\ \mu\text{m}$ . The laser power was attenuated to the single photon level with the combination of neutral density filters and polarizers. The light was coupled to a single mode fiber and passed through a polarization controller which consists of a polarizer, a half-wave plate, and a quarter-wave plate. Using this system, the input photon polarization was optimized to maximize the detection count by the SNSPD. The output port of SNSPD was connected to an oscilloscope to observe the waveform of the output voltage pulse from SNSPD or a pulse counter to obtain the detection count. Here, FIG. 1(b) shows the waveform of the output voltage pulse from the SNSPD. We set threshold voltage of a pulse counter for each bias current with this result. Using these voltages, we evaluated dark count and the linearity of detection count by changing the input photon number and the bias current. In this presentation, we will report the evaluation results in more detail.

This work was supported by MEXT Q-LEAP Grant Number JPMXS0118067634. JST-CREST Grant Number JPMJCR1674, Grant-in-Aid for JSPS Fellows Grant Number 20J23408

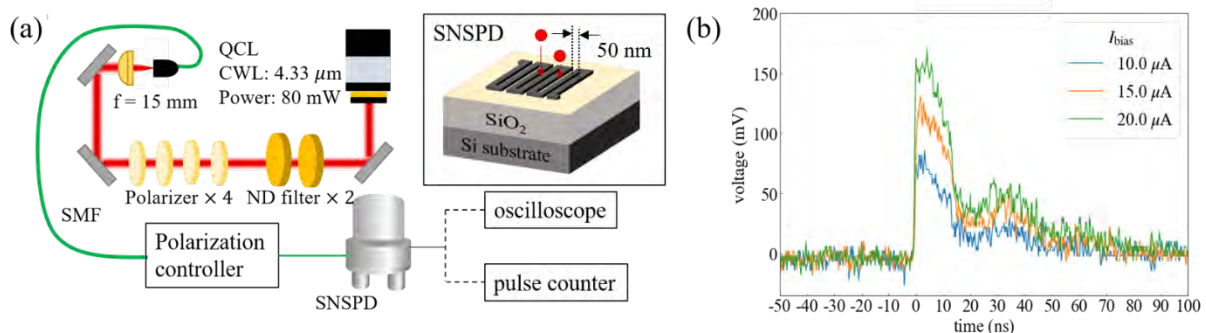


FIG. 1. (a) Experimental setup for the evaluation of mid-infrared SNSPD. ND filter: Neutral density filter, SMF: Single mode fiber. The inset shows the schematic of SNSPD. (b) The waveform of the output voltage pulse from mid-infrared SNSPD.

### Reference

- <sup>1</sup>D. Kalashnikov, A. Paterova, S. Kulik, and L. Krivitsky, *Nat. Photonics*, **10**, 98 (2026).
- <sup>2</sup>Y. Mukai, M. Arahata, T. Tashima, R. Okamoto, and S. Takeuchi, *Phys. Rev. Applied*, **15** (2021).
- <sup>3</sup>G. Taylor, D. Morozov, N. Gemmell, K. Erotokritou, S. Miki, H. Terai, and R. Hadfield, *Opt. Express* **27** (2019)
- <sup>4</sup>V. B. Verma *et al.*, *APL Photonics*, **6**, 056101 (2021).

## Phase retrieval of joint spectral amplitude

Kemeng Chen and Ryousuke Shimizu

*The University of Electro-Communications Fundamental Science and Engineering*

*c2033074@edu.cc.uec.ac.jp*

### Introduction

Tailored and energy tunable entangled photons are required rather than polarization entanglement on quantum information and communication technologies. To characterize the entanglement in a qubit system, such as polarization entanglement, quantum state tomography has been developed. On the other hand, the evaluation of entanglement for infinite dimension can be achieved by von Neumann entropy obtained by Schmidt decomposition. However, to implement Schmidt decomposition, the complex probability amplitude of a two-photon state should be required. Today, we can measure the two-photon spectral or temporal distributions in 2D space, but it is still challenging to evaluate phase distributions of the two-photon state. Here we develop Gerchburg-Saxton (GS) algorithm to retrieve the phase distribution. In addition, the original intensity data should be corrected by Wiener filter to suppress the noise fluctuation of the retrieved data.

### Method

To implement GS algorithm, we need a pair of data connected with Fourier transformation. Recently we proposed synthesizing time-frequency entangled photons and verified it by measuring joint spectral and temporal intensities. We applied GS algorithm to these data in the following procedure. At first, we added a random phase distribution to the frequency domain data and applied fast Fourier transform (FFT). Then, we extracted the transformed phase distribution in the time domain and reconstructed the joint temporal amplitude. Next, FFT was performed on the joint temporal amplitude repeatedly applied the same operation in the time and frequency domains. The transformed amplitudes were compared with the measured amplitudes and estimated an error. FFT was continued until the error values were below 5%, and eventually, the retrieved phase distribution was obtained. After the algorithm was completed, the resolution of the measured data should be considered to correct the retrieved result. Compared with time-domain data, the resolution in the frequency domain can be ignored and the time domain resolution was about 200 fs. So, we created ten point-spread functions (PSF) and use the Wiener filter to recorrect the original data. While the noise signal rate is 18, the best retrieval result was shown as the resolution is 197 fs. Figure 2 shows the retrieved phase distribution extracting the area that exceeds 50% of maximum intensity. Additionally, the retrieved phase distribution can be used on Hong-Ou-Mandle (HOM) interference conjecture. We also tried to evaluate the visibility of the retrieved result and compare it to its HOM interference experiment result.

This work was supported by MEXT Q-LEAP Grant Number JPMXS011806924.

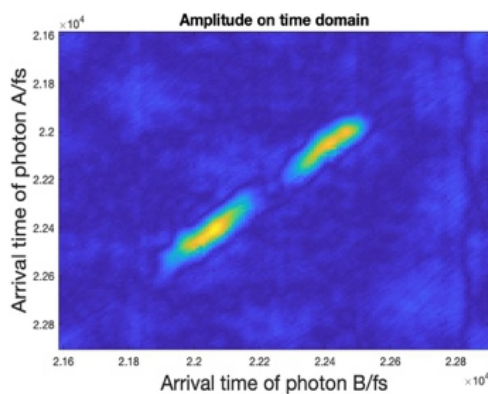


Fig. 1 Amplitude on time domain after phase retrieval and recorrected through point spectral function with 197 fs resolution

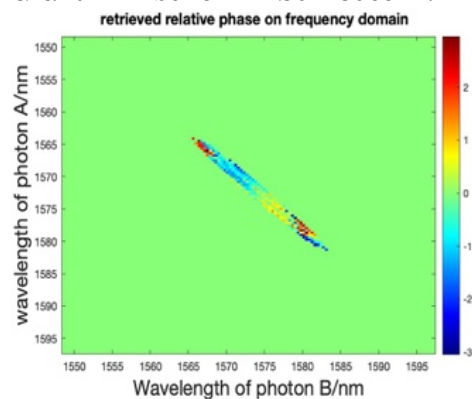


Fig. 2 Retrieved relative phase on frequency domain corrected by point spectral function with 197 fs resolution

## Temporal shaping of an entangled-photon wave packet by Fourier optical synthesis

H. Oshima<sup>1</sup>, F. China<sup>2</sup>, M. Yabuno<sup>2</sup>, S. Miki<sup>2</sup>, H. Terai<sup>2</sup>, and R. Shimizu<sup>1</sup>

<sup>1</sup>Univ. of Electro-Comm, <sup>2</sup>NICT

o2033021@edu.cc.uec.ac.jp

### Introduction

Temporal waveform control of ultrashort optical pulses is based on the one-dimensional Fourier transform relationship between the time and frequency domains, known as "optical synthesis" (OS). On the other hand, we have demonstrated that a two-dimensional Fourier transform (2D-FT) connects two-photon probability distributions of entangled photon pairs in time and frequency domains [1]. Based on this, we have developed manipulating the two-photon wave packet via 2D-FT, termed "quantum optical synthesis" (QOS) [2]. In this experiment, we created two discrete modes in 2D frequency space. However, the two-mode manipulation allows us to control the temporal waveform of entangled photons only in sinusoidal modulations. Our research aims to arbitrarily shape the time-domain structure of two photons with the 2D-FT manner. In this work, we present the extension of the frequency mode of the entangled photons toward arbitrary waveform shaping.

### Method

The experimental results are shown in Fig. 1. Figure 1 (a) is a two-photon spectral distribution, bidirectionally pumped for one nonlinear crystal. We can see two discrete frequency modes in the  $-45^\circ$  direction. The corresponding temporal distribution of the two-photon is shown in Fig. 1(b), which has a sinusoidal modulation in the  $-45^\circ$  direction. The temporal distribution with the sub-picosecond resolution was measured by up-conversion detection of single-photon with ultrashort pulses. Figure 1(c) is the measurement results obtained when creating four frequency modes using two nonlinear crystals. The corresponding time distribution is shown in Fig. 1(d). Setting the relative phase among all the frequency modes to be nearly 0, we can see slightly complicated temporal modulation as represented by  $|\cos(2\pi \times 0.33\tau_x) + \cos(2\pi \times 1.0\tau_x)|^2$

This work was supported by MEXT Q-LEAP Grant Number JPMXS0118069242.

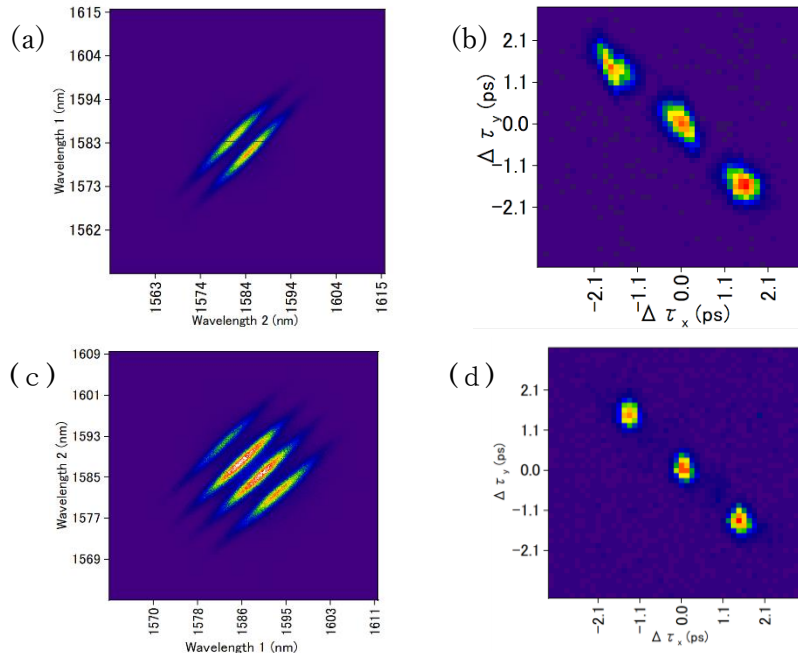


Fig.1 Upper plots are the experimental result of two-frequency mode (a) two-photon frequency and (b) temporal distribution. Lower plots are the experimental result of four-frequency mode (c) two-photon frequency and (d) its corresponding temporal distributions.

### Reference

<sup>1</sup>R.-B. Jin, T. Saito, and R. Shimizu, Phys. Rev. Appl. **10**, 034011 (2018).

<sup>2</sup>R.-B. Jin, K. Mihoshima, R. Shimizu *et al.*, APL Photonics **6**, 086104 (2021).

## Cryogenic Monolithic Interferometer for Sensing Gravity Gradient

Satoru Takano<sup>1</sup>, Ching Pin Ooi<sup>1</sup>, Yuka Oshima<sup>1</sup>, Yuta Michimura<sup>1</sup>, and Masaki Ando<sup>1</sup>

<sup>1</sup>Department of Physics, School of Science, The University of Tokyo

satoru.takano@phys.s.u-tokyo.ac.jp

### Introduction

Gravity gradient fluctuations are essential observation targets for precise measurement of motion of masses. From their measurement we obtain information about their source behavior. Recently fluctuations at low frequency, around 0.1 Hz, has been aimed for earthquake early alert using transient change of gravity potential [1] and for observation of GWs from mergers of intermediate-mass black holes [2].

A torsion-bar antenna (TOBA) is a ground-based gravity gradiometer proposed for measurement of gravity gradient fluctuations in such frequencies [2]. It measures torsional rotation angle of horizontally suspended mass(es) induced by gravity gradient fluctuations. Several prototypes and related technologies have been developed [3,4], and now we are planning to make a 30-cm scale prototype (Phase-III TOBA). Figure 1 shows the design setup of Phase-III TOBA

The goal of Phase-III TOBA is to achieve the strain sensitivity  $10^{-15} / \sqrt{\text{Hz}}$  at 0.1 Hz and demonstrate noise reduction, especially thermal noise by cooling the suspension system down to 4 K. To achieve this target sensitivity, reduction of sensing noise of interferometer is necessary. One solution is to make the readout system monolithically. Figure 2 shows the basic concept of the readout interferometer. We present development plan of the monolithic interferometer and current situation.

### Method

Monolithic interferometer consists of optical components directly glued on a plate. Thanks to this configuration we can reduce readout noise caused by vibration of optical components, thermal drift, etc. On the contrary, unlike ordinary interferometers we cannot adjust optics after gluing. Therefore, its construction requires special care. Recently the technology of construction has been well studied and validity of noise suppression has been proved in many fields.

Monolithic interferometers have been studied for applications in room temperatures. However, for TOBA case the interferometer is under cryogenic environment. Therefore, we have to revise usual way of construction of monolithic interferometer in order to survive in cryogenic temperatures. We have tested alternatives suitable for cryogenic environment and the results will be reported in the presentation.

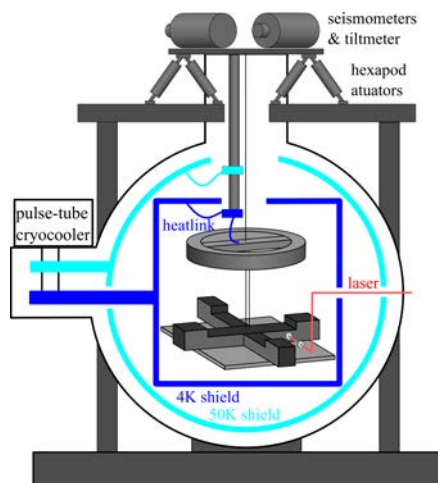


FIG. 1. Setup of Phase-III TOBA.

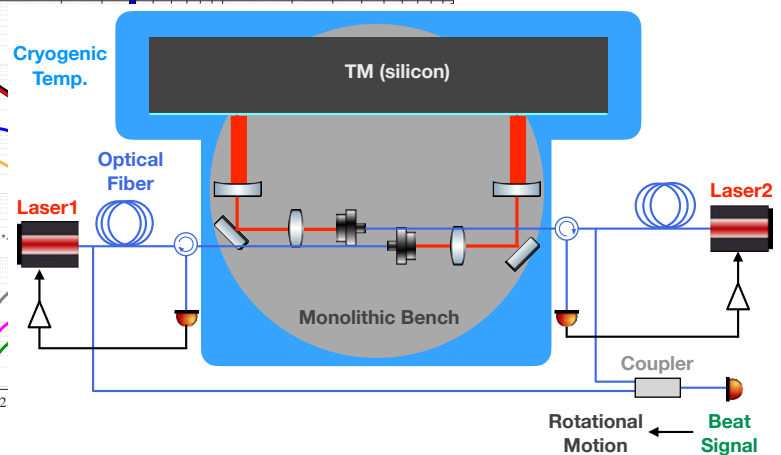


FIG. 2. Schematic of readout interferometer.

### Acknowledgement

This work was supported by MEXT Q-LEAP Grant Number JPMXS0118070351.

### Reference

- <sup>1</sup>J. Harms *et al.*, *Geophys. J. Int.*, 201, 1416-1425 (2015) <sup>2</sup>M. Ando *et al.*, *Phys. Rev. Lett.*, 105, 161101 (2010)  
<sup>3</sup>K. Ishidoshiro *et al.*, *Phys. Rev. Lett.*, 106, 161101 (2011) <sup>4</sup>A. Shoda *et al.*, *Phys. Rev. D*, 95, 082004 (2017)

## Suspension Noise measurements of Cryogenic Torsion Pendulums with Crystalline Fibres

Ching Pin Ooi<sup>1</sup>, Satoru Takano<sup>1</sup>, Yuka Oshima<sup>1</sup>, Yuta Michimura<sup>1</sup>, and Masaki Ando<sup>1</sup>

<sup>1</sup>Department of physics, School of Science, The University of Tokyo

ooichingpin@g.ecc.u-tokyo.ac.jp

### Introduction

Thermal noise in mechanical sensors are a fundamental noise source and a limit for sensitivity. Torsion Bar Antenna (TOBA), a proposed ground-based gravity gradiometer targeting the frequencies 0.1 - 10 Hz [1], naturally has this noise source. TOBA utilises torsion pendulums at high sensitivities to detect these gravitational fluctuations, which can be used for early earthquake detection [2] and sensing the gravitational waves from the mergers of intermediate mass black holes [1]. In this work, we study the suspension noise of torsion pendulums, and study how the use of two key technologies, cryogenic temperatures and crystalline fibres can reduce it.

To quantify the suspension thermal noise, we focus on measuring the Q factor, with which we can calculate the suspension thermal noise, given other parameters such as the temperature, and the relevant frequencies.

### Method

A copper beryllium torsion pendulum with a sapphire suspension fibre was placed in a cryogenic chamber. The Q factor of the torsion pendulum was then measured via the ringdown method as the setup was thermally cycled from room temperature to 4 K and back. The radial position of the torsion pendulum was measured using an optical lever. The torsion pendulum was excited using coil-coil actuators, to allow for the ringdown measurement to take place.

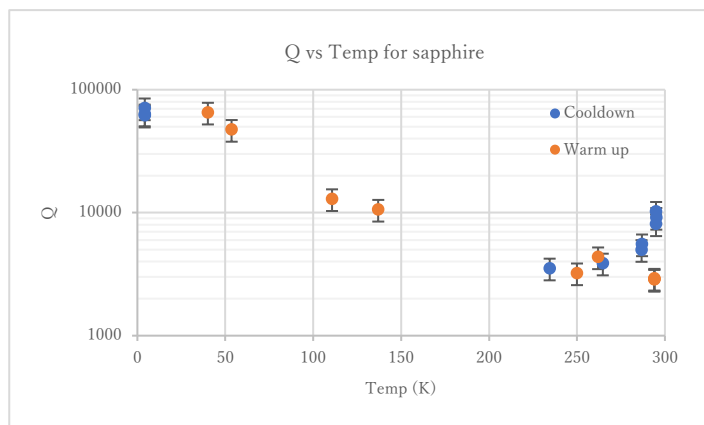


FIG 1. Graph of Q vs Temperature for a sapphire suspension fibre. The Q values ranged from 3 000 to 70 000 at 4 K, showing a great dependence on temperature, and follows the expectation that Q should increase at cryogenic temperatures. The resonance frequency was at 6 Hz, within the TOBA targeted frequencies of 0.1 – 10 Hz.



FIG 2. Picture of torsion pendulum, with attached mirror for optical lever readout, and coils for coil-coil actuation. The sapphire fibre used for suspension is 1 mm in diameter

### Acknowledgments

This work is supported by MEXT Q-LEAP Grant Number JPMXS0118070351.

### Reference

<sup>1</sup>M. Ando *et al.*, *Phys. Rev. Lett.*, 105, 161101 (2010)

<sup>2</sup>J. Harms *et al.*, *Geophys. J. Int.*, 201, 1416-1425 (2015)

## Angular Sensor with a Coupled Cavity for Gravity Gradient Sensing

Yuka Oshima<sup>1</sup>, Satoru Takano<sup>1</sup>, Ching Pin Ooi<sup>1</sup>, Yuta Michimura<sup>1</sup>, and Masaki Ando<sup>1</sup>

<sup>1</sup>Department of Physics, University of Tokyo

yuka.oshima@phys.s.u-tokyo.ac.jp

### Introduction

Torsion-Bar Antenna (TOBA) is a highly sensitive gravity gradient sensor using torsion pendulums [1]. The resonant frequency of torsional motion is  $\sim 1$  mHz, therefore TOBA has good design sensitivity in low frequencies (0.1 - 10 Hz). A prototype detector Phase-III TOBA with a 35 cm-scale pendulum is under development to demonstrate noise reduction [2]. The target sensitivity is set to  $10^{-15}$   $\sqrt{\text{Hz}}$  at 0.1 Hz. Phase-III TOBA can detect earthquakes with magnitude 7 or larger within 10 seconds from 100 km distance, therefore Phase-III TOBA is useful for gravity-based earthquake early warning [3]. To achieve our target sensitivity, we need to measure the pendulum rotation precisely. We propose a coupled wavefront sensor as an angular sensor for Phase-III TOBA. We show the principle and experimental demonstration status of a coupled wavefront sensor.

### Method

For a conventional wavefront sensor, we build a linear cavity with two mirrors (FIG. 1. Top). When a mirror tilts, a part of the zero-order Hermite-Gaussian (HG) modes converts into the first-order HG modes. We detect it as angular signal. In the cavity, the first-order HG modes are anti-resonant since they get non-zero Gouy phase shift compared to the zero-order HG modes.

A coupled wavefront sensor is a new wavefront sensor using an optical coupled cavity. In our method, we put one more mirror behind a main cavity and build an auxiliary cavity (FIG. 1. Bottom). An auxiliary cavity can compensate Gouy phase of main cavity, therefore the zero-order and the first-order HG modes are resonant simultaneously. As a result, angular signal is enhanced in the main cavity.

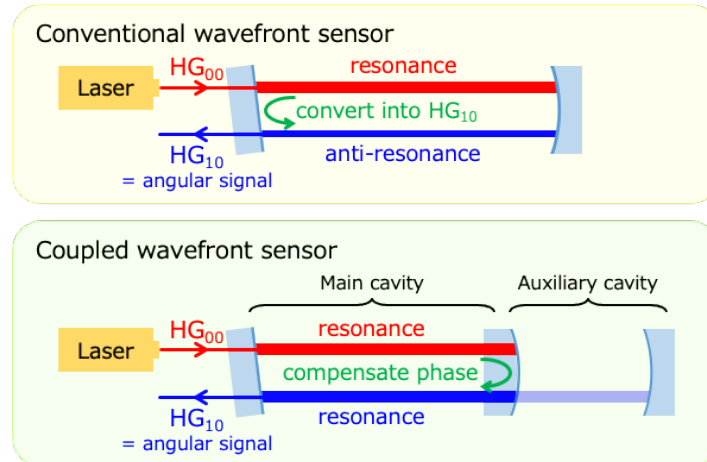


FIG. 1. Top: The schematic of a conventional wavefront sensor. Bottom: The schematic of a coupled wavefront sensor.

### Acknowledgments

This work was supported by MEXT Quantum Leap Flagship Program (MEXT Q-LEAP) Grant Number JPMXS0118070351.

### Reference

- <sup>1</sup>M. Ando *et al.*, *Phys. Rev. Lett.*, **105**, 161101 (2010).
- <sup>2</sup>T. Shimoda *et al.*, *International Journal of Modern Physics D*, **29**, 1940003 (2020).
- <sup>3</sup>T. Shimoda, PhD thesis, The University of Tokyo (2019).

## Towards sensitive accelerometers with levitated single nanoparticles

K. Aikawa<sup>1</sup>, M. Kamba<sup>1</sup>, H. Kiuchi<sup>1</sup>, K. Okuda<sup>1</sup>, N. Suyama<sup>1</sup>, and R. Shimizu<sup>1</sup>

<sup>1</sup>*Department of Physics, School of Science, Tokyo Institute of Technology*

*aikawa@phys.titech.ac.jp*

### Introduction

Single nanoparticles levitated in vacuum are a promising platform for sensitive accelerometers as well as for exploring macroscopic quantum physics. Cooling of their motion to the ground state of a trapping potential, corresponding to temperatures of about 10  $\mu$ K, has recently been demonstrated. We plan to use levitated nanoparticles as sensitive accelerometers. For this purpose, we develop two experimental setups: one with an optical lattice, and one with an ion trap. In this presentation, we briefly introduce the latest results from both setups.

### Method

In a setup with an optical lattice, we find that the phase noise of the trapping laser has a crucial impact on the motion along optical lattice. When the phase noise as well as the intensity noise are decreased, the center-of-mass motion along the optical lattice is cooled to near the ground state via electric feedback cooling<sup>1</sup>. The position sensitivity demonstrated in our setup is better than  $10 \text{ fm}/\sqrt{\text{Hz}}$ , suggesting that nanoparticles is a promising system as a sensitive accelerometer.

In a setup with an ion trap, we design and fabricate a novel electrode geometry allowing us to place a high-numerical-aperture lens, required for observing the motion of nanoparticles, close to the electrodes. In this ion trap, we demonstrate the stable confinement of nanoparticles and observe their three-dimensional motion via the high-numerical-aperture lens. Due to the low oscillation frequency of nanoparticles in the ion trap, the ion-trap setup is also a promising setup for the sensitive detection of acceleration.

### Reference

<sup>1</sup>M. Kamba, H. Kiuchi, T. Yotsuya, and K. Aikawa, *Phys. Rev. A* **103**, L051701 (2021).

# Interferometric gyroscope using slow and continuous atomic beam

Tomoya Sato<sup>1</sup>, Ryotaro Inoue<sup>1</sup>, Mikio Kozuma<sup>2,1</sup>

<sup>1</sup>*Institute of Innovative Research, Tokyo Institute of Technology*

<sup>2</sup>*Department of Physics, School of Science, Tokyo Institute of Technology*

sato@qnav.iir.titech.ac.jp

## Introduction

A self-localization method, which does not rely on external signals, complements methods such as satellite positioning by the GPS signal, ensuring safety and improving estimation accuracy by hybridization. Such a method is also essential for navigation in environments where other methods cannot be applied, for example, under the sea.

One can estimate their position by integrating the angular velocity and acceleration in time. Such a self-localization method consists of a gyroscope and accelerometer is called inertial navigation. The accuracy of the current high-end inertial navigation system is dominated by the performance of the gyroscope, which employs the optical Sagnac effect, such as the ring laser gyroscope. The magnitude of the phase difference between counter-propagating waves for the Sagnac interferometer is inversely proportional to the product of wavelength and velocity of the wave. Thus, the matter-wave interferometer is a promising way to improve the phase sensitivity of the gyroscope since the wavelength and velocity of the matter-wave are much smaller than those of the light wave [1]. We aim to develop the matter-wave gyroscope utilized by the slow and continuous atomic beam interferometer, which can be mounted on a vehicle.

## Method

A pair of atomic beams which is extracted from the 2D+MOT [2] is introduced into the interferometer region, where three pairs of counter-propagating Raman beams form the  $\pi/2$ - $\pi$ - $\pi/2$  Mach-Zehnder type interferometer [3]. The Sagnac effect causes the sinusoidal variation between populations of internal states of the atom as a function of the angular velocity on the Sagnac loop. Thus, the rotation of the system can be deduced from the phase shift in the interference signal.

The measured phase shift reflects the rotation of the system, but at the same time, acceleration and environmental disturbances also change the phase. It is necessary to eliminate these effects for accurate measurement. It can be achieved by using a pair of atomic interferometers with atomic beams that share Raman lights and travel in opposite directions [4]. Since the sign of phase shift induced by the rotation depends on the velocity vector, but that induced by the spurious effect is not. By measuring the differential phase shift between two interferometers, we can extract the phase shift caused by rotation while eliminating that caused by common-mode noises.

We measured the phase shift in the interference signal as a function of the tilting angle of the optical table on which the apparatus was installed (FIG.1). The linear phase shift due to the gravitational acceleration was observed as a function of the tilting angle. It was also confirmed that the common-mode rejection reduced that linear phase shift. The remaining phase shift after the rejection was consistent with the shift caused by the angular velocity of the Earth's rotation. To the best of our knowledge, this is the first demonstration of a gyroscope using the slow and continuous atomic beam.

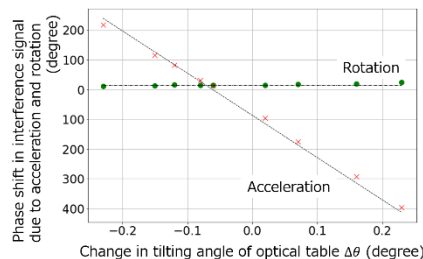


FIG. 1 Phase shift in interferometer due to the acceleration and rotation. Dashed lines indicate theoretical values.

This work was supported by JST-Mirai Program, Grant Number JPMJMI17A3 and COI-NEXT, Grant Number JPMJPF2015.

## Reference

- <sup>1</sup>J. F. Clauser, *Physica B*, **151**, 262 (1988).
- <sup>2</sup>K. Dieckmann, R. J. C. Spreeuw, M. Weidemüller, and J. T. M. Walraven, *Phys. Rev. A*, **58**, 3891 (1998).
- <sup>3</sup>M. Kasevich and S. Chu, *Phys. Rev. Lett.*, **67**, 181 (1991).
- <sup>4</sup>T. L. Gustavson, P. Bouyer and M. A. Kasevich, *Phys. Rev. Lett.*, **78**, 2046 (1997).

## Development of a quantum gyroscope based on a single ion trapping techniques

Ryoichi Saito<sup>1,2</sup>, and Takashi Mukaiyama<sup>1,2</sup>

<sup>1</sup> Graduate school of Engineering, Osaka University

<sup>2</sup>QIOB, Osaka University

*r\_saito@ee.es.osaka-u.ac.jp*

### Introduction

Atoms in a coherent superposition of different momentum states enable high-precision measurement of physical quantities. Matter-wave interferometers typically exploit entanglement between the internal state and the motional state of matter. The accumulated matter-wave phases for different paths are obtained from the interference signal of the internal states after the closing pulse of the interferometer. In order to achieve precise sensing, exquisite control of internal and external states of individual quanta is essential. Atoms and ions are ideal matter for such use since they provide us with the precise control of their quantum states using optical means. So far, neutral atoms have been used for various sensing applications such as detection of gravitational acceleration<sup>1</sup>, electric and magnetic field<sup>2</sup>, rotation<sup>3</sup> and so on. On the other hand, a trapped ion has not been considered for a platform to realize sensing of external perturbations until recently. This may partly be because of the difficulty in realizing a large interference area due to the tight confinement of the ion trap, which is inextricably linked with the advantage of a capability of stable trapping. Quite recently, Campbell and Hamilton proposed to utilize a trapped ion for a precise rotation sensing application. In the proposal, a trapped ion in a circular motion constructs a Sagnac interferometer. By taking an arbitrary number of ion rotations, the sensitivity of the rotation sensing can be tuned, and the ions with multiple circular motions may provide us with a large interference area and a compact physical size at the same time.

### Method

The Sagnac interferometer, which utilizes the single trapped ion, is realized by circularly propagating wave packet of the ion. The protocol to generate the two-dimensional circular interferometer is as below. First, we apply the microwave half pi pulse to the ion in a two-dimensional isotropic potential for creating the superposition of the internal spin state. Then, we irradiate a mode-locked laser at 355 nm to apply the momentum kick, depending on the internal spin state, to generate the one-dimensional interferometer<sup>5</sup>. After the generating spin-motion entangled state by spin-dependent momentum kick, non-adiabatic trap potential shift in a perpendicular direction to the momentum kick is applied by step voltage to the electrode<sup>6</sup>. Then, the wave packet of the ion propagates an elliptical orbit. The rotation of the system produces the path difference between clockwise and counterclockwise. The phase shift of the ion matter-wave due to the rotation is measured by the detection probability of the internal state.

In the presentation, we will talk about our experimental detail and the current achievement.

### Reference

- <sup>1</sup>M. Kasevich and S. Chu, *Phys. Rev. Lett.* 67, 181 (1991).
- <sup>2</sup>K. Zeiske, G. Zinner, F. Riehle, and J. Helmcke, *Appl. Phys. B* 60, 205 (1995).
- <sup>3</sup>T. L. Gustavson, P. Bouyer, and M. A. Kasevich, *Phys. Rev. Lett.* 78, 2046 (1997).
- <sup>4</sup>W. C. Campbell and P. Hamilton, *J. Phys. B: At. Mol. Opt. Phys.* 40
- <sup>5</sup>A. Shinjo, M. Baba, K. Higashiyama, R. Saito, and T. Mukaiyama, *Phys. Rev. Lett.* 126, 153604 (2021).
- <sup>6</sup>R. Saito and T. Mukaiyama, *Phys. Rev. A* 104, 053114 (2021)..

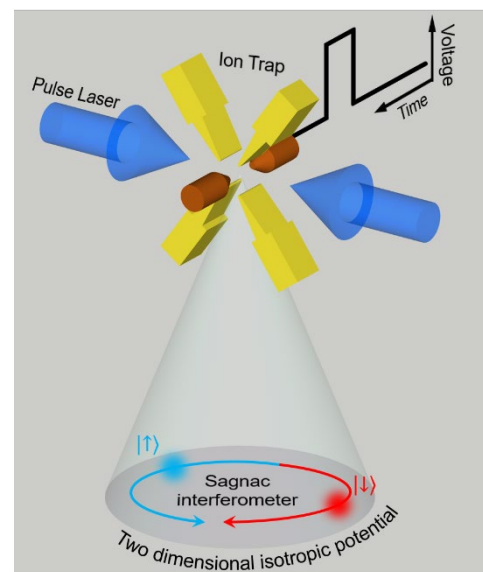


FIG. 1. Schematic diagram of rotation sensing using a trapped ion

SE-03A- $\delta$ 1-07

## Exponentially Enhanced Quantum Metrology by Quenching Superradiant Light-Matter Systems Beyond the Critical Point

Karol Gietka, Lewis Ruks, and Thomas Busch

*Okinawa Institute of Science and Technology, Quantum Systems Unit*

*Karol.Gietka@oist.jp*

### Introduction

We present a quantum metrology protocol which relies on quenching a light-matter system exhibiting a superradiant quantum phase transition beyond its critical point. In the thermodynamic limit these systems can exhibit an exponential divergence of the quantum Fisher information in time, whose origin is the exponential growth of the number of correlated photons on an arbitrarily fast time scale determined by the coupling strength. This provides an exponential speed-up in the growth of the quantum Fisher information over existing critical quantum metrology protocols observing power law behavior. We demonstrate that the Cramer-Rao bound can be saturated in our protocol through the standard homodyne detection scheme. We explicitly show its advantage in the archetypal setting of the Dicke model and explore a quantum gas coupled to a single-mode cavity field as a potential platform. In this case an additional exponential enhancement of the quantum Fisher information can in practice be observed with the number of atoms  $N$  in the cavity, despite existing works suggesting a requirement of  $N$ -body coupling terms.

### Reference

K. Gietka, L. Ruks, T. Busch, *arXiv*, S. Schmitt, *Science*, [2110:04048](#), (2021).

## Three-layered Magnetically Shielded Room for Ultrahigh-sensitivity Quantum Sensing of Biomagnetic Signals

Motofumi Fushimi<sup>1</sup>, Akihiro Kuwahata<sup>2</sup>, Shinichi Chikaki<sup>1</sup>,  
Takao Yamaguchi<sup>3</sup>, Yuuki Niwa<sup>3</sup>, and Masaki Sekino<sup>1</sup>

<sup>1</sup>Graduate School of Engineering, The University of Tokyo

<sup>2</sup>Graduate School of Engineering, Tohoku University

<sup>3</sup>Ishida Ironwork's Co., Ltd.

*motofumi-fushimi@g.ecc.u-tokyo.ac.jp*

### Introduction

Measurement of biomagnetic fields generated from biological tissues such as the brain and heart has attracted great attention since it enables us to observe physiological activities of living organisms. Quantum sensors such as the optically pumped atomic magnetometer and the nitrogen-vacancy center in diamond have achieved ultrahigh-sensitivity sensing of magnetic fields and opened the field of biomagnetic signal sensing at room temperature. However, to measure the extremely weak biomagnetic signals (typically at the order of picotesla), a magnetically shielded room (MSR) that prevents the ambient magnetic field (typically at the order of microtesla) from contaminating the target biomagnetic signals is essential [1].

In this study, we developed an MSR made of three-layered permalloy plates and measured its shielding factor to validate the efficacy of the shield in biomagnetic sensing such as magnetoencephalography (MEG) of small animals.

### Methods

Figure 1 shows the developed MSR consisting of three layers of permalloy plates and one layer of aluminum plate for shielding high frequency fields. The inside dimension of the MSR is 3 m x 2 m x 2 m, and thus available for wide range of biomedical applications including human subjects. For the measurement of the magnetic fields, we used a highly sensitive fluxgate sensor (502A, APPLIED PHYSICS SYSTEMS). While applying the external AC magnetic fields at 0.1-100 Hz, we evaluated the shielding factor defined here as the ratio of magnetic field strength inside to outside the MSR.



FIG. 1. Three-layered MSR developed in this study.

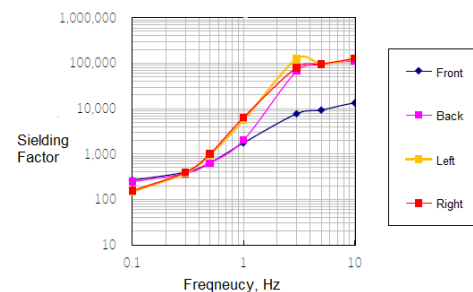


FIG. 2. The shielding factor at each four side of the MSR

### Results and Discussion

Figure 2 shows the shielding factor of four each side of the MSR. The shielding factor increases with frequency thanks to the aluminum layer and the factor of about  $10^4$ - $10^5$  is achieved at 10 Hz, which corresponds to the frequency of the alpha wave of humans. The shielding factor measured at the front side is relatively low. This is because the door of the shield deteriorates the effect of the aluminum layer. Although the MSR greatly suppresses the magnetic field, an additional shielding factor of about  $10^2$  is required to achieve the sensing of picotesla-scale biomagnetic signals. Introducing an active cancelling coil in the MSR would provide the sufficient shielding capability [2,3], evaluation of which is our future work.

### Acknowledgements

This work was supported by MEXT Quantum Leap Flagship Program (Q-LEAP) Grant Number JPMXS0118067395.

### References

- <sup>1</sup>T. J. Sumner *et al.*, *J. Phys. D: Appl. Phys.*, **20**, 1095 (1987).
- <sup>2</sup>K. Harakawa *et al.*, *IEEE Trans. Mag.*, **32**(6), 5256-5260 (1996).
- <sup>3</sup>E. Boto *et al.*, *Nature*, **555**, 657-661 (2018).

## Super-resolution in nano-NMR

Nicolas Staudenmaier<sup>1,\*</sup>, Santiago Oviedo-Casado<sup>2</sup>, Anjusha Vijayakumar-Sreeja<sup>1</sup>, Genko Genov<sup>1</sup>,  
Alex Retzker<sup>2</sup> and Fedor Jelezko<sup>1,4</sup>

<sup>1</sup>*Institute for Quantum Optics, Ulm University, D-89081 Ulm, Germany*

<sup>2</sup>*Racah Institute of Physics, The Hebrew University of Jerusalem, Jerusalem 91904, Givat Ram, Israel*

<sup>4</sup>*Center for Integrated Quantum Science and Technology, Ulm University, D-89081 Ulm, Germany*

\**nicolas.staudenmaier@uni-ulm.de*

### Introduction

There is increasing interest in reducing the size of NMR and MRI devices to gain new insights to processes on the nanoscale. These include for example NMR studies of single cells, neurons<sup>1</sup>, or surfaces and surface chemistry<sup>2</sup>. Nitrogen-vacancy (NV) centers in diamond show to be promising sensors for such applications. In the past years nano- to microscale NMR has been proven using single<sup>3,4</sup> or ensemble NV centers<sup>5</sup>. Importantly, unlike in conventional NMR, signal pickup with NV centers does not depend on the strength of an applied external magnetic field, allowing for the acquisition of information-rich spectra from zero and low-field<sup>6</sup> as well as high-field NMR. On the other side nanoscale NMR resorts to statistical nuclear spin polarization rather than directional such as thermal polarization. For that reason, spectral resolution is limited by diffusion of a liquid sample in the detection volume. However, there is theoretical evidence that the signal correlation does not drop off exponentially but that there is a polynomial tail for longer times allowing a sharp peaked signal in the spectrum<sup>7,8</sup>. We will show experimental evidence that promotes such a model that overcomes any resolution limit and ultimately enables super-resolution of signals with nearby frequencies.

### Method

Experimental measurements are done on a homebuilt confocal microscope using single shallow NV centers located about 10nm below the diamond surface. Hydrogen nuclear spins, naturally present in the used immersion oil, are sensed via a nuclear spin sensitive dynamical decoupling sequence in combination with the quantum heterodyne (Qdyne) measurement protocol<sup>9</sup>, that correlates all individual readouts. From the data the autocorrelation of the NMR signal is obtained and analyzed using different statistical tools.

### References

- <sup>1</sup> M. Grisi et al., *Sci. reports* **7**, 44670 (2017).
- <sup>2</sup> G. A. Somorjai and Y. Li, *Proc. Natl. Acad. Sci.* **108**, 917–924 (2011).
- <sup>3</sup> H. J. Mamin et al., *Science* **339**, 557-560 (2013).
- <sup>4</sup> T. Staudacher et al., *Science* **339**, 561-563 (2013).
- <sup>5</sup> D. Glenn et al., *Nature* **555**, 351–354 (2018).
- <sup>6</sup> M. Ledbetter et al., *J. Magn. Reson* **199**, 25-29 (2009).
- <sup>7</sup> D. Cohen et al., *Sci. Rep.* **10**, 5298 (2020).
- <sup>8</sup> S. Oviedo-Casado et al., *Sci. Rep.* **10**, 19691 (2020).
- <sup>9</sup> S. Schmitt et al., *Science* **356**, 832-837 (2017).

## Sensitivity of weight imaging using a hybrid system based on piezoactive magnetic material and diamond quantum sensor

Ryota Kitagawa<sup>1</sup>, Shunsuke Nagata<sup>1</sup>, Soki Urashita<sup>1</sup>, Keigo Arai<sup>1,2</sup>, Kosuke Mizuno<sup>1</sup>,  
Hitoshi Ishiwata<sup>1,2</sup>, Yota Takamura<sup>1</sup>,

Takayuki Iwasaki<sup>1</sup>, Shigeki Nakagawa<sup>1</sup>, and Mutsuko Hatano<sup>1</sup>

<sup>1</sup>Department of Electrical and Electronics Engineering, School of Engineering, Tokyo Institute of Technology

<sup>2</sup>PRESTO, Japan Science and Technology Agency  
kitagawa.r.ab@m.titech.ac.jp

### Introduction

Imaging weight over multiple length scales from single cells to biological tissues, remaining a key challenge, introduces a new modality for studying biological systems. Such a high dynamic range in length scale can be realized by a hybrid sensor based on magnetostrictive (MS) magnetic material [3] and nitrogen-vacancy (NV) centers in diamonds [4]. To detect the weight of human egg cells, the weight accuracy of  $\sim 1$  Pa is required. In this research, we evaluated the weight sensitivity of the hybrid system. We measured weight-to-magnetic field conversion efficiency and magnetic field sensitivity.

### Method

We fabricated a hybrid sensor by gluing a MS magnetic material of a  $\text{SmFe}_2$  thin film [3], deposited on an ultra-thin quartz substrate, and NV centers in a diamond film deposited on a type-Ib diamond (111) substrate (Fig. (a)) [5]. Various weight was applied through a rivet in an area of  $3.1 \text{ mm}^2$  by changing the number of calibrated weights ( $0 \sim 125 \text{ kPa}$ ). Due to the inverse MS effect, weight is converted into the rotation of magnetization in the MS layer (Fig. (b)). This rotation induces a change in the stray magnetic field, imaged by NV centers via optically-detected magnetic resonance (ODMR). We imaged the magnetic field by continuous-wave ODMR while changing the weight. One pixel of the image is  $(4.9 \mu\text{m})^2$ .

### Result

Fig. (c) shows a magnetic field image at  $0 \text{ kPa}$ . We successfully imaged the magnetic field from  $\text{SmFe}_2$ . Fig. (d) shows the  $B_z$ -pressure dependence of one pixel. Weight-to-magnetic field conversion efficiency was  $70 \text{ nT/kPa}$ . The estimation accuracy of  $B_z$  was about  $2 \mu\text{T}$  per one pixel. Thus, the estimation accuracy of weight was  $28 \text{ kPa}$ . Depositing  $\text{SmFe}_2$  on the NV center will improve the conversion efficiency by an order. Further improvement of magnetic field sensitivity is required, such as utilizing pulsed measurement, improvement of coherence time and generation rate of NV center, and spatial integration of the ODMR signal.

This work was supported by MEXT Quantum Leap Flagship Program (MEXT Q-LEAP) Grant Number JPMXS0118067395.

### Reference

[1] G. Popescu et al., Lab Chip **14**, 646-652 (2014).

[2] D. Martínez-Martín et al., Nature **550**, 500-505 (2017)

[3] Y. Takamura, et al., 2019 Annu. Conf. on MMM, Las

Vegas, AQ-11,5 Nov. 2019.

[4] J. Cai et al., Nat. Commun. **5**, 1 (2014).

[5] K. Tahara et al., Appl. Phys. Lett. **107**, 193110 (2015)

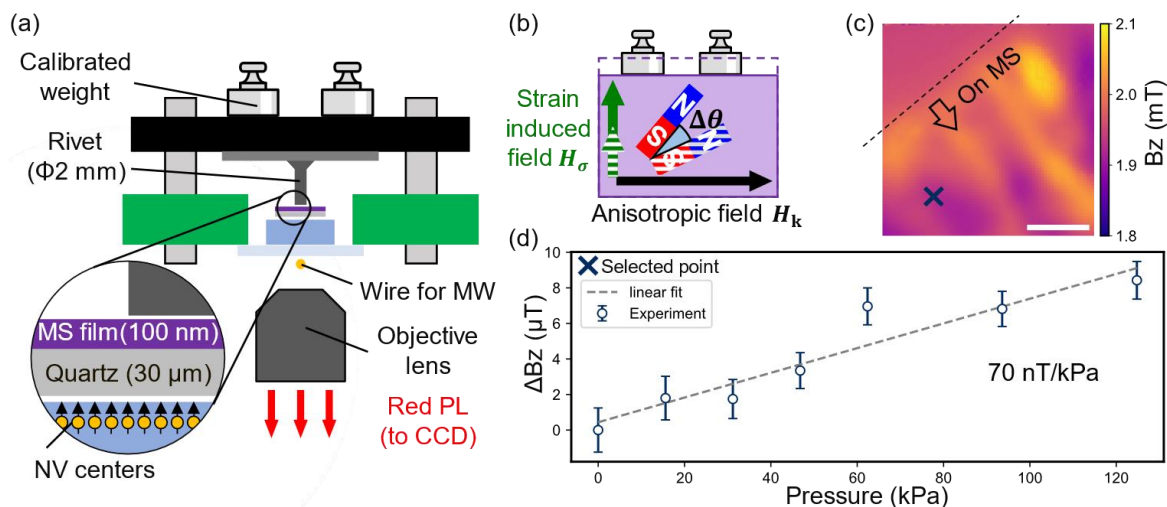


Fig. (a) Setup of hybrid weight imaging system. (b) Weight-dependent rotation of magnetization due to inverse MS effect. (c) Magnetic field image at  $0 \text{ kPa}$ . The upper light area is off MS film. The scale bar is  $100 \mu\text{m}$ . (d)  $B_z$ -pressure dependence of a selected point. Error bar is the  $\pm 1.96\sigma$  confidence interval. Weight-to-magnetic field conversion efficiency was  $70 \text{ nT/kPa}$ .

SE-03A- $\alpha$ 2-04**Study on electron spin control method for high-sensitivity diamond quantum sensor**Hiroyoshi Tomioka<sup>1</sup>, Yuji Hatano<sup>1</sup>, Takeharu Sekiguchi<sup>1</sup>, Keigo Arai<sup>1</sup>, Hiromitsu Kato<sup>2</sup>,  
Shinobu Onoda<sup>3</sup>, Takeshi Ohsima<sup>3</sup>, Takayuki Iwasaki<sup>1</sup>, and Mutsuko Hatano<sup>1</sup><sup>1</sup>Department of Electrical and Electronics Engineering, School of Engineering, Tokyo Institute of Technology<sup>2</sup>National Institute of Advanced Industrial Science and Technology<sup>3</sup>National Institutes for Quantum and Radiological Science and Technology

tomioka.h.ac@m.titech.ac.jp

**Introduction**

A diamond quantum sensor utilizing the NV center, a paramagnetic defect composed of nitrogen and vacancy in diamond, is expected to be applied to life-science [1] and automotive fields due to its high sensitivity and room temperature operation. However, further improvements in DC-field sensitivity and miniaturization are demanded for practical applications. To achieve such improvements, we focus on CE (continuously excited)-Ramsey method [2] as an alternative to the conventional method of continuous-wave optically detected magnetic resonance (CW-ODMR) or regular Ramsey.

**Methods**

In CE-Ramsey measurement, the excitation light is continuously applied while the microwaves are pulsed to control the electron spin states. Our experimental setup is shown in Fig. 1(a). In this study, we performed CW-ODMR, CE-SQ (single quantum)-Ramsey, and CE-DQ (double quantum)-Ramsey measurements to compare the magnetic sensitivities between them. We also estimated the shot noise limited sensitivities of CW-ODMR and CE-SQ-Ramsey methods. For this calculation, we solved the rate equations involving only five levels [3]: two ground states, two excited states, and a metastable state. The diamond sample used was grown by CVD (100  $\mu\text{m}$  thickness) using <sup>12</sup>C-enriched methane on a IIa substrate with a (111) surface, followed by electron beam irradiation ( $5 \times 10^{17} \text{cm}^{-2}$ ) and annealing.

**Results and discussion**

The magnetic sensitivities obtained by CW-ODMR, CE-SQ-Ramsey, and CE-DQ-Ramsey methods are plotted in Fig. 1(b). The CE-SQ-Ramsey and CE-DQ-Ramsey measurements showed better magnetic sensitivities than CW-ODMR for the modulation frequency between 10 and 90 kHz. Fig. 1(c) shows the calculation result of the shot noise limited sensitivity. This sensitivity is better for CE-SQ-Ramsey than CW-ODMR at high modulation frequencies (above 20 kHz). In addition to the sensitivity improvement, CE-Ramsey is suitable for miniaturization because it does not require pulsing of a high-power laser, which is essential for the regular Ramsey. Therefore, we expect it to be used for applications such as battery monitoring in electric vehicles.

This work was supported by MEXT Q-LEAP Grant Number JPMXS0118067395.

**Reference**

- [1] J. F. Barry *et al.*, Proc. Natl. Acad. Sci. USA, **113**, 14133 (2016). [2] C. Zhang *et al.*, Phys. Rev. Appl. **15**, 064075(2021). [3] K. Jensen *et al.*, Phys. Rev. B **87**, 014115 (2013).

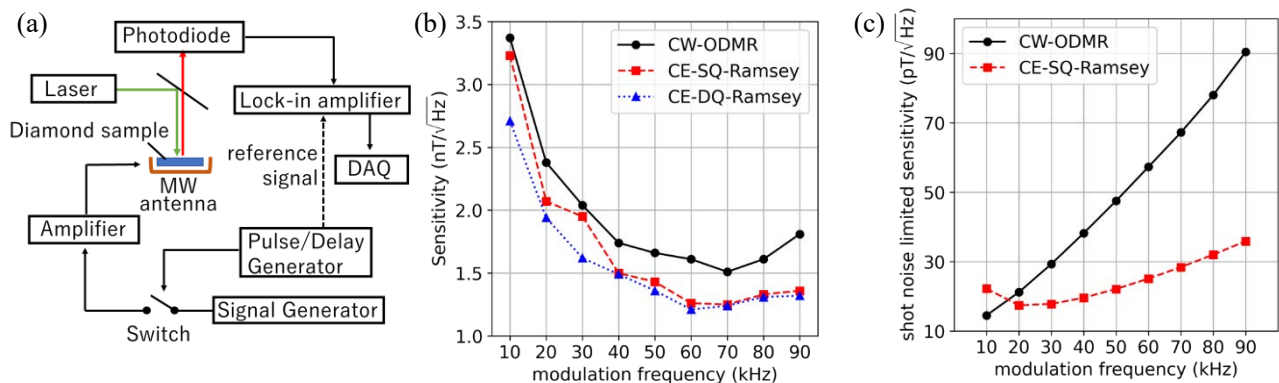


FIG. 1. (a) Schematic of the experimental setup. (b) Comparison of the experimental magnetic sensitivities with different modulation frequencies. (c) Comparison of the shot noise limited sensitivities calculated by using five level model with different modulation frequencies.

## Optically detected magnetic resonance spectra of silicon vacancies in 4H-SiC with different temperatures

S. Motoki<sup>1,2</sup>, S.-I. Sato<sup>2</sup>, Y. Masuyama<sup>2</sup>, Y. Yamazaki<sup>2</sup>, Y. Hijikata<sup>1</sup>, T. Ohshima<sup>2</sup>

<sup>1</sup> *Science and Engineering, Course in Electrical and Electronic Systems, Saitama University*

<sup>2</sup> *National Institutes for Quantum Science and Technology*

*E-mail: s.motoki.639@ms.saitama-u.ac.jp*

### Introduction

Silicon vacancy ( $V_{Si}^-$ ) centers in silicon carbide have attracted attention because of their potential applications to quantum sensors (high-sensitivity magnetic field and temperature sensors).  $V_{Si}^-$  centers are also expected to be used for magnetic sensors under harsh environments such as space and undergrounds, since they have structural stability and the potential of high-fidelity spin manipulation at high temperatures<sup>1</sup>. To realize  $V_{Si}^-$  based magnetic sensors operating at high temperature, understanding of optically detected magnetic resonance (ODMR) in the ground states of  $V_{Si}^-$  centers, which is the basic principle of magnetic sensing, is crucial. In particular, the effects of temperature on the ODMR spectra are less well understood. Here, we demonstrate the potential of  $V_{Si}^-$  magnetic sensors at high temperatures by showing the ODMR spectra with different temperatures. We also systematically investigate the effects of high energy electron irradiations on the ODMR spectra of formed  $V_{Si}^-$  centers. The concentration of  $V_{Si}^-$  centers increases with increasing electron irradiation dose, resulting in the enhancement of sensitivity, but increase in undesired defects which can cause decoherence is also expected. Hence, the effects of electron irradiation dose should be clarified to obtain better sensitivity of  $V_{Si}^-$  based magnetic sensors.

### Method

High purity semi-insulating (HPSI) 4H-SiC was irradiated with 2 MeV electrons at room temperature up to the dose of  $3 \times 10^{18} \text{ cm}^{-2}$  to form  $V_{Si}^-$  centers. The samples were then thermally annealed at 873 K for 30 minutes in vacuum to obtain stability during measurements at high temperature. FIG. 1 shows ODMR spectra of  $V_{Si}^-$  centers in 4H-SiC at different temperatures. The 785 nm laser at 40 mW was used for excitation and the emitted photons above 900 nm were collected by an InGaAs photo detector. Under zero magnetic field, a resonant peak at 70 MHz due to zero-field splitting of  $V_{Si}^-$  ground states appeared even at 600 K, being reduced with increase temperature. The resonant peak was split into two peaks by applying external magnetic field (Zeeman splitting). These results suggest that spin manipulation of  $V_{Si}^-$  centers is possible at 600 K and thus high temperature operation of  $V_{Si}^-$  based magnetic sensor is feasible. At the presentation, the mechanism of change in ODMR spectra with different temperatures is discussed. In addition, the relationship between the ODMR spectra and the electron irradiation dose is reported.

### Acknowledgement

This presentation is based on results obtained from a NEDO Feasibility Study Program (Uncharted Territory Challenge 2050). Part of this study was supported by MEXT Q-LEAP grant numbers JPMXS0118067395, and JSPS KAKENHI grant numbers 20H00355, and was carried out within the framework of IAEA CRP F11020.

### Reference

<sup>1</sup> H. Kraus et al., Sci. Rep. 4: 5303 (2014).

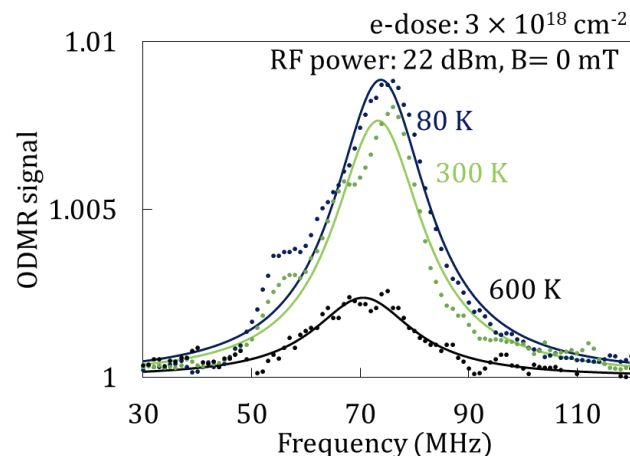


FIG. 1. ODMR spectra of  $V_{Si}^-$  centers in 4H-SiC at different temperatures. Experimental data (symbols) are fitted by the Lorentzian function (solid lines).

## High efficiency formation of NV center inside diamond by femtosecond laser

Ryusei Yanoshita<sup>1</sup>, Torataro Kurita<sup>1</sup>, Yasuhiko Shimotsuma<sup>1</sup>,  
Masanori Fujiwara<sup>2</sup>, Norikazu Mizuochi<sup>2</sup>, Masahiro Shimizu<sup>1</sup>, Kiyotaka Miura<sup>1</sup>

<sup>1</sup>Department of Material Chemistry, School of Engineering, Kyoto University

<sup>2</sup>Institute for Chemical Research, Kyoto University

yanoshita.ryuusei.66a@st.kyoto-u.ac.jp

### Introduction

The ensemble of NV centers, consisting of impurity nitrogen and adjacent vacancies in diamond, are expected as quantum sensors due to their long coherence time and possible coherent control of a single spin at room temperature [1]. Although the single NV center formation by femtosecond laser irradiation has been reported [2], the formation mechanism is not fully understood. Especially, the transformation of diamond to graphite [3] and the effective laser irradiation parameters for the formation of NV center ensemble remain unexplored. More recently, we have demonstrated that the pulse width and the number of pulses are effective to generate a higher density NV center ensemble [4, 5]. Here we report on the relation between the impurity nitrogen concentration and the laser irradiation parameters for the NV center formation. In particular, we focused on the efficiency of the NV center formed by the femtosecond laser irradiation with different pulse repetition rates.

### Method

A femtosecond laser beam with a central wave length of 800 nm (bandwidth 37 nm) and a pulse width of 60 fs was focused in a diamond sample through the objective lens (50× NA 0.80). The focus was located at a depth of 50 μm below the sample surface. In the experiments, two diamonds with different nitrogen concentrations (Sample A: CVD synthesized Type IIa diamond, [N] ≤ 1 ppm, Sample B: HPHT synthesized Type Ib diamond, [N] ≈ 33 ppm) were used. The laser pulses were irradiated from the normal to the (100) plane. To reveal the effect of the impurity nitrogen concentration, the PL intensity originated from the NV- center ranging from 640 nm to 660 nm between the different diamond samples was compared. Since the threshold of NV center formation by the femtosecond laser irradiation depends on the impurity nitrogen concentration, we tuned the pulse energy ( $E_p$ ) according to the samples. The  $E_p$  between 50 nJ and 200 nJ was applied for sample A, on the other hand, the  $E_p$  was set to 2000 nJ for sample B. Other laser parameters such as the pulse width (60 fs), pulse repetition rate (250 kHz), and the number of pulses ( $2.5 \times 10^5$ ) were set the same. Table 1 shows the PL intensity ( $I_{PL}$ ) normalized by that in the unirradiated region. Despite the fact that the  $E_p$  for sample A was lower than that for sample B in all experiments, the PL intensity for sample A reached approximately 4.4 times higher than that for sample B. Assuming the PL intensity is proportional to the NV center concentration, this result indicates that the formation efficiency for the NV center is high when the impurity nitrogen concentration is low. We have also confirmed the formation efficiency of the NV center by the femtosecond laser irradiation with various pulse repetition rates ranging from 5 kHz to 250 kHz. In the laser experiments, the irradiated number of pulses was set to be  $2.5 \times 10^5$  pulses by changing the irradiation time. Fig. 2 shows the normalized PL intensity was changed by the pulse repetition rate, despite that the same total pulse energy was irradiated. In particular, the NV center concentration decreased at 10 kHz or less and 100 kHz or more. In the case below 10 kHz, corresponding to the pulse interval of 100 μs, such timescale is quite longer than that for thermalization and the lifetime of the exciton in diamond (~ 1 μs). Furthermore, the decrease of NV center concentration at 100 kHz or more could be interpreted in terms of the annihilation of NV center or the transformation into the different defects such as H3 center.

Table1. Normalized PL intensity of NV center in two different types of diamonds.

Type	$E_p$ [nJ]	$I_{PL}$
Ib	2000	8.21
IIa	50	4.05
IIa	100	17.4
IIa	200	35.8

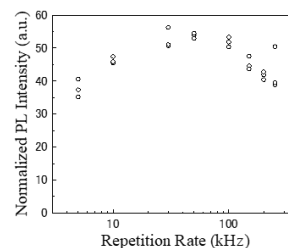


Fig. 2. Normalized PL intensity of NV center induced by the femtosecond laser pulses with various pulse repetition rates.

### Reference

- [1] A. Gruber, et al., *Science* 276 2012 (1997).
- [2] Y. Chen, et al., *Nat. Photonics* 11 77 (2017).
- [3] M. Sakakura, et al., *J. Laser Micro/Nanoeng.* 11 346 (2016).
- [4] T. Kurita, et al., *Appl. Phys. Lett.* 113 211102 (2018).
- [5] T. Kurita, et al., *Appl. Phys. Lett.* 118 214001 (2021).

## AC magnetic field sensing with ensemble NV centers using electrical detection methods

Hiroki Morishita<sup>1</sup>, Naoya Morioka<sup>1</sup>, Tetsuri Nishikawa<sup>1</sup>, Hajime Yao<sup>1</sup>, Shinobu Onoda<sup>2</sup>,

Hiroshi Abe<sup>2</sup>, Takeshi Ohshima<sup>2</sup>, and Norikazu Mizuochi<sup>1</sup>

<sup>1</sup>Institute for Chemical Research, Kyoto University, Uji, Kyoto 611-0011, Japan.

<sup>2</sup>National Institutes for Quantum and Radiological Science and Technology, Takasaki, Gunma, 370-1292, Japan.

*h-mori@scl.kyoto-u.ac.jp*

### Introduction

Nitrogen-vacancy (NV) centers in diamond have a long coherence time at room temperature, and hence they are candidates for quantum sensors and quantum information processing devices [1]. While electrical detection of NV spins is essential to develop and integrate these quantum devices [2-8], to the best of our knowledge, there are no demonstrations of AC magnetic field sensing using electrical detection methods. In the electrical detection of the NV spins, the change in the photocurrent is measured when resonant microwaves are applied to the NV spins. In the demonstration of the AC magnetic field sensing using electrical detection methods, the current generated by the AC magnetic field flows in the diamond sample. This current generated by the AC magnetic field can cause an increase in noise in the electrical detection method. Thus, the AC magnetic field sensing using the electrical detection method is still challenging. In this study, we demonstrate for the first time AC magnetic field sensing using the electrical detection method by reducing the influence of such a current.

### Method & Results

In this study, we performed the AC magnetic field sensing with an electrical detection method using the ensemble of NV centers (concentration of  $\sim 1.4 \times 10^{17} \text{ cm}^{-3}$ ) created by electron-beam irradiation followed by annealing. Figure 1 shows a result of AC magnetic field sensing with the electrical detection method with the bias voltage of 5 V. The result indicates that we observe  $\sim 3 \times 10^{-8} \text{ T}/\text{Hz}$  of the sensitivity of the AC magnetic field. In this presentation, we discuss the results of AC magnetic field sensing using the electrical detection method.

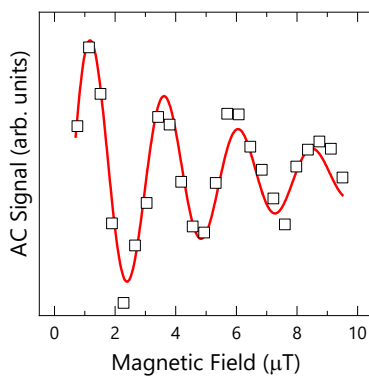


Fig.1 AC magnetic field sensing with an electrical detection method.

### Acknowledgments

We thank T. Ono and T. Moriyama for their technical help. This work was supported by MEXT Q-LEAP (No. JPMXS0118067395), KAKENHI (No. 15H05868, No. 19H02546), and Kyoto University Nano Hub.

### References

- <sup>1</sup> E. D. Herbschleb et al., *Nat. Commun.* **10**, 3766 (2019).
- <sup>2</sup> E. Bourgeois et al., *Nat. Commun.* **6**, 8577 (2015).
- <sup>3</sup> F. M. Hrubesch et al., *Phys. Rev. Lett.* **118**, 037601 (2017).
- <sup>4</sup> M. Gulka et al., *Phys. Rev. Applied* **7**, 044032 (2017).
- <sup>5</sup> P. Siyushev, et al. *Science* **363**, 728 (2019).
- <sup>6</sup> H. Morishita et al., *Sci. Rep.* **10**, 792 (2020).
- <sup>7</sup> T. Murooka et al., *App. Phys. Lett.* **118**, 253502 (2021).
- <sup>8</sup> M. Gulka et al., *Nat. Commun.* **12**, 4421 (2021).

## OPuS-MAGNM - Miniaturized Optically Pumped Solid State Quantum Magnetometers for Space Applications

Hannes Kraus<sup>1</sup>, Corey J. Cochrane<sup>1</sup>

<sup>1</sup>NASA Jet Propulsion Laboratory, California Institute of Technology, Pasadena, California, USA

*hannes.kraus@jpl.nasa.gov*

The OPuS-MAGNM project proposes to develop a novel low-cost low-power rad-hard miniaturized solid-state magnetometer for planetary magnetic field sensing. This technology leverages optically active, spin-carrying quantum centers (QC) in wide-bandgap semiconductors such as diamond or silicon carbide. External magnetic fields cause changes in the QC spin energy conformation, which can be detected optically. Wide-bandgap solid-state systems, in comparison to gas-cell based optically pumped magnetometers are interesting because of the material's intrinsic extensive temperature range (QC deterioration starts above Venus surface temperatures, at about 700C), and radiation hardness (QC implantation fluence  $\sim 10^{17}$  e/cm<sup>2</sup> vs. Europa orbit 30 day fluence  $\sim 10^{13}$  e/cm<sup>2</sup>). Additionally, the sensor lends itself to miniaturization, as QC are sensitive down to single emitters, i.e. small, sub-mm ensembles are sufficient sensor volumes.

The U.S. Planetary Science Decadal Survey identifies the need for a number of scientific instruments addressing the three crosscutting themes of planetary science: (1) understanding solar system beginnings, (2) searching for the requirements for life and (3) revealing planetary processes. Magnetometers are unassuming, but powerful tools aiding in all of these themes.

The proposed technology is an extension to the recent Silicon Carbide solid-state magnetometer (SiCMAG<sup>1</sup>), adding substantially better sensitivities at the expense of requiring optical readout<sup>2</sup>. We leverage optical readout noise being shot noise in nature, while all-electrical systems suffer from 1/f noise. This gives the optical readout approach a significant advantage in low-frequency and long-term stability performance metrics.

Consider the two most commonly used magnetometer technologies flown in space: Fluxgate systems exhibit high sensitivities and all-electrical simplicity, but require multiple coils per spatial direction. Additionally, fluxgates are not self-calibrating; drifts in absolute field values necessitate either augmenting the fluxgate system with a self-calibrating system or incorporating complicated spacecraft roll maneuvers into mission planning.

Optically pumped He cell systems can counter this issue, operating both in scalar and vector mode, also with very high sensitivities. Their downside is the added complexity of the gas cell, with Helium being notoriously prone to outgas. Also, vector-helium systems are larger and more expensive than fluxgates. OPuS-MAGNM now marries the solid-state simplicity of fluxgates and SiCMAG with the precision and self-calibration capabilities of an atomic gas magnetometer system, with improving longevity over gas cells. It has the potential to provide self-calibrated, heritage-level vector magnetic field science in a radiation-hard and thermal/vacuum-rugged miniaturized package; well suited for all kinds of planetary science missions.

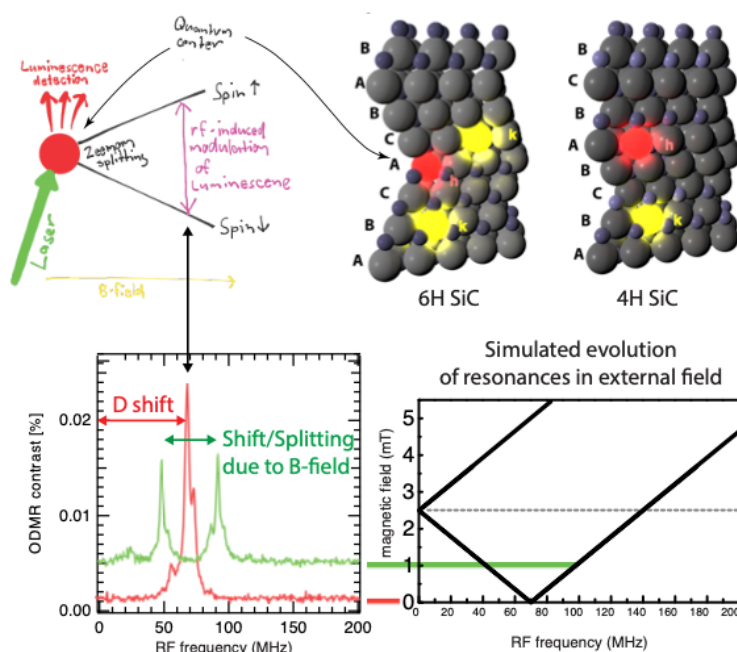


FIG. 1. Illustration of the signal genesis of the optically detected magnetic resonance (ODMR) in wide-bandgap solid-state semiconductors. Silicon vacancies in Silicon Carbide (h,k) are optically active spin carrying quantum centers, addressable by resonant excitation of electronic and radio frequency transitions. An exemplary ODMR spectrum at zero magnetic field and 1mT field is shown at the bottom left. A calculation of the resonance positions depending on the magnetic field is shown on the bottom right.<sup>3</sup>

### References

1. C.J. Cochrane, J. Blacksberg, M.A. Anders, P.M. Lenahan. Vectorized magnetometer for space applications using electrical readout of atomic scale defects in silicon carbide. *Sci. Rep.* 2016, 6 (1), 1239.
2. H. Zheng, J. Xu, G.Z. Iwata, et al. Zero-Field Magnetometry Based on Nitrogen-Vacancy Ensembles in Diamond. *Phys. Rev. Applied* 2019, 11 (6), 064068.
3. H. Kraus, V.A. Soltamov, F. Fuchs, et al. Magnetic field and temperature sensing with atomic-scale spin defects in silicon carbide. *Sci. Rep.* 2014, 4, 5303.

## Development of phthalocyanine ion beam for creation of multiple NV centers

Kosuke Kimura<sup>1,2</sup>, Shinobu Onoda<sup>1</sup>, Keisuke Yamada<sup>1</sup>, Wataru Kada<sup>2</sup>, Tokuyuki Teraji<sup>3</sup>,

Junichi Isoya<sup>4</sup>, Osamu Hanaizumi<sup>2</sup>, and Takeshi Ohshima<sup>1</sup>

<sup>1</sup> National Institutes for Quantum Science and Technology

<sup>2</sup> Graduate School of Science and Technology, Gunma University

<sup>3</sup> National Institute for Materials Science

<sup>4</sup> Faculty of Pure and Applied Sciences, University of Tsukuba

t201d208@gunma-u.ac.jp, kimura.kosuke@qst.go.jp

### Introduction

A nitrogen vacancy (NV center in diamond is known as a solid-state spin qubit worked at room temperature. NV centers coherently coupled by dipole-dipole interactions have a potential to accomplish quantum registers operatable at room temperature. Since the dipole-dipole interaction is inversely proportional to the cube of the distance between the NV centers, it is necessary to create NV centers in close proximity to each other. One of the methods to create NV centers in close proximity is nitrogen (N ion implantation via a nanohole mask [1]. This method has been reported to create double coupled NV centers. However, for reason of nanohole purification technology, it has been difficult to create multiple coupled NV centers with this method. The other method is molecular ion implantation [2,3]. In 2013, Yamamoto *et al.* reported the dipolar coupled NV center pair via nitrogen molecular ion ( $N_2^+$  implantation [2]. In 2019, Haruyama *et al.* reported the implantation of molecular ion from an adenine ( $C_5N_5H_5$  ion source and demonstrated to create triple coupled NV centers [3]. It is expected to create further multiple coupled NV center by implantation of molecular ion with a higher number of nitrogen atoms than  $C_5N_5H_5$ . In this study, we report to develop a phthalocyanine ( $C_{32}N_8H_{18}$  ion beam containing eight nitrogen atoms for creation of multiple NV centers.

### Method and result

The  $C_{32}N_8H_{18}$  ion beam was developed using an ion implanter. Firstly,  $C_{32}N_8H_{18}$  powder was vaporized and ionized by a heater at 336°C in the support gas (Ar ambient. Secondly, positive ions were electrically extracted by energy of 3 keV. Thirdly, the extracted beam was analyzed by mass spectrometry. The result of mass spectra was showed FIG. 1. The fragments, such as  $C_6H_4$ ,  $C_8H_4$ ,  $C_8N_2H_5$ , etc., and Ar were detected in mass number ranging from 0 to 250.  $C_{32}N_8H_{18}$  ion was detected around the mass number of 505. finally, the  $C_{32}N_8H_{18}$  ion beam extracted by mass spectrometry magnet was accelerated at the energy of 281 keV and implanted into the sample.

The NV centers created by  $C_{32}N_8H_{18}$  ion implantation were observed using confocal fluorescence microscopy (CFM). The measurement of photon counts and optically detected magnetic resonance (ODMR) were performed with 532 nm laser and microwaves. FIG. 2(a) shows a typical image observed by a CFM with area of  $20 \times 20 \mu m^2$ . Isolated spots are clearly found from  $C_{32}N_8H_{18}$  implanted region. FIG. 2(b) shows the ODMR spectra of the spot indicated by the circles and pentagon in FIG. 2(a). It is clear from the spectra that the spots labeled  $NV_A$ ,  $NV_B$ ,  $NV_C$ , and  $NV_D$  contain a single NV center with different axes. The spectrum labeled  $NV_{ABCD}$  is the result of the ODMR measurement of the spot indicated by the pentagon symbol in FIG. 1(a). from the number of dips in this spectrum, the creation of four NV centers with different orientation axes was observed per spot.

Therefore, we succeeded to create four NV centers in a spot by  $C_{32}N_8H_{18}$  ion implantation. In the presentation, I will report on the probability of the creation of multiple NV centers.

### Reference

- [1] I. Jakobi, *et al.*, *J. Phys.*, **752**, 012001 (2016).  
 [2] T. Yamamoto, *et al.*, *Phys. Rev. B*, **88**, 201201 (2014).  
 [3] M. Haruyama, *et al.*, *Nat. Commun.*, **10**, 2664 (2019).

### Acknowledgement

This work was supported by MEXT Q-LEAP Grant Number JPMXS0118067395 and JST Moonshot R&D Grant Number JPMJMS2062.

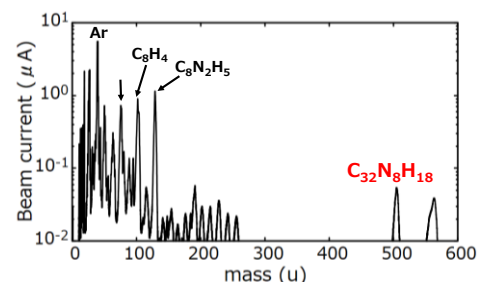


FIG. 1. Mass spectra from the  $C_{32}N_8H_{18}$  ion source.

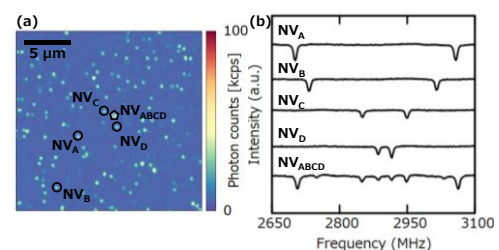


FIG. 2. (a) Typical CFM image ( $20 \times 20 \mu m^2$ ). (b) The ODMR spectra of the single NV centers and quadruple NV center.

## Fabrication of diamond protective film using microwave plasma CVD towards high-quality quantum emitters

K. Hirokawa<sup>1</sup>, K. Fukuda<sup>1</sup>, P. Wang<sup>1</sup>, T. Taniguchi<sup>2</sup>, M. Hatano<sup>1</sup> and T. Iwasaki<sup>1</sup>

<sup>1</sup>Department of Electrical and Electronics Engineering, School of Engineering, Tokyo Institute of Technology

<sup>2</sup>International Center for Materials Nanoarchitectonics, National Institute for Materials Science,

hirokawa.k.ab@m.titech.ac.jp

### Introduction

Quantum networks are expected to realize secure communication by using the transfer of quantum states. Quantum emitters which can generate a quantum entanglement state are necessary to construct quantum networks. Group-IV color centers in diamond has attracted due to the sharp zero photon line (ZPL) and resistance to external electric noise. Among the group-IV color centers, SnV and PbV are expected to have a long spin coherence time in the milli-seconds at Kelvin temperatures [1,2]. However, the fabrication process includes high-temperature anneal at 2100°C, resulting in deterioration of the sample surface, which frequently etches the incorporated color centers and hinders the fabrication of nanophotonic structures. To overcome this issue, in this study, diamond films were deposited on a diamond substrate containing SnV centers to protect during the high- temperature anneal.

### Method and Results

Figure 1 illustrates the fabrication process. We used a Iia-type diamond substrate (Element Six). Sn ions were implanted into the substrate with an acceleration energy of 700 keV and a dose of  $2 \times 10^9/\text{cm}^2$ . Then, diamond films were deposited by two microwave plasma CVD systems for 40 hours in total. At the first growth stage, diamond films with low impurity concentrations were synthesized at the low growth rate. Then, at the next stage, thicker diamond films were grown using a high-power plasma CVD system. This sample was treated at 2100°C under 7.7 GPa to form SnV centers in the Iia-type diamond substrate. Confocal fluorescence microscope observations were carried out at a cryogenic temperature.

The CVD film remained on the substrate after anneal at 2100°C. Figure 2 shows ZPL from the SnV centers after the high-temperature anneal. The two lines correspond to C- and D-peaks, originating from split energy levels of the SnV centers. These observations indicate that the deposited diamond films worked as a protective layer to form SnV centers.

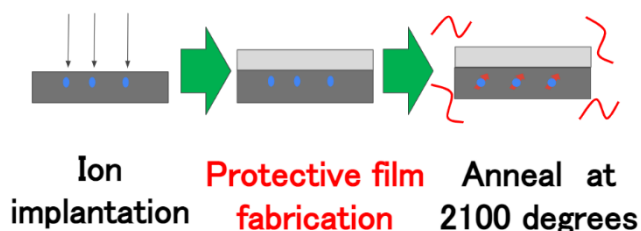


FIG.1. Schematic diagram of protective film fabrication for the SnV center formation.

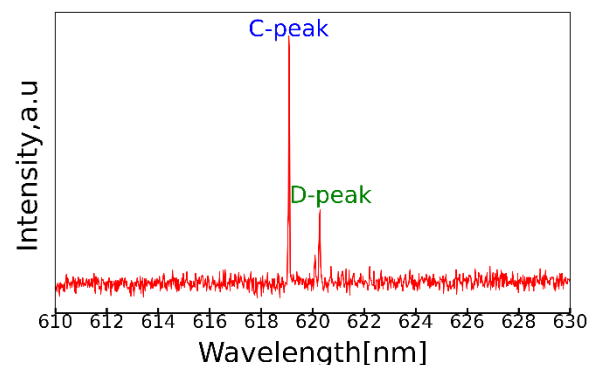


FIG.2. PL spectrum of SnV

### Reference

<sup>1</sup>T.iwasaki et al, Phys. Rev. Lett, 119, 253601 (2017)

<sup>2</sup>P.Wang et al, ACS photonics,2947,2954(2021)

### Acknowledgments

This work was supported by the Toray Science Foundation, the MEXT Quantum Leap Flagship Program (MEXT Q-LEAP) Grant No. JPMXS0118067395 and "Nanotechnology Platform Program" of the Ministry of Education, Culture, Sports, Science and Technology (MEXT), Japan, Grant Number JPMXP09F-21-IT-013.

## A compact quantum sensor head with side excitation of CVD diamond

Yuki Nishio<sup>1</sup>, Yuji Hatano<sup>1</sup>, Jaewon Shin<sup>2</sup>, Daisuke Nishitani<sup>1</sup>, Ryo Matsuki<sup>1</sup>, Hiromitsu Kato<sup>3</sup>, Shinobu Onoda<sup>4</sup>, Takeshi Oshima<sup>4</sup>, Keigo Arai<sup>1</sup>, Mutsuko Hatano<sup>1</sup>, and Takayuki Iwasaki<sup>1</sup>

<sup>1</sup>Department of Electrical and Electronics Engineering, School of Engineering, Tokyo Institute of Technology

<sup>2</sup>Yazaki Corporation

<sup>3</sup>National Institute of Advanced Industrial Science and Technology

<sup>4</sup>National Institutes for Quantum Science and Technology

nishio.y.ac@m.titech.ac.jp

### Introduction

A compact sensor system is important for practical applications of quantum diamond sensors using NV centers. There have been reports on nanotesla to sub-nanotesla sensitivities for the small modular diamond sensor, such as  $3 \text{ nT}/\sqrt{\text{Hz}}$  by side excitation on a (100 crystal<sup>1</sup>,  $310 \text{ pT}/\sqrt{\text{Hz}}$  by perpendicular excitation on a (100 crystal<sup>2</sup>, and  $344 \text{ pT}/\sqrt{\text{Hz}}$  by perpendicular excitation on a (111 crystal<sup>3</sup>. In this report, we investigate the side excitation of a CVD diamond layer on a (111 crystal including a large volume of NV centers.

### Method

The configuration of the sensor head fabricated in this experiment is shown in FIG.1. A  $110 \mu\text{m}$ -thick  $^{12}\text{C}$ -enriched CVD film grown on  $2.0 \times 2.0 \times 0.3 \text{ mm}^3$  4H (111) substrate was used as the diamond sensor. The NV centers were formed by  $5.0 \times 10^{17} \text{ cm}^{-2}$  EB irradiation and high-temperature anneal. The excitation green laser was introduced on a sidewall of the CVD film, and the fluorescence emitted from the NV centers was then collected by a CPC lens and led into a photodiode through LPFs. The microwave antenna was made of copper tape and the microwave magnetic field was applied horizontally. The antenna was placed on an AlN heatsink plate. In order to excite only the NV-rich region in the diamond sample, the laser diameter was adjusted using a beam expander and focusing lens. A part of the excitation laser was extracted as a reference light to cancel the laser noise from the fluorescence. The optical system was placed in a 1 mm-thick permalloy single layer magnetic shielded box.

### Result

First, we investigated the magnetically insensitive noise and slope of the lock-in ODMR by varying the deviation frequency (Fig. 2a). Although the slope takes the maximum value at a deviation frequency of 500 kHz, in this experiment, we set the deviation frequency around 350 kHz, where the noise/slope becomes small. The measured magnetic field noise spectrum is shown in Fig. 2b. The sensitivity was estimated to be  $770 \text{ pT}/\sqrt{\text{Hz}}$  and the noise floor was  $400 \text{ pT}/\sqrt{\text{Hz}}$  between 30-100 Hz. In this frequency range, the noise floor of magnetically sensitive is comparable to that of the magnetically insensitive. The shot-noise limit sensitivity, calculated from the contrast and linewidth measured from the ODMR, is  $15 \text{ pT}/\sqrt{\text{Hz}}$ , expecting a higher magnetic field sensitivity by improving the measurement system. This work was supported by MEXT Q-LEAP Grant Number JPMXS0118067395.

### Reference

<sup>1</sup>J. Webb et al., Appl. Phys. Lett. 114, 231103 (2019)

<sup>2</sup>R. Patel et al., Phys. Rev. Appl. 14, 044058 (2020)

<sup>3</sup>F. Stürner et al., Adv. Quantum Technol. 4, 2000111 (2021)

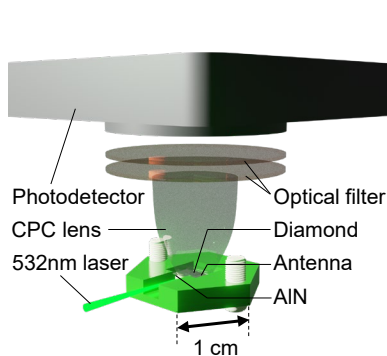


FIG.1 Sensor module for side laser excitation.

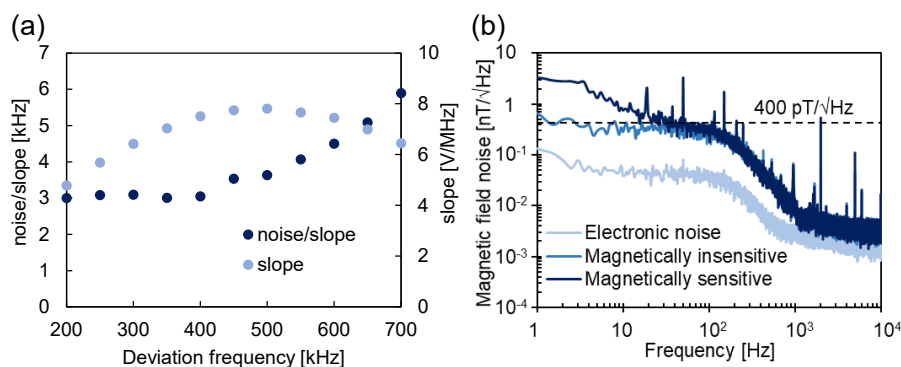


FIG.2 (a) Ratio of the magnetically insensitive noise to the slope of the lock-in ODMR and the slope depending on the deviation frequency. (b) Measured FFT spectrum of sensitivity. The black dotted line indicates  $400 \text{ pT}/\sqrt{\text{Hz}}$ .

## Hybrid integration of Si<sub>3</sub>N<sub>4</sub> grating structure on diamond NV substrate for efficient photon extraction

Ryota Katsumi<sup>1,2</sup>, Takeshi Hizawa<sup>1</sup>, Akihiro Kuwahata<sup>2,3</sup>, Takayuki Iwasaki<sup>4</sup>, Mutsuko Hatano<sup>4</sup>,

Fedor Jelezko<sup>5</sup>, Masaki Sekino<sup>2</sup>, and Takashi Yatsui<sup>1,2</sup>

<sup>1</sup> Graduate School of Engineering, Toyohashi University of Technology

<sup>2</sup> Graduate School of Engineering, The University of Tokyo

<sup>3</sup> Graduate School of Engineering, Tohoku University

<sup>4</sup> School of Engineering, Tokyo Institute of Technology

<sup>5</sup> Institute of Quantum Optics, Ulm University

katsumi.ryota.ti@tut.jp

### Introduction

Nitrogen-vacancy (NV) centers in diamond is a promising candidate for a quantum sensor, especially a sensitive magnetometer thanks to their excellent spin property<sup>1,2</sup>. However, their demonstrated magnetic field sensitivity is far beyond those based on superconducting quantum-interference devices. One of the critical issues is the low extraction efficiency of the emitted photons from the diamond NV substrate<sup>3</sup>. This can be overcome by implementing the nanostructure on diamond including gratings, but the fabrication of such structure on diamond is technically difficult.

### Method

In this work, we demonstrate the hybrid integration of grating structure on a diamond NV substrate using transfer printing, which is based on a simple pick-and-place operation<sup>4</sup>. Figure 1(a) displays the SEM image of the grating based on Si<sub>3</sub>N<sub>4</sub>, which is transparent for the NV emission wavelength of around 700 nm. To pick them up, we employed the air-bridged structure for the grating. By using the transfer printing [Fig. 1(b)], the Si<sub>3</sub>N<sub>4</sub> grating was integrated on the diamond NV substrate. Figure 1(c) displays the optical microscope image of the fabricated device. The grating is indeed bonded with the diamond NV substrate. The detailed design and characterization will be discussed in the presentation.

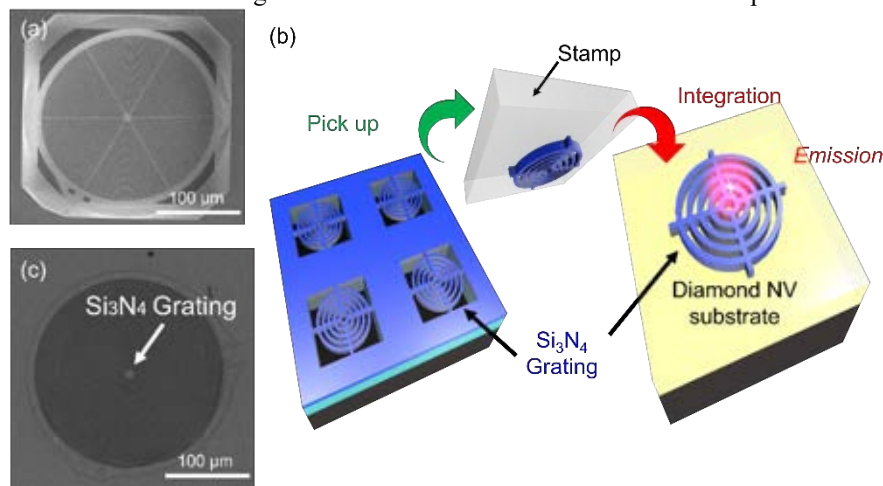


FIG. 1. (a) SEM image of the fabricated Si<sub>3</sub>N<sub>4</sub> grating. (b) Schematics of the transfer printing-based integration of Si<sub>3</sub>N<sub>4</sub> grating on diamond. (c) Optical microscope image of the fabricated device.

### Acknowledgement

This work was supported by MEXT Q-LEAP Grant Number JPMXS0118067395 and Kakenhi (18H01470, 20H02197, 20H05091, 20K21118).

### References

- <sup>1</sup> J. M. Taylor, *et al.*, Nat. Phys. **4**, 810 (2008).
- <sup>2</sup> A. Kuwahata, *et al.*, Sci Rep **10**, 2483 (2020).
- <sup>3</sup> D. Le Sage, *et al.*, Physical Review B **85**, 121202 (2012).
- <sup>4</sup> R. Katsumi, *et al.*, Optica **5**, 691 (2018).

## Superconducting nanostrip single-photon detectors with dielectric multilayer cavities

Fumihiko China<sup>1</sup>, Shigehito Miki<sup>1,2</sup>, Satoru Mima<sup>1</sup>, Masahiro Yabuno<sup>1</sup>, Shigeyuki Miyajima<sup>1</sup> and Hirotaka Terai<sup>1</sup>

<sup>1</sup> Advanced ICR Research Institute, National Institute of Information and Communications Technology

<sup>2</sup> Graduate School of Engineering, Kobe University

f-china@nict.go.jp

### Introduction

Superconducting nanostrip single-photon detectors (SNSPDs) have attractive features such as high detection efficiency, low dark count rate, and low timing jitter, and are promising instruments in various fields, including quantum information science [1]. The superconducting nanostrip consisting of a thin and narrow meandering line potentially has photon sensitivity in a wide wavelength range from ultraviolet to mid-infrared, but the optical absorptance of only a single nanostrip layer is as low as few tens of percent. The SNSPDs integrated with dielectric multilayer (DML) cavities, as shown in FIG. 1, are effective structures to enhance the optical absorptance of the nanostrips at the target wavelengths. The DMLs are composed of two dielectric materials with different refractive indexes. By optimizing the layer structure such as the number of layers and film thickness of each layer, the optical properties of SNSPDs can be designed flexibly according to the requirement [2]. In this presentation, we show the development of SNSPDs with DMLs for various wavelength regions.

### Method

We have designed and developed SNSPDs with DMLs using SiO<sub>2</sub> and TiO<sub>2</sub> for the visible wavelength, SiO<sub>2</sub> and Si for the telecom wavelength, and Ta<sub>2</sub>O<sub>5</sub> and Si for the mid-infrared region, respectively. FIG. 1 shows a schematic of an SNSPD with a DML composed of SiO<sub>2</sub> and TiO<sub>2</sub>, which is designed for 780 nm wavelength region. First, the layer structure of the DML was optimized for the target wavelength using a thin film calculation software. Subsequently, we simulated the absorptance dependence on the polarization state of incident photons by finite-element analysis. As results, the optimized number of layers and the total thickness of the DML are 17 layers and 2.02 μm, respectively. Since it was also confirmed that the optical absorptance of the nanostrip depends on the polarization state of the incident photon, SiO film is deposited on the nanostrip to minimize the polarization sensitivity at the wavelength of 780 nm. Then, we fabricated the nanostrip devices according to the optimized design of SNSPD with the DML and evaluated the wavelength dependence of the system detection efficiency (DE) using a supercontinuum light source. FIG. 2 shows the wavelength dependence of the optical absorptance and measured system DE. The obtained dependence of the system DE well agrees with optical absorptance dependence in the simulations, and we obtained a high system DE of 85% at 780 nm. The developments of SNSPDs for other wavelengths will be talked in the presentation.

### Acknowledgment

This work was supported by MEXT Q-LEAP Grant Number JPMXS0118067634, JST CREST Grant Number JPMJCR1671, and JST Moonshot R&D Grant Number JPMJMS2066.

### Reference

<sup>1</sup>R. H. Hadfield, *Nat. Photon.*, **3**, 696–705 (2009).

<sup>2</sup>T. Yamashita, K. Waki, S. Miki, R. A. Kirkwood, R. H. Hadfield, H. Terai, *Sci rep.*, **6**, 35240 (2016).

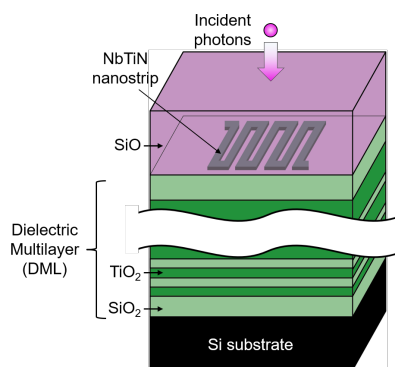


FIG. 1. Schematic of the device structure of an SNSPD with a DML. The number of layers and total thickness of the DML are 17 layers and 2.02 μm, respectively.

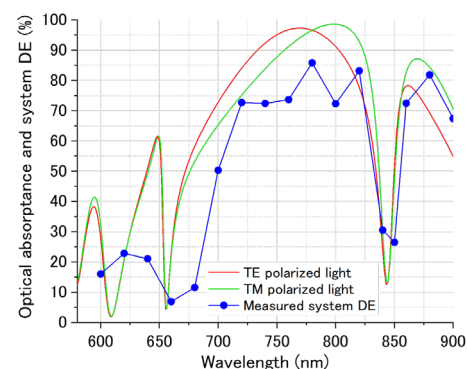


FIG. 2. Comparison of the simulated optical absorptance of the NbTiN nanostrip and the measured system DEs.

## Estimation of the quantum efficiency of the up-conversion system based on injection-locked dual oscillators

Masayuki Hojo<sup>1</sup>, Shuntaro Tani<sup>2</sup>, Yohei Kobayashi<sup>2</sup>, and Koichiro Tanaka<sup>1</sup>

<sup>1</sup>Department of Physics, School of Science, Kyoto University

<sup>2</sup>ISSP, The University of Tokyo

hojo.masayuki.33e@st.kyoto-u.ac.jp

### Introduction

Spontaneous parametric down-conversion (SPDC) is essential tool for a quantum light source in the infrared region ranging 2-5  $\mu\text{m}$  for the purpose of material identification, chemical analysis, and gas sensing. However, SPDC process has a technical limitation of low efficiency and can be detected only by sensitive detectors. Up-conversion detecting system has been demonstrated to bridge such a gap. So far, existing technique<sup>1</sup> has been concentrated into the conversion efficiency, in which the temporal duration of the light source was highly broad. In this work, we implement the up-conversion detector using two Er- and Yb-doped fiber lasers (EDFL and YDFL) with the duration narrower than the conventional one.

### Method

Figure 1 illustrates the schematics of the up-conversion system. The EDFL output at 1.56  $\mu\text{m}$  was split into two ports, which served as the injecting seed and the pump for down frequency generation (DFG) process in PPSLT, respectively. The repetitions of EDFL and YDFL was synchronized at 57.9 MHz. The YDFL output had the spectral shape narrowed by Fiber-Bragg-Grating (FBG) and was boosted to 100mW. Similarly, the amplified pulse was divided into two portions, the DFG port and the up-conversion port. In the DFG port, the two pulses at 1.03 and 1.56  $\mu\text{m}$  were spatially combined with a wavelength division multiplexer (WDM) and produced a MIR pulse by DFG process. The MIR light source was then introduced into PPLN crystal. The pump for the up-conversion was focused into PPLN in the collinear configuration with the MIR pulse. The SFG signal in the visible region was detected by a sensitive detector.

In our presentation, we will report the result of up-conversion detection and discuss about the system improvement.

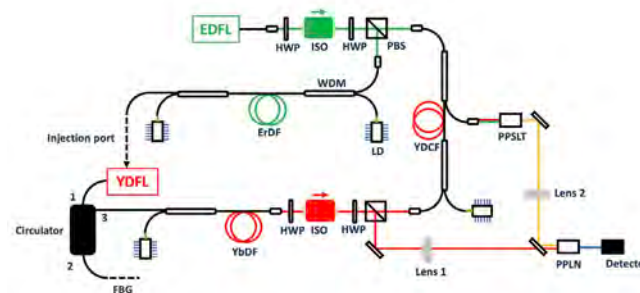


Fig. 1 Schematics of the whole system.

### Acknowledgement

This work was supported by MEXT Q-LEAP Grant Number JPMXS0118067634.

### Reference

1. Huang, K. *et al. Photonics Res.* **9**, 259 (2021).

## Selective measurement of biexciton luminescence by photon correlation spectroscopy

Hiroya Seki<sup>1</sup>, Keita Hashimoto<sup>2</sup>, Jun Ishihara<sup>2</sup>, Kensuke Miyajima<sup>2</sup>, Ryosuke Shimizu<sup>1</sup>

<sup>1</sup>Department of Engineering Science, The University of Electro-Communications

<sup>2</sup>Department of Applied Physics, Tokyo University of science

s2043006@edu.cc.uec.ac.jp

### Introduction

Coincidence measurement performed by two detectors is a common technique to detect photon pairs in quantum optical experiments [1] and allows us to extract two-photon events from the input state of light [2]. This technique has been used in demonstrating fundamental concepts of quantum mechanics, quantum information protocols, and quantum imaging. On the other hand, we also expect the application of coincidence measurement to spectroscopy as a new development of quantum technology. Combining the coincidence counting with frequency-resolved measurement could bring us a new approach to spectroscopy in a quantum manner. Hereafter we refer to it as photon correlation spectroscopy (PCS) [3]. The Photon-number-resolving ability of PCS may provide a powerful tool to analyze a complex quantum system in condensed matter. Here we present a proof-of-concept experiment of PCS with biexciton luminescence.

### Method

Biexciton is generated via a two-photon resonant excitation by the second harmonic of a mode-locked Ti: sapphire laser, and then decays into two polaritons; a higher energy polariton (HEP) and a lower energy polariton (LEP). After propagating in the crystal, the polaritons are converted into photons at the crystal surface. In this process, the sum of the two-photon energy should be the same as biexciton energy due to the phase-matching condition. We employed a femtosecond laser with the bandwidth of 4.4 nm, corresponding energy width of 9.0 eV, to clarify the photon-number-resolving ability. In this situation, the spectrum of Rayleigh scattering light of the laser overlaps that of biexciton luminescence. Therefore, it is difficult to distinguish the biexciton luminescence from the laser spectrum. In contrast, PCS enables us to observe HEP and LEP due to the photon-number-resolving ability.

In order to characterize two-photon spectral distributions, joint spectral intensity (JSI) plotted in a two-dimensional space has been employed in the quantum optics field [4]. The JSI represents the two-photon probability distribution as a function of the energy of the constituent photon. Experimentally, we recorded the coincidence counting values by scanning the transmission frequency of two monochromators for the JSI measurement.

Figure 1 shows the measured JSI of biexciton luminescence. We can see a single peak distribution caused by coincidence counts of HEP and LEP. We estimated the spectral width of HEP (LEP) as 0.94 (1.2) meV from the projection of the JSI onto the vertical (horizontal) axis, which is narrower than the bandwidth of the laser. This result implies a successful demonstration of PCS.

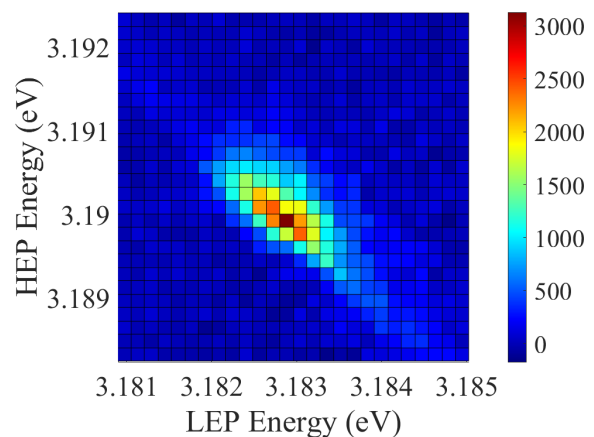


FIG. 1. JSI of biexciton luminescence.

### Acknowledgment

This work was supported by MEXT Q-LEAP Grant Number JPMXS0118069242.

### Reference

- <sup>1</sup> C. K. Hong, Z. Y. Ou, and L. Mandel, *Phys. Rev. Lett.*, **59**, 2044-2046 (1987).
- <sup>2</sup> H. Seki, K. Miyajima, R. Shimizu, arXiv:2109.03715 (2021)
- <sup>3</sup> C. M. Muñoz, and F. Schlawin, *Phys. Rev. Lett.*, **124**, 203601 (2020).
- <sup>4</sup> P. G. Evans, R. S. Bennink, W. P. Grice, and T. S. Humble, *Phys. Rev. Lett.*, **105**, 25361 (2010).

## Towards Optical Manipulation of Gold-Nanoparticles for Efficient Single Photon Sources

Rui Sun<sup>1</sup>, Yining Xuan<sup>1</sup>, Soyoung Baek<sup>1</sup>, and Keiichi Edamatsu<sup>1</sup>

<sup>1</sup>Research Institute of Electrical Communication, Tohoku University

sun@quantum.riec.tohoku.ac.jp

Quantum dot is a promising candidate for constructing a single photon source because of its broad and continuous excitation spectrum, adjustable wavelength, high photochemical stability, and long fluorescence lifetime<sup>1</sup>. Our research focuses on the single photon source based on quantum-dot-gold-nanoparticle coupled system on optical nanofiber<sup>2</sup>. Combining with the Purcell effect<sup>3</sup>, the rise time of the second order intensity correlation function for quantum dot can be enhanced. However, the position of gold-nanosphere on nanofiber is entirely random, which makes the quantitative study of single-photon emission rate difficult. We propose a non-contact method to control the position of a gold-nanoparticle on the nanofiber making use of an optical tweezer. We calculate the optical responses and heating effects of a gold-nanoparticle trapped in optical tweezer to define the optimal wavelength and laser power for the experiment.

The optical response of a gold-nanoparticle submerged in water and trapped in an optical tweezer is calculated based on Mie theory. Figure 1 is the scattering and absorption efficiencies of a gold-nanoparticle in an optical tweezer. The red and blue curves are the scattering ( $Q_{sca}$ ) and absorption ( $Q_{abs}$ ) factors, respectively. The abscissa is the size parameter ( $ka$ ) of the gold-nanoparticle;  $k$  is the wave number of the light and  $a$  is the radius of gold-nanosphere. Here, the gold-nanoparticle size ranges from 0 to 200 nm. For the same particle size, the longer the optical wavelength is, the weaker the effect of absorption and scattering.

This work was supported by MEXT Q-LEAP Grant Number JPMXS0118067581.

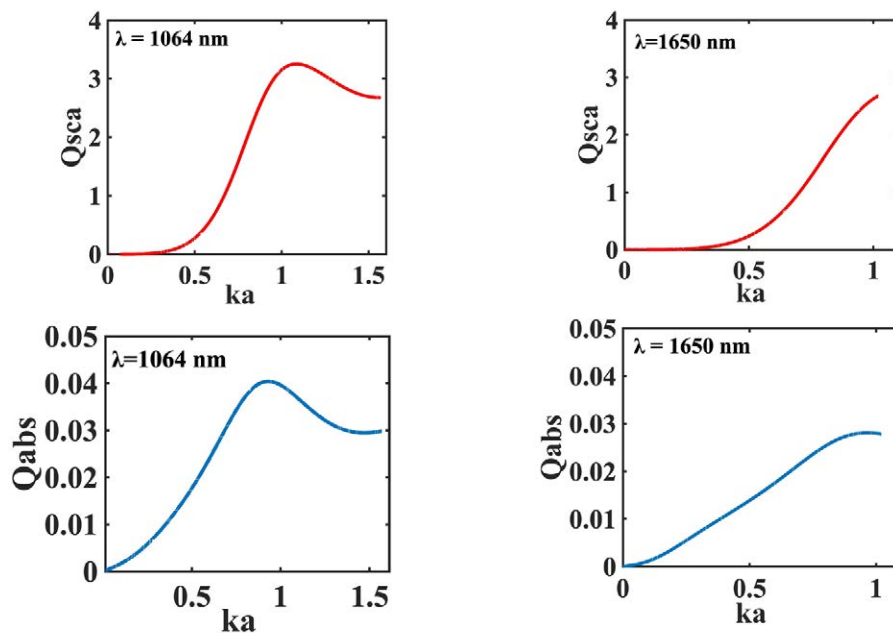


FIG. 1. Scattering and absorbing efficiencies of gold-nanoparticle trapped in optical tweezer.

### References

- <sup>1</sup> O. Gazzano and G. Solomon, *J. Opt. Soc. Am. B*, **33**, C160-C175 (2016).
- <sup>2</sup> M. Sadgrove, M. Sugawara, Y. Mitsumori and K. Edamatsu, *Sci Rep*, **7**, 17085 (2017).
- <sup>3</sup> Q. Gu, and Y. Fainman, *Semiconductor Nanolasers*, (pp. 65-90) (2017).

# Single photon emission from a quantum-dot-gold-nanostar coupled system on an optical nanofiber

Yining Xuan<sup>1</sup>, Masakazu Sugawara<sup>1</sup>, Rui Sun<sup>1</sup>, Soyoung Baek<sup>1</sup>, Keiichi Edamatsu<sup>1</sup>, and Mark Sadgrove<sup>2</sup>

<sup>1</sup>Research Institute of Electrical Communication, Tohoku University

<sup>2</sup>Department of Physics, Faculty of Science, Tokyo University of Science

xuan@quantum.riec.tohoku.ac.jp

Single-photon emitters play an important role in many leading quantum technologies such as quantum communications and quantum cryptography. Therefore, coupling them to existing fiber network can be a promising candidate for the various applications in quantum network. As a carrier of photon transportation, optical nanofiber has the advantage of ultra-low loss, low cost and high coupling efficiency [1]. Since the nanofiber has a diameter of hundreds of nanometers, photons emitted from single photon emitters can be coupled into nanofiber through the evanescent field directly. Therefore, single-photon source's effective incorporation into nanofibers shows great potential in the construction of fiber-based quantum information network. In 2012, Yalla *et al.* demonstrated the coupling of single photons from quantum dots into the nanofiber [2]. After that, Liebermeister *et al.* succeed in coupling single photons from color centers in a diamond into the nanofiber [3]. Nevertheless, how much we can improve the coupling between the single-photon emitters and the nanofiber is still an open question that needs to be addressed. In this research, in order to achieve Purcell-enhanced single-photon emission from a quantum dot (QD, we place gold nanoparticles, especially gold nanostars (GNS, in the vicinity of the quantum dot located on the surface of an optical nanofiber. By measuring the rise time of the second order correlation function  $g^{(2)}(\tau)$  for both the GNS-QD system and the sole QD system, Purcell-enhancement can be verified.

We fabricate a nanofiber with the diameter of 474 nm by heating-stretch method [4][5], and place a GNS and a QD on the surface of a nanofiber. Figure 1 shows scanning electron microscope (SEM) image of GNS-QD coupled system. By scanning a laser beam spot along the nanofiber axis and measuring the photoluminescence (PL signal from the QD and the scattered light from the GNS, we confirm the GNS and the QD is located within 1.5  $\mu\text{m}$  interval. Next, we measure second order correlation function  $g^{(2)}(\tau)$  for both the GNS-QD system and the sole QD system on the same nanofiber. See Figure 2. The obtained  $g^{(2)}(0)$  for the GNS-QD and Sole QD was less than 0.5, a signature of anti-bunched single photons. The rise time of  $g^{(2)}(\tau)$  for the GNS-QD and the SQD are obtained to be 167 ns and 107 ns, respectively; the GNS-QD exhibited ~36 % reduction of the rise time in comparison to the SQD. Although it is likely to originate from Purcell enhancement, more detailed and complete measurement and analysis are necessary to conclude.

This work was supported by MEXT Q-LEAP Grant Number JPMXS0118067581.

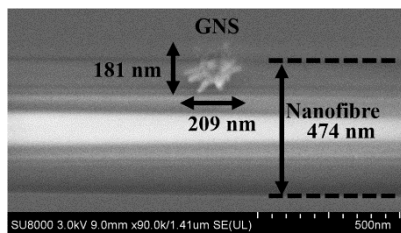


FIG. 1. SEM image of GNS-QD coupled system.

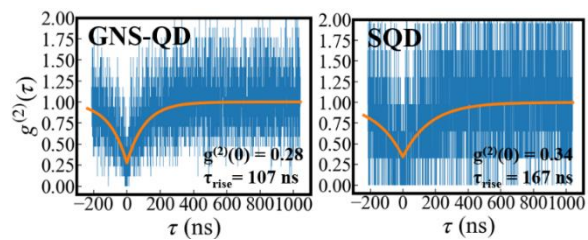


FIG. 2.  $g^{(2)}(\tau)$  measurement of GNS-QD coupled system and sole QD system, respectively.

## Reference

- <sup>1</sup>M. Sadgrove, M. Sugawara, Y. Mitsumori, and K. Edamatsu, *Sci. Rep.*, **7**, 17085 (2017).
- <sup>2</sup>R. Yalla, K. Nayak, and K. Hakuta, *Opt. Express*, Vol. **20**, Issue **3**, 2932 (2012).
- <sup>3</sup>L. Liebermeister *et al.*, *Appl. Phys. Lett.*, **104**, 031101 (2014).
- <sup>4</sup>M. Sugawara, Y. Mitsumori, K. Edamatsu, and M. Sadgrove, *Opt. Express*, **28**, 18938 (2020).
- <sup>5</sup>M. Sadgrove, T. Yoshino, M. Sugawara, Y. Mitsumori, and K. Edamatsu, *Phys. Rev. Applied*, **16**, 044034 (2021).

SE-03A-γ2-06

## Focusing constraints on coupling efficiency of collinear type-I degenerated SPDC photon pairs into a single-mode fiber

Nicolas Schwaller<sup>1,2</sup>, Geobae Park<sup>1</sup>, Ryo Okamoto<sup>1,3</sup>, and Shigeki Takeuchi<sup>1</sup>

<sup>1</sup>Department of Electronic Science and Engineering, Kyoto University

<sup>2</sup>Institute of Physics, Swiss Federal Institute of Technology Lausanne (EPFL), Lausanne, Switzerland

<sup>3</sup>Japan Science and Technology Agency, PRESTO

schwaller.nicolas.52z@st.kyoto-u.ac.jp

### Introduction

Entangled photon pairs represent an essential resource for various quantum technologies, such as quantum key distribution, quantum computing or quantum imaging. A common process to produce correlated pairs is spontaneous parametric downconversion (SPDC) of pump photons into pairs of entangled photons which are then coupled into a single-mode (SM) fiber. For most applications, it is desirable to maximize the coupling efficiency of the entangled pairs into the SM fiber, as well as the rate of pairs that can be collected. Systematic studies about the maximization of these quantities have been carried out for specific parameters of SPDC, e.g. using type-II phase-matching condition [1]. However, despite advances on theoretical modelling [2,3], other SPDC configurations still lack experimental evidence to confirm the dependence of the coupling efficiency on the main parameters of the setup. This study focuses on collinear degenerated co-polarized SPDC photon pairs. They are relevant for various applications such as single mode squeezed states for gaussian boson sampling, and non-linear interferometers.

### Method

We investigate the dependence of the correlated-mode coupling efficiency  $\eta_c$  on pump and collection beam waists by continuously varying their size thanks to two beam expanders (FIG. 1). We generate type-I SPDC by pumping a bulk beta barium borate (BBO) crystal of  $L=3$  mm length with a continuous wave (CW) 404 nm laser. We measure the coupling efficiency using coincident detections from single photon counting modules (SPCMs), and study the impact of different focusing conditions of the pump and collection beam. The estimated coupling efficiency was obtained by considering the losses of the optics and the experimentally determined quantum efficiencies of the SPCMs. The observed  $\eta_c$  reached up to 98%.

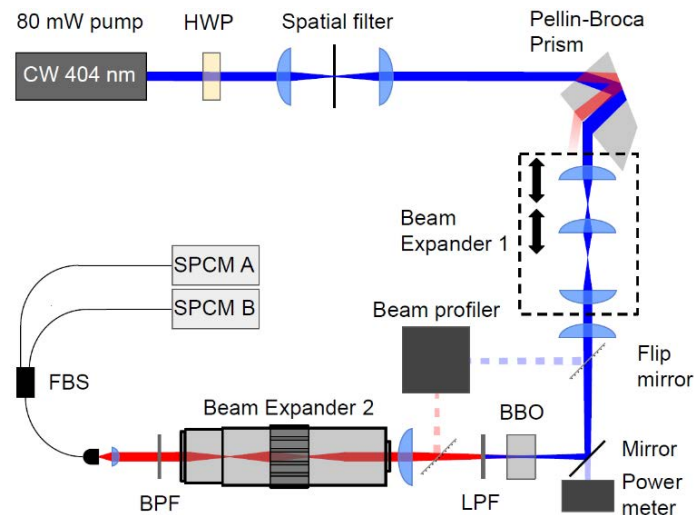


FIG. 1: Experimental setup enabling to change the focus of pump and collection beam in the crystal.

This work is supported in part by JST CREST Grant Number JPMJCR1674, Japan, MEXT Quantum Leap Flagship Program (MEXT Q-LEAP) Grant Number JP-MXS0118067634, JST-PRESTO (JPMJPR15P4), and KAHENHI Grants-in-Aid No. 21H04444.

### Reference

<sup>1</sup>P. Ben Dixon *et al.*, *Phys. Rev. A*, **90**(4), 1-9 (2014).

<sup>2</sup>R. S. Bennink, R. S., *Phys. Rev. A*, **81**(5), 1-10 (2010).

<sup>3</sup>H. E. Guilbert *et al.*, *IEEE Journal of Selected Topics in Quantum Electronics*, **21**(3), 215-224 (2015).

# 4<sup>th</sup> IFQMS

The 4th International Forum  
on Quantum Metrology and Sensing

## PROCEEDINGS

Short Presentations by Young Researchers  
Part 2: SE-03B

December 8th, 2021  
Online Conference (Zoom)

Joint Program Session with Quantum Innovation 2021



**Quantum Sensing Track : Short Presentations by Young Researchers**
**SE-03B. Short Presentations by Young Researchers on SE-02, 05 Topics [4th IFQMS]**

\*Note: Depending on the program, the order of presentations may change within the same group.

All the times in the program are Japan Standard time (GMT+9)

Dec 8 (Wed.)	Session / Presentation	Mentor Chair Co-chair / Presenter	Affiliation	Abstract ID
<b>13:10-14:30 SE-03B-01</b>				
	Mentor	Johnjoe McFadden	U Surrey	
	Mentor	Shigenori Tanaka	Kobe U	
	Mentor	Kiminori Maeda	Saitama U	
	Chair	Noriaki Yahata	QST	
	Co-chair	Akinari Yokoya	QST	
	Intracellular thermal conductivity determined by dual-functionalized diamond nanosensor	Madoka Suzuki	Osaka U	SE-03B-01-01
	Label-free analysis of diffusion constant in lipid bilayers using nanoscale diamond magnetometry	Hitoshi Ishiwata	QST	SE-03B-01-02
	Temperature sensing using silicon vacancy centers in detonation nanodiamonds	Masanori Fujiwara	Kyoto U	SE-03B-01-03
	Quantum-inspired machine learning for exponentially big neural data analysis	Kei Majima	QST	SE-03B-01-04
	Empirical verification of the violation of the temporal Bell inequality in bistable perception	Yasunori Aizawa	QST	SE-03B-01-05
	Tracking radiation damage induction pathway following core-hole creation of DNA molecules in aqueous solution	Yoshiaki Kumagai	TUAT	SE-03B-01-06
<b>14:50-16:10 SE-03B-02</b>				
	Mentor	Peter Hore	U Oxford	
	Mentor	Akihito Ishizaki	IMS	
	Mentor	Yasuteru Shigeta	U Tsukuba	
	Chair	Yoichi Takakusagi	QST	
	Co-chair	Tatsuhiko Imaoka	QST	
	High-resolution structure of an electron-transfer protein by neutron crystallography	Yuya Hanazono	TMDU	SE-03B-02-01
	Fabrication of a quantum sensor to reveal a topic in thermal physiology	Shuya Ishii	QST	SE-03B-02-02
	Investigation of irradiation induced nitrogen-vacancy centers in 5-nanometer-sized detonation nanodiamonds	Kit So	Kyoto U	SE-03B-02-03
	Formation of flavin anion and tyrosine radicals in avian Cryptochrome4	Hiroaki Otsuka	Waseda U	SE-03B-02-04
	Do neural activities of binocular rivalry follow a quantum probability model? A test of temporal Bell inequalities	Takahiro Hirao	QST	SE-03B-02-05
	X-ray absorption spectroscopy of a silicon phthalocyanine derivative, IR700, for X-ray excited photoimmunotherapy	Yudai Izumi	QST	SE-03B-02-06
	Magnetically sensitive radical pairs in avian cryptochrome 4 proteins	Jingjing Xu	U Oldenburg	SE-03B-02-07

## Intracellular thermal conductivity determined by dual-functionalized diamond nanosensor

Madoka Suzuki<sup>1</sup>

<sup>1</sup>*Institute for Protein Research, Osaka University*

*suzu\_mado@protein.osaka-u.ac.jp*

### Introduction

Cellular thermogenesis is an origin of rising body temperature. However, it is difficult to examine thermal effects in a small scale such as a cell or a nanoparticle. The difficulty is caused by a simple reason; i.e., the thermogenesis occurs within the volume of the heat source, while the heat escapes from its surface. When the size of a heat source (a fixed shape and volume is considered) decreases by half, the volume of the heat source becomes 1/8, whereas the surface area decreases only by 1/4. Therefore, as the scale of a system is reduced, the temperature rise can be orders of magnitude smaller and quicker than in larger systems such as a tissue and an organism. This difficulty has been eased recently by a variety of temperature nanoproboscopes and local heating methods. We can measure and manipulate temperature locally at the subcellular scale. Yet, the heat diffusion in cells, an essential knowledge to understand the results provided by those new methods, have never been determined experimentally [1]. In many cases, the heat diffusion in a cell has been considered as similar to that in cells.

### Method

Here, our recent study provided a new methodology to measure the thermal conductivity at the nanoscale [2]. The method utilizes a dual-functionalized diamond nanosensor that functions as both a nanothermometer and a nanoheater. We found that the thermal conductivity in HeLa and MCF-7 cell lines is surprisingly smaller (about 1/6) than in water. This new finding that the heat diffusion in a cell is significantly hindered than in water may suggest a new role of cellular thermogenesis in biology beyond the conventional understanding of rising body temperature. Now we can expect that larger or longer heat pulses are formed by metabolic processes in cells [3]. Intracellular signaling is a biochemical reactions caused by a diffusion of molecules. We propose that "thermal" signaling could also be a part of this intracellular process.

This work was supported by JSPS KAKENHI Grant No. 19H03198 and by the Human Frontier Science Program No. RGP0047/2018.

### References

- <sup>1</sup>M. Suzuki and T. Plakhotnik, *Biophysical Reviews*, 12, 593–600 (2020). doi: 10.1007/s12551-020-00683-8
- <sup>2</sup>S. Sotoma, C. Zhong, J.C.Y. Kah, H. Yamashita, T. Plakhotnik, Y. Harada and M. Suzuki, *Science Advances*, 7, eabd7888 (2021). doi: 10.1126/sciadv.abd7888
- <sup>3</sup>M. Suzuki and T. Plakhotnik, *Applied Physics Letters*, 119, 190502 (2021). doi: 10.1063/5.0063089

## Label-free analysis of diffusion constant in lipid bilayers using nanoscale diamond magnetometry

Hitoshi Ishiwata<sup>1</sup>, Hiroshi C. Watanabe<sup>2</sup>, Shinya Hanashima<sup>3</sup>,  
Takayuki Iwasaki<sup>4</sup>, Mutsuko Hatano<sup>4</sup>, Ryuji Igarashi<sup>1,5</sup>

<sup>1</sup>Institute for Quantum Life Science, National Institutes for Quantum and Radiological Science and Technology

<sup>2</sup>Quantum Computing Center, Keio University

<sup>3</sup>Department of Chemistry, Graduate School of Science, Osaka University

<sup>4</sup>Department of Electrical and Electronics Engineering, School of Engineering, Tokyo Institute of Technology

<sup>5</sup>PRESTO, Japan Science and Technology Agency

ishiwata.hitoshi@qst.go.jp

### Introduction

The NV center in a diamond is a quantum sensor with exceptional quality for highly sensitive nanoscale analysis of NMR spectra. In this study, we investigate diffusion constant of a lipid bilayer, a biological parameter that determines the dynamics of the lipid bilayer, utilizing ensemble-averaged nuclear spin detection from small volume  $\sim (6 \text{ nm})^3$ , which was determined by the depth of the NV center [1]. Observation of diffusion constant at different temperature reveals different phases of lipid bilayer [2]. The result builds foundation for label-free imaging of cell membranes for observation of phase composition and pristine dynamics that determines cellular functions.

### Result

In Figure 1, the result of the correlation spectroscopy was compared with the 2D molecular diffusion model constructed by Monte Carlo simulation combined with results from molecular dynamics simulation. There is a change in diffusion constant from  $1.5 \pm 0.25 \text{ nm}^2/\mu\text{s}$  to  $3.0 \pm 0.5 \text{ nm}^2/\mu\text{s}$  when the temperature changes from  $26.5 \text{ }^\circ\text{C}$  to  $36.0 \text{ }^\circ\text{C}$ . Observation of diffusion constant reveals different phases of lipid bilayer which identifies sub-compartment domains that are critical for cellular functions. In Figure 2, diffusion constant obtained from various different methods are shown. Previous results from Fluorescence Recovery After Photobleaching (FRAP) vary significantly depending on the selected markers as shown in Figure 2. Our results obtained from nanoscale diamond magnetometry are consistent with the results obtained from label-free bulk measurement using Magic-Angle Spinning Pulse Field Gradient NMR (MAS PFG NMR). Our method builds foundation for label-free imaging of cell membranes for observation of phase composition that determines cellular functions.

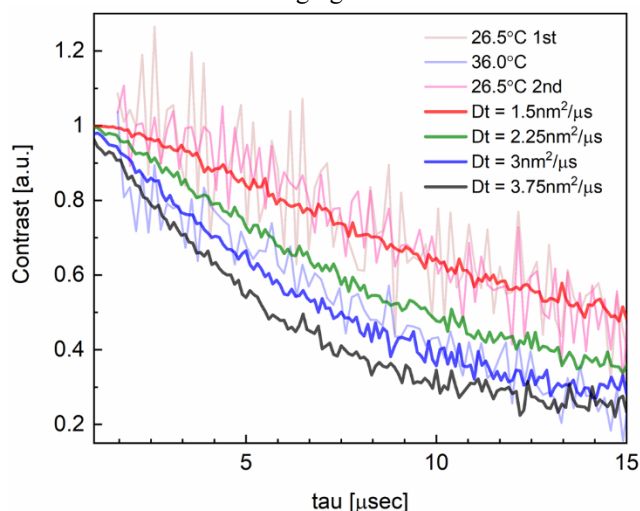


FIG. 1. Absolute value of correlation spectrum at  $26.5 \text{ }^\circ\text{C}$  (1st and 2nd) and  $36.0 \text{ }^\circ\text{C}$  are shown and compared with results of 2D molecular diffusion

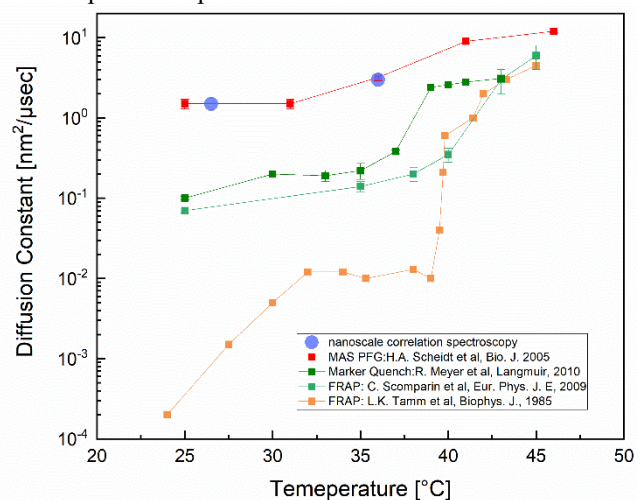


FIG. 2. Diffusion constant obtained from various measurement method compared with nanoscale correlation spectroscopy

### Reference:

<sup>1</sup>H. Ishiwata, et al, *APL*, 111, 043103 (2017). <sup>2</sup>H. Ishiwata, et al, *Adv. Quantum Technol.* 4, 2000106 (2021)

This research was supported by JST PRESTO Grant number JPMJPR17G1 and the MEXT Quantum Leap Flagship Program (MEXT Q-LEAP) Grant Number JPMXS0118067395, JPMXS0120330644.

## Temperature sensing using silicon-vacancy centers in detonation nanodiamonds

Masanori Fujiwara<sup>1</sup>, Gaku Uchida<sup>1</sup>, Izuru Ohki<sup>1</sup>, Ming Liu<sup>2</sup>, Akihiko Tsurui<sup>2</sup>, Taro Yoshikawa<sup>2</sup>, Masahiro Nishikawa<sup>2</sup>, and Norikazu Mizuochi<sup>1</sup>

<sup>1</sup>Institute for Chemical Research, Kyoto University, Gokasho, Uji, Kyoto 611-0011, Japan

<sup>2</sup>Business Development Center, Daicel Corporation, 1239, Shinzaike, Aboshi-Ku, Himeji, Hyogo 671-1283, Japan

masafuji@scl.kyoto-u.ac.jp

### Introduction

Nanodiamonds containing silicon-vacancy centers (SiV-NDs) are promising candidates for all-optical nanoscale thermometry. For the practical application of SiV-NDs into a biological system like a living cell, NDs smaller than 30 nm are suitable to pass through their membrane with minor damage. However, since the particle size of SiV-NDs reported for temperature sensing is larger than 200 nm<sup>1</sup>, it is difficult to introduce such NDs into the target position without invasive and complicated methods. As one of the efforts to overcome this problem, we developed SiV containing NDs via detonation process (SiV-DNDs)<sup>2</sup> since the detonation method can create small-size and massive NDs at a low cost. In this presentation, we show the photoluminescence (PL) spectral response to the temperature of SiV-DNDs.

### Method

We first prepared polyglycerol-coated SiV-DNDs after purification and dispersion processes. The particle size of SiV-DNDs is distributed at around 20 nm judging from the size histogram of 208 DNDs selected from a transmission electron microscope (TEM) image as shown in Fig. 1(a). The particle size of the DNDs is small enough to use inside the cell. We next prepared the SiV-DND suspension, dropped them on a coverslip, and dried them in ambient conditions. We observed the PL image and spectrum by a homebuilt confocal microscope with a thermoplate to control the sample temperature. From the confocal image, we found several bright spots (SiV-DND's aggregations) with the SiV center's zero phonon line (ZPL) at a wavelength of 737 nm. Figure 1(b) shows ZPL peak wavelength ( $\lambda_p$ ) as a function of the sample temperature for a bright spot. We confirmed the  $\lambda_p$  linearly red-shifted with increasing temperature ranging from 22 °C to 40.5 °C. The peak wavelength sensitivity to temperature ( $\Delta\lambda/\Delta T$ ) is 0.015 nm K<sup>-1</sup>, which agrees with the result of SiV center's ensemble in a diamond substrate (0.0124 nm K<sup>-1</sup>)<sup>1</sup>. Using  $\Delta\lambda/\Delta T$ , we evaluated the temperature sensitivity  $\eta_T$ , which is defined the uncertainty  $\sigma_T$  at a unit measurement time  $t_{\text{int}}$  (Fig. 1c). We found a bright spot with  $\eta_T = 1.1 \text{ K}/\sqrt{\text{Hz}}$ , which indicates sub-Kelvin precision was realized for 10 s integration time. All-optical thermometers such as small nanoparticles will be a key factor for thermometry of nanosystems like organelle in the living cell.

This work was supported by MEXT Q-LEAP No. JPMXS0120330644.

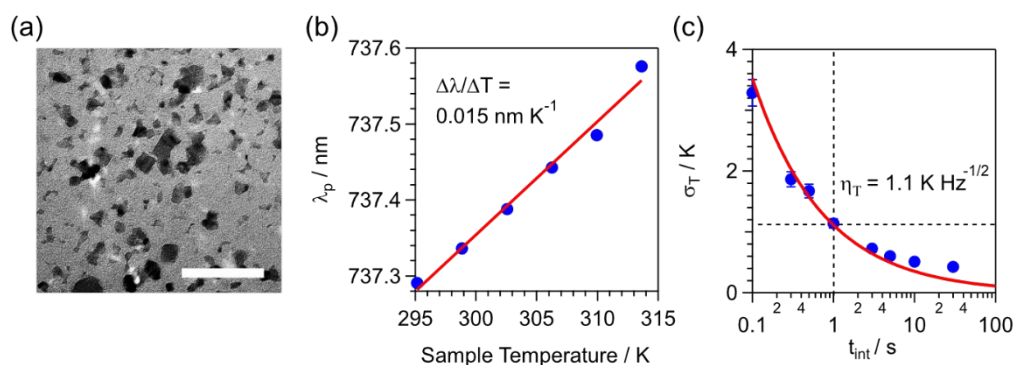


**Figure 1** (a) TEM image of SiV-DNDs. Scale bar indicates 100 nm. (b) ZPL peak wavelength ( $\lambda_p$ ) as a function of the sample temperature for a bright spot (SiV-DNDs' aggregation) selected from a confocal image. The peak sensitivity to temperature ( $\Delta\lambda/\Delta T$ ) was obtained by a line fit from the experimental data (filled circles). (c) Temperature uncertainty ( $\sigma_T$ ) of the spot as a function of measurement time  $t_{\text{int}}$ . The experimental data (filled circles) are fitted on a curve  $\propto 1/\sqrt{t_{\text{int}}}$ .

### Reference

<sup>1</sup>C. T. Nguyen, et al., *Appl. Phys. Lett.*, **112**, 203102 (2018).

<sup>2</sup>Y. Makino, et al., *Diam. Relat. Mater.*, **112**, 108248 (2021).

# Quantum-inspired machine learning for exponentially big neural data analysis

Kei Majima<sup>1,2</sup>

<sup>1</sup>*Institute for Quantum Life Science, National Institutes for Quantum Science and Technology (QST), Chiba, Japan*

<sup>2</sup>*PRESTO, Japan Science and Technology Agency (JST), Japan*

*majima.kei@qst.go.jp*

## Introduction

Machine learning algorithms specialized for neural data have allowed the extraction of information encoded in the brain. As an example, in previous studies, the images human subjects see were reconstructed from their brain activity measured via functional magnetic resonance imaging (fMRI) [1]. However, the application of those machine learning algorithms to high-resolution fMRI data, which may become mainstream in the near future, is limited due to their high computational cost. To solve this problem, scalable machine learning algorithms are being designed by utilizing computational techniques developed in the field of quantum computation [2,3]. In this report, taking one of the popular statistical methods, principal component analysis (PCA), as an example, we show that machine algorithms can be approximated with the use of such quantum-inspired techniques. The computational time and approximation performance of quantum-inspired PCA are demonstrated. The main results of this report have been presented in a previous paper by the author [3].

## Methods

In this report, the computational time and performance were compared between quantum-inspired PCA and its exact counterpart (*i.e.*, exact PCA). Due to space limitations, the details of the algorithms and datasets used are omitted in this report; however, they have been explained in the previous study [3]. Briefly, the computational times of the two algorithms were measured by applying them to simulation data. To characterize the dependence on the input dimensionality, the number of input dimensions in the simulation data was systematically changed. The performances of those two algorithms were evaluated by applying them to five benchmark datasets, and the variance explained by the top 100 PCs was measured and used as a performance metric in this report.

## Results

Both the computational time and performance (*i.e.*, explained variance) are shown in Figure 1. Results show that quantum-inspired PCA was significantly faster than the exact PCA, and its performance was maximally 7% worse than the exact PCA for these five datasets.

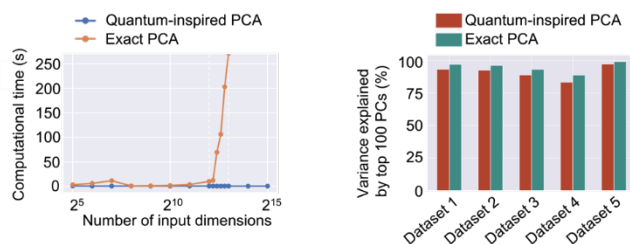


FIG 1. Comparison of the computational time and performance between quantum-inspired PCA and its exact counterpart.

## Discussion and Conclusions

In this report, quantum-inspired PCA was applied to simulation and real benchmark datasets, and its computational time and performance were compared with those of the exact PCA. As results, quantum-inspired PCA was significantly faster than its exact counterpart, and it showed moderate approximation performance on the five datasets. These results suggest a possibility that high-dimensional neural data whose size is intractable with previous machine learning algorithms can be efficiently analyzed using such quantum-inspired algorithms.

## References

- <sup>1</sup>G. Shen, T. Horikawa, K. Majima, Y. Kamitani, *PLOS Computational Biology*, Volume **15**, e1006633 (2019).
- <sup>2</sup>E. Tang, *Physical Review Letters*, Volume **127**, 060503 (2021).
- <sup>3</sup>N. Koide-Majima, K. Majima, *Neural Networks*, Volume **135**, 55–67 (2021).

This research was supported by MEXT Q-LEAP (JPMXS0120330644), JSPS KAKENHI (20K16465), JST ERATO (JPMJER1801), and JST PRESTO (JPMJPR2128).

## Empirical verification of the violation of the temporal Bell inequality in bistable perception

Yasunori Aizawa<sup>1,2</sup>, Naotsugu Tsuchiya<sup>3</sup>, Emmanuel Pothos<sup>4</sup>, Jerome Busemeyer<sup>5</sup>, Peter Bruza<sup>6</sup>,  
and Makiko Yamada<sup>1,7</sup>

<sup>1</sup>*Institute for Quantum Life Science, National Institutes for Quantum Science and Technology*

<sup>2</sup>*Graduate School of Medicine, Tohoku University*

<sup>3</sup>*School of Psychological Sciences, Monash University*

<sup>4</sup>*School of Arts and Social Sciences, Department of Psychology, City, University of London*

<sup>5</sup>*Department of Psychological and Brain Sciences, Indiana University Bloomington*

<sup>6</sup>*Faculty of Science and Technology, Queensland University of Technology*

<sup>7</sup>*Institute for Quantum Medical Science, National Institutes for Quantum Science and Technology*  
aizawa.yasunori@qst.go.jp

### Introduction

The purpose of the present study is to investigate quantum-like properties of mental states in bistable perception. In order to do this, we tested whether the temporal Bell inequality applied to bistable perception experiments[1] can be violated. In the present study, we used visual stimuli [2], where we can continuously and systematically manipulate two types of ambiguities in the perceived rotation of dots. When the rotation angle is large, the stimuli induce bistable percept. When the angle is small, the direction of rotation of the stimuli becomes difficult to judge. We use the stimuli to test if the temporal Bell inequality can be violated, and if so, under what parameter regime, it can be violated.

### Method

Two patterns were presented alternately: a visual stimulus consisting of four disks, and one in which the disks were rotated by a specific angle (5–45 degrees) in each trial [FIG. 1(A)]. When the angle of rotation was close to 45 degrees, stimuli were perceived to rotate in one of the two directions for a while with occasional reversals at random times (i.e., bistable perception). When the angle of rotation was close to 5 degrees, no rotation was perceived beyond the angle of rotation of the stimulus, and left and right rotations were perceived alternately, but the angle of rotation was so small that it was difficult to determine the direction of rotation [FIG. 1(B)]. At two time points after the beep, the participants responded by pressing a button in the direction of rotation that they saw at that time [FIG. 1(C)].

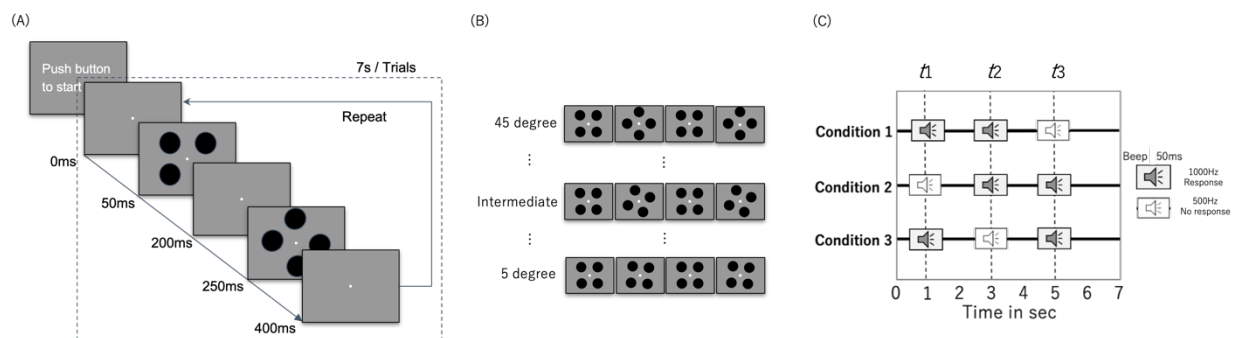


FIG. 1. (A) Schematic illustration of the task. (B) A set of rotation angles (5–45 degrees in 5 degree steps). (C) Three timings on the measurement of perceived stimuli. The perceived rotation direction was measured at two out of three timepoints for the calculation of the temporal Bell inequality.

### Reference

<sup>1</sup>H. Atmanspacher, and T. Filk, *J. Math. Psychol.* **54**, 314-321 (2010).

<sup>2</sup>S. Takei and S. Nishida, *J. Vision.* **10**, 23 (2010).

<sup>3</sup>M. M. Wilde and A. Mizel, *Found. Phys.* **42**, 256 (2012).

### Acknowledgement

This work was supported by JSPS KAKENHI JP20H05711 and MEXT Q-LEAP Grant Number JPMXS0120330644.

## Tracking radiation damage induction pathway following core-hole creation of DNA molecules in aqueous solution

Yoshiaki Kumagai<sup>1,2</sup>, Masatoshi Ukai<sup>1,2</sup>, Akinari Yokoya<sup>3</sup>

<sup>1</sup>*Department of Applied Physics, Tokyo University of Agriculture and Technology*

<sup>2</sup>*Institute of Engineering, Tokyo University of Agriculture and Technology*

<sup>3</sup>*Institute for Quantum Life Science, National Institute for Quantum Science and Technology*

kumagai@go.tuat.ac.jp

### Introduction

Ionizing radiation often causes irreversible DNA damage in a living cell of tissue and the mutation or cell death are thought to arise from localization of damage known as a clustered DNA damage site [1]. Recently, it is recognized that the production of the DNA molecules with inner-shell vacancies after irradiation can be a cause of clustered DNA damages [2]. We have reported the x-ray absorption near-edge structure (XANES) spectra at photon energies near the nitrogen K-shell ionization potential of the base moieties of aqueous nucleotides [3]. The measuring excitation energies and binding energies of the electrons in the nitrogen K-shell orbitals at different pH conditions predicted the hydration interaction of bases in nucleotides with hydrated water molecules. This hydration interaction has been further confirmed by the spectroscopy of the secondary and Auger electrons [4] (FIG.1). These findings gave rise to a possible deposition of excess charge from doubly ionized DNA to water molecules, which may suppress the clustered DNA damage induction. We studied the reaction pathways and dynamics of core-hole DNA molecules in the aqueous solution with their identified electronic states toward chemically stable and irreparable damages.

### Results

We used monochromatic soft x-rays at SPring-8 BL23SU to selectively excite or ionize an inner shell electron of a specific atom in aqueous nucleotide molecules, which have been introduced into the vacuum using a liquid micro-jet technique. In order to track the chemical reaction sequences following initial core-hole states created by the primary radiations, we have focused on particular events by excitation and to probe outcoming luminescences [5]. This is a nondestructive analysis of the excited intermediate species produced in a molecular reaction on the damage induction pathway. We obtained the first evidence of luminescence spectra of aqueous uridine-5'-monophosphate (UMP) after x-ray absorption (FIG.2). The cause of luminescence can be due to the parent species produced following the double ionization of aqueous UMP, and emission of excess positive charge and excess internal energy from double charged UMP.

We also established the mass spectroscopy for the secondary ion fragments produced via the relaxation of core-hole nucleotide molecules in aqueous solution which extended the adaptabilities of the soft x-ray spectroscopy for the DNA damaging using a liquid-jet technique.

### Acknowledgement

This work was supported by JSPS KAKENHI (Grant Nos. 20H04338).

### Reference

- <sup>1</sup>D. Goodhead, *Int. J. Radiat. Bio.*, **65**, 7 (1994).
- <sup>2</sup>A. Yokoya *et al.*, in *Charged Particle and Photon Interaction with Matter*, (CRC Press: Boca Raton, 2011), pp.543-574.
- <sup>3</sup>H. Shimada *et al.*, *Chem. Phys. Lett.*, **591**, 137 (2014); H. Shimada *et al.*, *J. Chem. Phys.*, **141**, 055102 (2014); H. Shimada *et al.*, *J. Chem. Phys.*, **142**, 175102 (2015).
- <sup>4</sup>Y. Takeda *et al.*, *Quantum Beam Sci.*, **4**, 10 (2020)
- <sup>5</sup>Y. Terao *et al.*, *Int. J. Radiat. Bio.*, (published online; 2021)

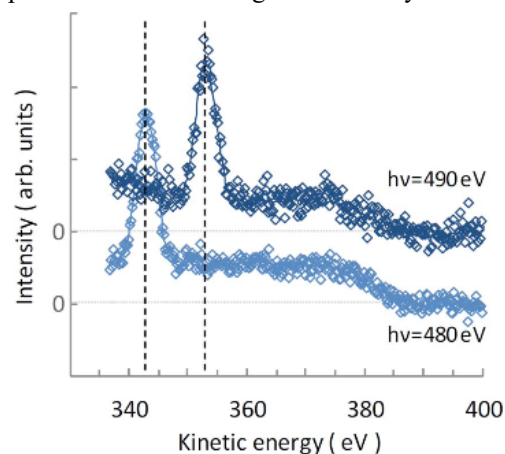


FIG. 1. Electron kinetic energy spectra for aqueous UMP at pH = 7.5 at the x-ray photon energies of 480 eV and 490 eV [4].

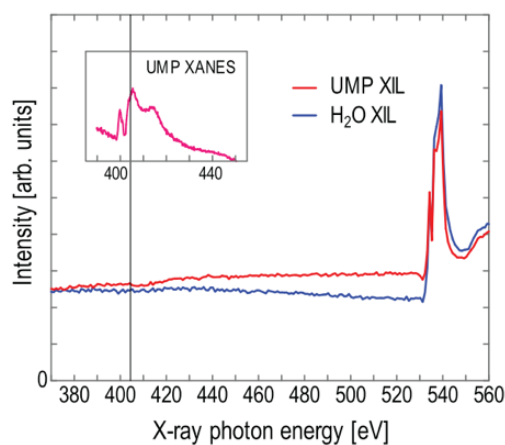


FIG. 2. Yields of x-ray induced luminescence for aqueous UMP and pure water as a function of x-ray photon energy [5]. The inset shows the XANES spectra for aqueous UMP.

## High-resolution structure of an electron-transfer protein by neutron crystallography

Yuya Hanazono<sup>1,2,3</sup>, Yu Hirano<sup>2,4</sup>, Kazuki Takeda<sup>1</sup>, Katsuhiko Kusaka<sup>5</sup>, Taro Tamada<sup>2</sup>, and Kunio Miki<sup>1</sup>

<sup>1</sup>*Department of Chemistry, Graduate School of Science, Kyoto University*

<sup>2</sup>*Institute for Quantum Life Science, National Institutes for Quantum Science and Technology*

<sup>3</sup>*Medical Research Institute, Tokyo Medical and Dental University*

<sup>4</sup>*PRESTO, Japan Science and Technology Agency*

<sup>5</sup>*Frontier Research Center for Applied Atomic Sciences, Ibaraki University*

hanazono.str@tmd.ac.jp

### Introduction

High-potential iron-sulfur protein (HiPIP) is a component of electron transfer from cytochrome *bc*<sub>1</sub> complex to light-harvesting-reaction center complexes (LH1-RC) in bacterial photosynthesis. HiPIP possesses a cubane-like Fe<sub>4</sub>S<sub>4</sub> cluster at its center with a redox potential of above +300 mV. This high potential arises from the hydrogen bonds and hydrophobic environment around the iron-sulfur cluster [1–3]. In order to clarify the effect of hydrogen bond on the redox potential and reaction mechanism, we determined the neutron structure of HiPIP and obtained the precise locations of the hydrogen nuclei.

### Methods

We collected X-ray and neutron diffraction data of oxidized HiPIP at 0.66 and 1.2 Å resolution, respectively, from the same crystal at a cryogenic temperature of 100 K. The initial refinement of X-ray data was performed at 1.2 Å resolution. Then, the refinements with anisotropic atomic displacement parameters were performed at 0.66 Å resolution. After that, the joint refinement of neutron and X-ray data was performed. The amide protons that had occupancies more than or equal to 0.60 that of deuterium or 0.75 that of protium and the deuterium atoms of the side chains in a single conformation were refined without geometry restraints.

### Results

In the case of the NH...O hydrogen bond, most of the nucleus positions of the amide protons shift toward the acceptor atoms. These hydrogen atoms are attracted by the electrostatic force. On the other hand, some hydrogen atoms point away from the acceptor atoms. Around these hydrogen atoms, there is another oxygen atom nearby that can form a hydrogen bond. Generally, the planarity of the peptide bond is discussed based on  $\omega$ -angles due to the insufficient structural data for the amide protons. In this study, we focus on the planarity of the H<sub>i</sub>-N<sub>i</sub>-C<sub>i-1</sub>=O<sub>i-1</sub> planes, where *i* represents the residue number, in the peptide bond. To evaluate the planarity of peptide bonds including hydrogen atoms, the positions of hydrogen atoms and oxygen atoms are defined with the in-plane angle ( $\gamma_H$ ,  $\gamma_O$ ), the out-of-plane angle with the C<sub>i-1</sub>-N<sub>i</sub>-C<sub>ai</sub> plane ( $\delta_H$ ,  $\delta_O$ ). There is a substantial correlation between  $\delta_H$  and  $\delta_O$ . When the amide protons deviate from the peptide plane owing to the electrostatic interaction, the position of the oxygen atoms of previous residues shifts in the opposite direction. Consequently, the planarity of the H<sub>i</sub>-N<sub>i</sub>-C<sub>i-1</sub>=O<sub>i-1</sub> planes is mainly preserved. Moreover, the orientation of the amide proton of Cys75 is different in the reduced and oxidized states possibly due to the electron storage capacity of the iron-sulfur cluster. The change in the electron storage capacity will facilitate the electron transfer from HiPIP to LH1-RC.

### References

- <sup>1</sup>T. Glaser *et al.*, Schmitt, *J. Am. Chem. Soc.*, **123**, 4859–4860 (2001).
- <sup>2</sup>S. Niu *et al.*, *J. Am. Chem. Soc.*, **131**, 5724–5725 (2009).
- <sup>3</sup>A. Dey *et al.*, *Science*, **318**, 1464–1468 (2007).

### Acknowledgements

This work was supported by the Photon and Quantum Basic Research Coordinated Development Program, Quantum Leap Flagship Program (Q-LEAP) JPMXS0120330644 from the Ministry of Education, Culture, Sports, Science and Technology (MEXT), PRESTO JPMJPR17G7 from the Japan Science and Technology Agency (JST), and Grants-in-Aid for Scientific Research (C) JP20K06523, for Research Activity Start-up JP25891030 and JP20K22642 and for Young Scientists (B) JP15K18494 from the Japan Society for the Promotion of Science (JSPS).

## Fabrication of a quantum sensor to reveal a topic in thermal physiology

Shuya Ishii<sup>1,2</sup>

<sup>1</sup>*Takasaki Advanced Radiation Research Institute, National Institutes for Quantum Science and Technology, 1233 Watanuki, Takasaki, Gunma 370-1292, Japan*

<sup>2</sup>*Institute for Quantum Life Science, National Institutes for Quantum Science and Technology, 4-9-1 Ana-gawa, Inage-ku, Chiba 263-8555, Japan*

### Abstract

At first, I'll talking about a topic of thermal physiology in myocardial contraction to introduce the importance of focusing on temperature in biological viewpoint. During excitation-contraction coupling of striated muscle, sarcomeres are activated via thin filament structural changes, i.e., from the "off" state to the "on" state, in response to a rise in the intracellular  $\text{Ca}^{2+}$  concentration. We systematically investigated the effects of rapid heating by infra-red (IR) laser irradiation on the sliding of thin filaments reconstituted with human cardiac  $\alpha$ -tropomyosin (Tm) and bovine ventricular troponin (Tn), or rabbit fast skeletal Tm-Tn complex in the *in vitro* motility assay. The findings in our studies suggest that the "on-off" equilibrium of the cardiac thin filament state is partially shifted toward the "on" state in diastole at the body temperature, enabling rapid and efficient myocardial dynamics in systole [1,2].

Next, I'll show you a study of fabricating a quantum sensor (under submission), which has been getting a lot of attention in biological field. Negatively charged nitrogen-vacancy ( $\text{NV}^-$ ) center in diamond is known as quantum sensor, can be used to measure small changes in physical quantities, such as temperature [3]. Electron beam irradiation into type-Ib diamond is known as a good method for the creation of high concentration negatively-charged nitrogen-vacancy ( $\text{NV}^-$ ) centers by which highly sensitive quantum sensors can be fabricated. In order to understand the creation mechanism of  $\text{NV}^-$  centers, we study the behavior of substitutional isolated nitrogen (P1 centers) and  $\text{NV}^-$  centers in type-Ib diamond, with an initial P1 concentration of 40-80 ppm by electron beam irradiation up to  $8.0 \times 10^{18}$  electrons/cm<sup>2</sup>. P1 concentration and  $\text{NV}^-$  concentration were measured using electron spin resonance and photoluminescence measurements. Comparing concentration of P1 centers with that of  $\text{NV}^-$  centers, it suggests that a part of P1 centers plays a role in the formation of other defects. The usefulness of electron beam irradiation to type-Ib diamonds was confirmed by the resultant conversion efficiency from P1 to  $\text{NV}^-$  center around 12-19%. The result obtained in this study is useful to understand the creation mechanism of  $\text{NV}^-$  centers, leading to realize highly sensitive quantum sensors.

### Acknowledgement

This work was supported by Quantum Leap Flagship Program (Q-LEAP; JPMXS 0118067395) of MEXT.

### Reference

1. Oyama K, Mizuno A, Shintani SA, Itoh H, Serizawa T, Fukuda N, et al. Microscopic heat pulses induce contraction of cardiomyocytes without calcium transients. *Biochem Biophys Res Commun* [Internet]. 2012;417(1):607–12. Available from: <http://dx.doi.org/10.1016/j.bbrc.2011.12.015>
2. Ishii S, Oyama K, Arai T, Itoh H, Shintani SA, Suzuki M, et al. Microscopic heat pulses activate cardiac thin filaments. *J Gen Physiol*. 2019;151(6):860–9.
3. Barry JF, Schloss JM, Bauch E, Turner MJ, Hart CA, Pham LM, et al. Sensitivity optimization for  $\text{NV}^-$ -diamond magnetometry. *Rev Mod Phys*. 2020;92(1):015004(68).

## Investigation of irradiation induced nitrogen-vacancy centers in 5-nanometer-sized Detonation nanodiamonds

Frederick T.-K. So<sup>1,2,3</sup>, Alexander I. Shames<sup>4</sup>, Daiki Terada<sup>2,3</sup>, Takuya Genjo<sup>2,3</sup>, Hiroki Morishita<sup>1</sup>, Izuru Ohki<sup>1</sup>, Takeshi Ohshima<sup>5</sup>, Shinobu Onoda<sup>5</sup>, Hideaki Takashima<sup>6</sup>, Shigeki Takeuchi<sup>6</sup>, Norikazu Mizuochi<sup>1</sup>, Ryuji Igarashi<sup>3,7</sup>, Masahiro Shirakawa<sup>2,3\*</sup>, Takuya F. Segawa<sup>2,8\*</sup>

<sup>1</sup>*Institute for Chemical Research, Kyoto University*

<sup>2</sup>*Department of Molecular Engineering, Graduate School of Engineering, Kyoto University*

<sup>3</sup>*Institute for Quantum Life Science, National Institutes for Quantum and Radiological Science and Technology*

<sup>4</sup>*Department of Physics, Ben-Gurion University of the Negev, Israel*

<sup>5</sup>*Takasaki Advanced Radiation Research Institute, National Institutes for Quantum Science and Technology*

<sup>6</sup>*Department of Electronic Science and Engineering, Kyoto University*

<sup>7</sup>*National Institute for Radiological Sciences, National Institutes for Quantum Science and Technology*

<sup>8</sup>*Laboratory for Solid State Physics, ETH Zurich, Switzerland*

so.kit.58a@st.kyoto-u.ac.jp

### Introduction

Nanodiamonds containing negatively-charged Nitrogen-Vacancy (NV<sup>-</sup>) centers are versatile room-temperature quantum sensors in a growing field of research. Yet, knowledge regarding the formation mechanism in very small particles is still limited. Here, the study was focused on the formation of the smallest NV<sup>-</sup>-containing diamonds, 5 nm detonation nanodiamonds (DNDs). As a reliable method to quantify NV<sup>-</sup> centers in nanodiamonds, half-field signals in electron paramagnetic resonance (EPR) spectroscopy are recorded. By comparing the NV<sup>-</sup> concentration in a series of nanodiamonds (5 - 100 nm), it was shown that the formation process in DNDs is unique in several aspects. NV<sup>-</sup> centers in DNDs are already formed during electron irradiation, without the need for high-temperature annealing. The effect was interpreted in terms of “self-annealing”, where size and type dependent effects enable vacancy migration at lower temperature. Although NV<sup>-</sup> concentration increases with particle size, the NV<sup>-</sup> concentration in NDs surpasses that of 20 nm-sized nanodiamonds. Using Monte-Carlo simulations, we show that the higher substitutional Nitrogen concentration compensates the vacancy loss induced by the large particle surface. Upon  $1.5 \times 10^{19}$  e<sup>-</sup>/cm<sup>2</sup> electron irradiation, DNDs show a 12.5-fold NV<sup>-</sup> increment with no sign of saturation. These findings can be of interest for the creation of defects in other very small semiconductor nanoparticles.

This work was supported by MEXT Q-LEAP Grant Number JPMXS0120330644 & JPMXS0118067395, KAKENHI (Grants 20H00453, 18K19297)

### Method

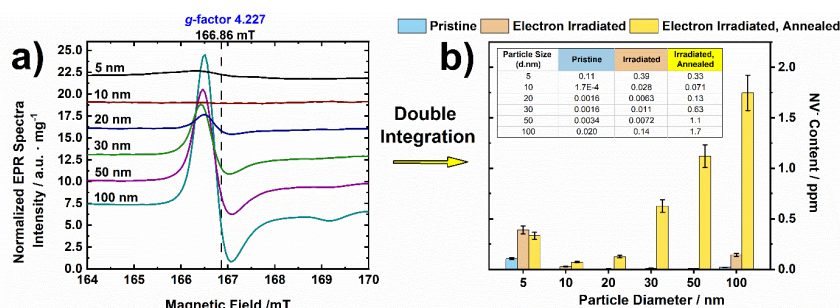


Figure 1. (a) Continuous-wave half-field EPR spectra of electron-irradiated (2 MeV,  $5 \times 10^{18}$  e<sup>-</sup>/cm<sup>2</sup>) nanodiamonds with different particle size after high-temperature annealing. The double integral of the signal at  $g_{\text{eff}} = 4.227$  provides the NV<sup>-</sup> concentration. (b) A summary graph of NV<sup>-</sup> content (ppm, in units of atomic ratio) in NDs of different sizes, measured via the half-field EPR technique. Blue bars are the pristine nanodiamonds; Orange bars are the electron-irradiated nanodiamonds; Yellow bars are the electron-irradiated and subsequently annealed nanodiamonds (derived from the  $g_{\text{eff}} = 4.227$  signal in the EPR spectrum of Fig. 1(a)). Electron irradiation was conducted with 2 MeV electrons at a fluence of  $5 \times 10^{18}$  e<sup>-</sup>/cm<sup>2</sup>; Annealing was performed at 800 °C in vacuum for 2 h. All samples were boiling acid treated to remove Fe<sup>3+</sup> impurities, which overlap with the half-field EPR NV<sup>-</sup> signal. Inset table shows the corresponding NV<sup>-</sup> concentrations in ppm. Errors in NV<sup>-</sup> concentration do not exceed  $\pm 15\%$ .

## Formation of flavin anion and tyrosine radicals in avian Cryptochrome4

Hiroaki Otsuka<sup>1</sup>, Hiromasa Mitsui<sup>1</sup>, Kota Miura<sup>1</sup>, Keiko Okano<sup>1</sup>, Yasushi Imamoto<sup>2</sup>, Toshiyuki Okano<sup>1</sup>

<sup>1</sup>Department of Electrical Engineering and Bioscience, School of Advanced Science and Engineering,  
Waseda University

<sup>2</sup>Department of Biophysics, Graduate School of Science, Kyoto University  
o1.2t5.8tt21.tf@ruri.waseda.jp

### Introduction

Many animals, such as avian and insects, exhibit light-dependent magnetoreception [1] that is likely mediated by the magnetic field-dependent chemical reaction of a pair of entangled radicals, called radical pair mechanism (RPM) [2].

Avian CRY4 is a plausible magnetoreceptor operating through RPM (FIG. 1) in the retina [3,4]. Our previous study suggested that chicken CRY4 (cCRY4) changes its conformation upon blue light irradiation [4] along with the formation of neutral radical FAD (FADH<sup>•</sup>) [5]. Together with the retinal localization of CRY4, it is a leading candidate of magnetoreceptor in birds. Therefore, analysis of the molecular changes after photoreception by CRY4 will be a key step for elucidation of RPM in the magnetoreception.

In this study, we measured the transient reactions up to the formation of FADH<sup>•</sup> after photoreception of CRY4 by millisecond timescale spectroscopy. Singular value decomposition (SVD) was applied to detailed analysis of the photoreactions. For comparative analysis, the recombinant CRY4 of magnetically migrating European robin (ErCRY4) was prepared.

### Method

Recombinant cCRY4 samples were purified by GST-tag purification system. Transient reactions of each sample were measured by laboratory-built, time-resolved spectrophotometry system. Obtained data were decomposed by SVD analysis and reconstructed into the spectra of each independent reaction (B spectra). SVD analysis yielded the spectrum representing steady state difference spectrum (B0 spectrum) and the two spectra representing the spectral changes occurring up to steady state (B1 and B2 spectra).

### Results and discussion

Regardless of the presence of dithiothreitol (DTT), flavin anion radical (FAD<sup>•-</sup>), a precursor of FADH<sup>•</sup>, was formed just after the blue light irradiation of ground state of cCRY4 and ErCRY4 (having oxidized FAD: FAD<sub>OX</sub>). FAD<sup>•-</sup> was then protonated to FADH<sup>•</sup> on the time scale of sub-seconds. In the absence of DTT, FAD<sup>•-</sup> was oxidized to FAD<sub>OX</sub> more rapidly than the protonation.

The spectral data were decomposed to three difference spectra (B0–B2) by SVD, representing two independent reactions; the oxidation and protonation. Time constants for the protonation from FAD<sup>•-</sup> to FADH<sup>•</sup> and the oxidation from FAD<sup>•-</sup> to FAD<sub>OX</sub> was 200 ms and 34 ms, respectively. Such a large difference in the time constants between the oxidation and protonation suggests the bifurcation of FAD<sup>•-</sup> bound to cCRY4 and ErCRY4. Furthermore, the presence of tyrosine neutral radical (Tyr-O<sup>•</sup>) was suggested by the spectrum for FAD<sup>•-</sup> oxidation in cCRY4. Based on these results, we speculate that FAD<sup>•-</sup> could be paired with Tyr-O<sup>•</sup>, and that magnetoreception may be achieved by detecting the ratio of the state of entangled [FAD<sup>•-</sup> Tyr-O<sup>•</sup>]. A comparison of photoreactions in cCRY4 and ErCRY4 would allow us to consider the differences in magnetoreception mechanisms between nesting and migrating birds.

### Reference

<sup>1</sup>R. Wiltschko and W. Wiltschko, *Sens. Nat.* **739**, 126 (2012); <sup>2</sup>T. Ritz, S. Adem, and K. Schulten, *Biophys. J.* **78**, 707 (2000); <sup>3</sup>Y. Kubo, M. Akiyama, Y. Fukada, and T. Okano, *J. Neurochem.* **97**, 1155 (2006); <sup>4</sup>R. Watari, C. Yamaguchi, W. Zemba, Y. Kubo, K. Okano, and T. Okano, *J. Biol. Chem.* **287**, 42634 (2012); <sup>5</sup>H. Mitsui, T. Maeda, C. Yamaguchi, Y. Tsuji, R. Watari, Y. Kubo, K. Okano, and T. Okano, *Biochemistry* **54**, 1908 (2015).

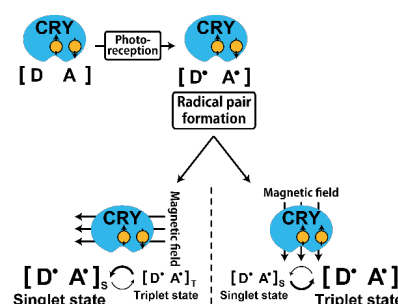


FIG. 1. Radical pair model mediated by cryptochrome CRYs photoactivation followed by formation of two entangled radicals are assumed to detect the geomagnetic field.

## Do neural activities of binocular rivalry follow a quantum probability model? A test of temporal Bell inequalities

Takahiro Hirao<sup>1,2</sup>, Naotsugu Tsuchiya<sup>3</sup>, Emmanuel Pothos<sup>4</sup>, Jerome Busemeyer<sup>5</sup>, Peter Bruza<sup>6</sup>, and Makiko Yamada<sup>1,2</sup>

<sup>1</sup>Institute for Quantum Life Science, National Institutes for Quantum Science and Technology

<sup>2</sup>Institute for Quantum Medical Science, National Institutes for Quantum Science and Technology

<sup>3</sup>School of Psychological Sciences, Monash University

<sup>4</sup>School of Arts and Social Sciences, Department of Psychology, City, University of London

<sup>5</sup>Department of Psychological and Brain Sciences, Indiana University Bloomington

<sup>6</sup>Faculty of Science and Technology, Queensland University of Technology

hirao.takahiro@qst.go.jp

### Introduction

Binocular rivalry refers to a phenomenon in which the perceived image changes spontaneously over time when the two eyes are presented with different images. The purpose of this study is to test whether the violation of temporal Bell inequality can be experimentally observed in binocular rivalry. If the temporal Bell inequality is violated (under no-signaling in time: NSIT), it implies that the perception of the rival stimuli cannot be assumed to be definite at each point in time (i.e., “realism” in the corresponding mental representations is violated), which is a key indication of non-classical behavior (as in, for example, quantum-like systems) [1]. Here, to test the violation of the inequality, we used binocular rivalry and measured both subjective reports and electroencephalogram (EEG). With EEG, we used frequency-tagging technique to track the cortical signal driven by each eye’s stimulus, known as the steady-state visual evoked potential (SSVEP). We present the conceptual and methodological approaches to test the temporal Bell inequality.

### Method

Two checkerboards flickering at different frequencies (red stimulus at 7.5 Hz; blue stimulus at 6.6 Hz) were dichoptically presented, one to each eye [FIG. 1(A) (B)]. Participants were asked to report their perception of the rival stimuli at two out of three different timepoints [FIG. 1(C)]. The electroencephalogram (EEG) was recorded from 28 scalp sites at a sampling rate of 1000 Hz. The EEG was re-referenced to the averaged mastoids and band-pass filtered with a 0.1-50 Hz cutoff. The prominent artifacts were identified and removed by the individual component analysis. The SSVEP signals were extracted by using an adaptive recursive least-square (RLS) filter [FIG. 1(D)].

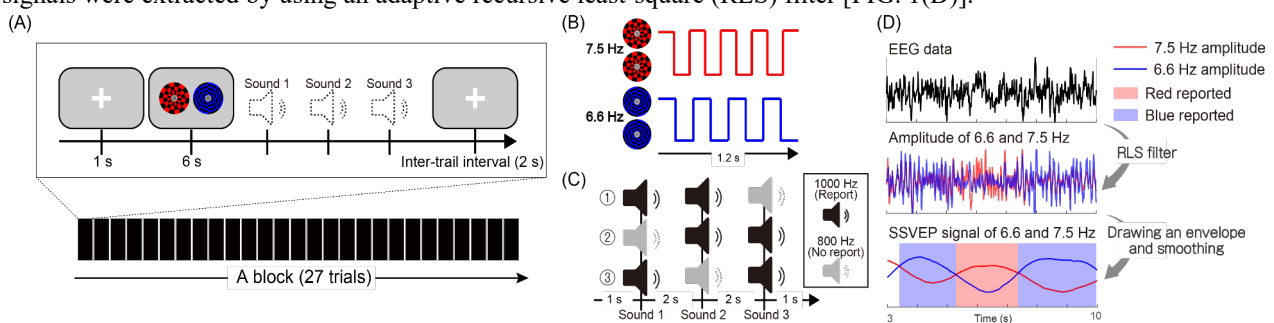


FIG. 1. (A) Schematic illustration of the task for a block. A participant conducted a total of 10 blocks. (B) Time-course modulation of checkerboard patterns. (C) Three timings on the measurement of perceived stimuli. The perceived stimulus was measured at two out of three timepoints for the calculation of the temporal Bell inequality. (D) Steps for SSVEP calculation using a 30-second binocular rivalry data. An adaptive RLS filter was applied to the raw EEG data in the top figure. In the middle figure, the extracted frequency-tagged amplitudes of 7.5 and 6.6 Hz were depicted. The bottom figure indicates that the frequency-tagged amplitude extracted by SSVEP was consistent with the subjective report.

### Reference

<sup>1</sup>H. Atmanspacher, and T. Filk, *J. Math. Psychol.* **54**, 314-321 (2010).

### Acknowledgement

This work was supported by JSPS KAKENHI JP20H05711 and MEXT Q-LEAP Grant Number JPMXS0120330644.

## X-ray absorption spectroscopy of a silicon phthalocyanine derivative, IR700, for X-ray excited photoimmunotherapy

Y. Izumi<sup>1</sup>, M. Ohara<sup>1</sup>, K. Fujii<sup>1</sup>, A. Yokoya<sup>1</sup>, R. Watanabe<sup>1</sup>, K. Nakagawa<sup>2</sup>, O. Inanami<sup>3</sup>, T. Taketsugu<sup>4</sup>, and M. Ogawa<sup>5</sup>

<sup>1</sup>*Institute for Quantum Life Science, National Institutes for Quantum Science and Technology (QST)*

<sup>2</sup>*Graduate School of Engineering, The University of Tokyo*

<sup>3</sup>*Graduate School of Veterinary Medicine, Hokkaido University*

<sup>4</sup>*Faculty of Science, Hokkaido University*

<sup>5</sup>*Graduate School of Pharmaceutical Sciences, Hokkaido University*

izumi.yudai@qst.go.jp

### Introduction

Photoimmunotherapy (PIT) has been recognized as one of the most promising methods in advanced cancer therapies [1]. A silicon phthalocyanine derivative (IR700) conjugated to a monoclonal antibody (mAb) targeting epidermal growth factor receptors of cancer membranes is used as a photosensitizing molecule. Irradiating the mAb-IR700-bound cancer cells with near-infrared (NIR) light, axial ligands of the IR700 are released. It makes the cell membranes brittle and, as a result, prompts cell death. Though the evidence clearly shows a strong potential of the PIT, the short penetration depth of NIR (a few centimeters) might be controversial when it is applied to deeply located tumors. We have focused on X-ray-induced core level excitations as alternative initiation probes owing to those long penetration depths. In this work, the reaction probability of the IR700 with X-rays was evaluated by measuring atom selective K-shell X-ray absorption spectra using a synchrotron radiation soft-X-ray beamline.

### Methods

Thin films of IR700 were prepared on gold plates by drying an aqueous solution of IR700 at room temperature. X-ray absorption spectroscopy of the films was performed in the BL23SU at SPring-8 in Japan. The absorption spectra were measured in the nitrogen, oxygen, and silicon K-edge energy regions, in which corresponding K-shell electrons were excited selectively. The optical absorption cross-section in each region was evaluated.

### Results and Discussion

The absorption cross-section of the oxygen K-shell resonance excitation  $\sigma_r$  (~536 eV) was almost two folds of that at the pre-edge region  $\sigma_p$  (~530 eV) in which the oxygen atoms were not excited (FIG. 1). It was larger than those of the nitrogen and silicon K-shell resonance excitations.

X-ray-induced bond breakages often occur in the vicinity of the excited atoms. Since the axial ligands and the phthalocyanine body of the IR700 are linked via oxygen atoms, the oxygen K-shell excitations could be effective to detach the axial ligands, similar to the NIR irradiations.

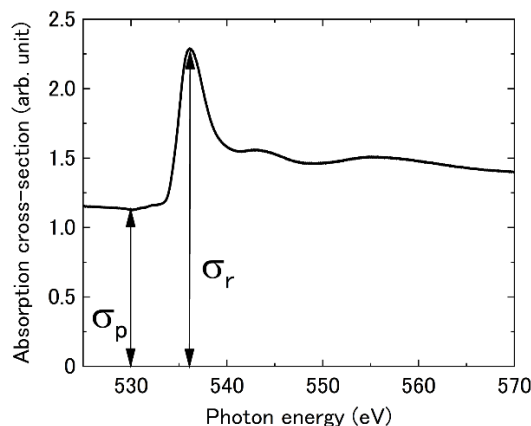


FIG. 1. X-ray absorption spectrum of the IR700 thin film in the oxygen K-edge energy region.

### Reference

<sup>1</sup>M. Kobayashi *et al.*, *ChemPlusChem*, **85**, 1959 (2020).

## Magnetically sensitive radical pairs in avian cryptochrome 4 proteins

Presenters: Jingjing Xu<sup>1</sup>, Siu Ying Wong<sup>2</sup>

<sup>1</sup>*Institute of Biology and Environmental Sciences, Carl-von-Ossietzky University Oldenburg,*

<sup>2</sup>*Department of Physics, Carl-von-Ossietzky Universität Oldenburg,*

*jingjing.xu@uni-oldenburg.de*

\*A list of authors and affiliations appears on the next page.

### Introduction

Migratory birds use the earth's magnetic field to navigate during their spectacular migratory journeys<sup>1</sup>. The avian magnetic compass was proposed to be based on quantum effects in radical pairs (RP) in cryptochrome (CRY) proteins<sup>2,3</sup>. Specifically, transfer of an electron along a chain of tryptophan residues to the photoexcited chromophore, flavin adenine dinucleotide (FAD), in CRY generates a spin-correlated flavin-tryptophan radical pair. An external magnetic field could alter the time-dependent fractions of RPs present in the singlet and triplet states and change the product yields of spin-selective RP chemical reactions<sup>4</sup>. However, there had been no experimental evidence showing a magnetic sensitivity of CRY proteins from any migratory bird.

### Method

Cryptochrome 4 proteins from the migratory European robin (*Erithacus rubecula*, *ErCRY4*) and non-migratory birds pigeon (*Columba livia*, *CiCRY4*) and chicken (*Gallus gallus*, *GgCRY4*) were produced using an *E. coli* expression system. Magnetic field effects on CRY4 proteins were measured optically using various spectroscopic techniques, including picosecond transient absorption spectroscopy, cavity ring-down spectroscopy, broadband cavity-enhanced absorption spectroscopy, and electron paramagnetic resonance.

### Results

A long-lived spin-correlated radical pair is formed via light-induced electron hopping along a tetrad of tryptophan residues to FAD in European robin CRY4 (FIG. 1A and 1B). *ErCRY4* is more sensitive to weak magnetic fields than the plant CRY given other factors being equal, e.g., pH7 and tryptophan-triad (FIG. 1C). Moreover, *ErCRY4* shows a more pronounced magnetic field effect than non-migratory pigeon and chicken CRY4s (FIG. 1D).

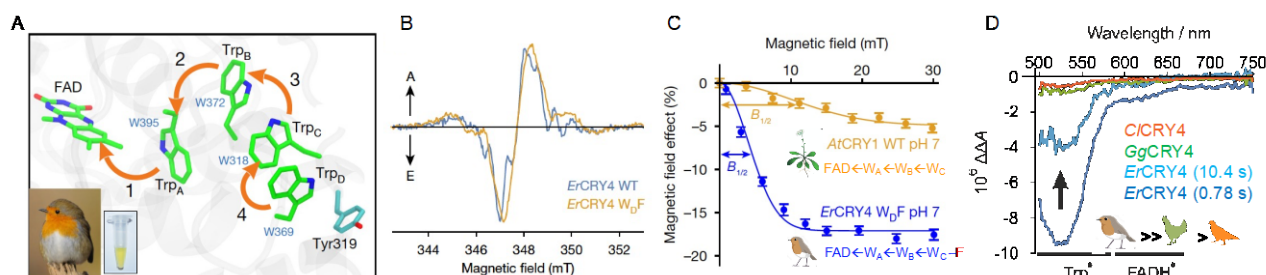


FIG. 1. A light-induced magnetically sensitive radical pair in cryptochrome proteins. A, Structural homology model of European robin CRY4 (*ErCRY4*) showing sequential electron transfer from tryptophan residues (Trp, W) to the FAD. Inset shows a robin and a CRY4 protein sample with FAD bound. B, Time-resolved X-band (9.75 GHz) electron paramagnetic resonance spectra of wild-type *ErCRY4* and the terminal tryptophan mutant (*W<sub>D</sub>F*) recorded at 1 °C, 0.5  $\mu$ s after a 450-nm laser pulse. In the *ErCRY4 W<sub>D</sub>F* mutant, the fourth tryptophan was replaced by a redox-inactive phenylalanine residue to block the fourth electron transfer step. C, Comparison of magnetic field effects on *ErCRY4 W<sub>D</sub>F* and *Arabidopsis thaliana* cryptochrome (*AtCRY*).  $B_{1/2}$  is the intensity of a magnetic field that produces 50% of the overall magnetic field effect. D, Change in the optical absorbance of photoinduced radicals in three avian CRY4 samples induced by a 30-mT magnetic field. *ErCRY4* spectra are shown at two different times after the start of illumination.

### Conclusion:

Cryptochrome 4 from the European robin is magnetically sensitive *in vitro* and could be the long sought-after magnetic sensor in night-migratory songbirds.

### Reference

<sup>1</sup>H. Mouritsen, *Nature* **558**, 50-59 (2018).

<sup>2</sup>K. Schulten, et al., *Z. Phys. Chem.* **111**, 1-5 (1978).

<sup>3</sup>T. Ritz, et al., *Biophys. J.*, **78**, 707-718 (2000)

<sup>4</sup>P. J. Hore & H. Mouritsen, *Annu. Rev. Biophys.* **45**, 299-344 (2016),

## **Authors:**

Jingjing Xu<sup>1+</sup>, Lauren E. Jarochoa<sup>2+</sup>, Tilo Zollitsch<sup>2+</sup>, Marcin Konowalczyk<sup>3+</sup>, Kevin B. Henbest<sup>2,3+</sup>, Sabine Richert<sup>4+</sup>, Matthew J. Golesworthy<sup>3+</sup>, Jessica Schmidt<sup>1</sup>, Victoire Déjean<sup>3</sup>, Daniel J. C. Sowood<sup>2</sup>, Marco Bassetto<sup>1,2</sup>, Jiatae Luo<sup>2</sup>, Jessica R. Walton<sup>2</sup>, Jessica Fleming<sup>2</sup>, Yujing Wei<sup>2</sup>, Tommy L. Pitcher<sup>3</sup>, Gabriel Moise<sup>3</sup>, Maike Herrmann<sup>1</sup>, Hang Yin<sup>5</sup>, Haijia Wu<sup>6</sup>, Rabea Bartölke<sup>1</sup>, Stefanie J. Käsehagen<sup>1</sup>, Simon Horst<sup>1</sup>, Glen Dautaj<sup>1</sup>, Patrick D. F. Murton<sup>2</sup>, Angela S. Gehrckens<sup>2</sup>, Yogarany Chelliah<sup>7,8</sup>, Joseph S. Takahashi<sup>7,8</sup>, Karl-Wilhelm Koch<sup>6,9</sup>, Stefan Weber<sup>4</sup>, Ilia A. Solov'yov<sup>9,10\*</sup>, Can Xie<sup>11\*</sup>, Stuart R. Mackenzie<sup>2\*</sup>, Christiane R. Timmel<sup>3,12\*</sup>, Henrik Mouritsen<sup>1,9\*</sup>, P. J. Hore<sup>2\*</sup>

<sup>1</sup>AG Neurosensory Sciences/Animal Navigation, Institut für Biologie und Umweltwissenschaften, Carl-von-Ossietzky Universität Oldenburg, 26111 Oldenburg, Germany

<sup>2</sup>Department of Chemistry, University of Oxford, Physical and Theoretical Chemistry Laboratory, Oxford OX1 3QZ, UK

<sup>3</sup>Department of Chemistry, University of Oxford, Inorganic Chemistry Laboratory, Oxford OX1 3QR, UK

<sup>4</sup>Institut für Physikalische Chemie, Albert-Ludwigs-Universität Freiburg, 79104 Freiburg, Germany

<sup>5</sup>Department of Medicinal Chemistry and Molecular Pharmacology, Purdue University, West Lafayette, IN 47907, USA

<sup>6</sup>Division of Biochemistry, Department of Neuroscience, Carl-von-Ossietzky Universität Oldenburg, DE-26111 Oldenburg, Germany

<sup>7</sup>Department of Neuroscience, University of Texas Southwestern Medical Center, Dallas, TX 75390-9111, USA

<sup>8</sup>Howard Hughes Medical Institute, University of Texas Southwestern Medical Center, Dallas, TX 75390-9111, USA

<sup>9</sup>Research Centre for Neurosensory Science, University of Oldenburg, 26111 Oldenburg, Germany

<sup>10</sup>Department of Physics, Carl-von-Ossietzky Universität Oldenburg, 26111 Oldenburg, Germany

<sup>11</sup>CAS Key Laboratory of High Magnetic Field and Ion Beam Physical Biology, High Magnetic Field Laboratory, Hefei Institutes of Physical Science, Chinese Academy of Sciences, Hefei, Anhui 230031, PR China

<sup>12</sup>Centre for Advanced Electron Spin Resonance (CAESR), Department of Chemistry, University of Oxford, Oxford OX1 3QR, UK